
Electronic Theses and Dissertations, 2004-2019

2012

The Dynamic Functions Of Bax Are Dependent On Key Structural And Regulatory Features

Rebecca Boohaker
University of Central Florida



Part of the [Molecular Biology Commons](#)

Find similar works at: <https://stars.library.ucf.edu/etd>

University of Central Florida Libraries <http://library.ucf.edu>

This Doctoral Dissertation (Open Access) is brought to you for free and open access by STARS. It has been accepted for inclusion in Electronic Theses and Dissertations, 2004-2019 by an authorized administrator of STARS. For more information, please contact STARS@ucf.edu.

STARS Citation

Boohaker, Rebecca, "The Dynamic Functions Of Bax Are Dependent On Key Structural And Regulatory Features" (2012). *Electronic Theses and Dissertations, 2004-2019*. 2292.

<https://stars.library.ucf.edu/etd/2292>

THE DYNAMIC FUNCTIONS OF BAX ARE DEPENDENT ON KEY STRUCTURAL
AND REGULATORY FEATURES

by

REBECCA JOSEPH BOOHAKER
B.S. University of Alabama at Birmingham, 2005

A dissertation submitted in partial fulfillment of the requirements
for the degree of Doctor of Philosophy
in the Department of Biomedical Sciences
in the College of Medicine
at the University of Central Florida
Orlando, Florida

Summer Term
2012

Major Professor: Annette R. Khaled

© 2012 Rebecca J. Boohaker

ABSTRACT

Bax is an essential mediator of cell fate. Since its discovery in 1985 as a protein that interacts with the anti-apoptotic protein, Bcl-2, key elements related to its function, structure and regulation remains to be determined. To this end, mitochondrial metabolism was examined in non-apoptotic Bax-deficient HCT-116 cells as well as primary hepatocytes from Bax-deficient mice. Although mitochondrial density and mitochondrial DNA content was the same in Bax-containing and Bax -deficient cells, MitoTracker staining patterns differed, suggesting the existence of Bax -dependent functional differences in mitochondrial physiology. Oxygen consumption and cellular ATP levels were reduced in Bax -deficient cells, while glycolysis was increased. These results suggest that cells lacking Bax have a deficiency in the ability to generate ATP through cellular respiration, supported by detection of reduced citrate synthase activity in Bax -deficient cells. Expression of either full length or C-terminal truncated Bax in Bax -deficient cells rescued ATP synthesis and oxygen consumption and reduced glycolytic activity, suggesting that this metabolic function of Bax was not dependent upon its C-terminal helix. Expression of BCL-2 in Bax-containing cells resulted in a subsequent loss of ATP measured, implying that, even under non-apoptotic conditions, an antagonistic interaction exists between the two proteins.

Bax is composed of nine alpha-helices. While three of these helices have features of a trans-membrane region, the contribution of each domain to the apoptotic or non-apoptotic functions of Bax remains unknown. To examine this, we focused on the C-terminal alpha-9 helix, an amphipathic domain with putative membrane binding

properties and discovered that it has an inherent membrane-binding and cytotoxic capacity. A peptide based on the last twenty amino acids (CT20p) of the alpha-9 helix was synthesized and proved a potent inducer of cell death independent of any apoptotic stimuli. The solubility of CT20p allowed it to be encapsulated in polymeric nanoparticles (NPs), and these CT20p-NPs caused the death of colon and breast cancer cells *in vitro* and induced tumor regression *in vivo*, using a murine breast cancer tumor model. CT20p caused increased mitochondrial membrane potential followed by cell death via membrane rupture, without the characteristic membrane asymmetry associated with apoptosis. Hence, while CT20p is based on Bax, its innate cytotoxic activity is unlike the parent protein and could be a powerful anti-cancer agent that bypasses drug resistance, can be encapsulated in tumor-targeted nanoparticles and has potential application in combination therapies to activate multiple death pathways in cancer cells.

While previous work revealed novel aspects of the biology of Bax that were unrecognized, new structural information is needed to fully elucidate the complexity of Bax's function. One approach is to use computational modeling to assess the solved structure of Bax and provide insight into the structural components involved in the activity of the protein. Use of molecular dynamics simulators such as GROMACS, as well as other computational tools provides a powerful means by which to test the feasibility of certain modifications in defined parameters. Such work revealed that the removal of the C-terminal alpha-9 helix of Bax, which normally resides within a hydrophobic pocket, significantly destabilized the protein, perhaps explaining how the protein transitions from soluble to membrane-bound form and maintain energy

production via aerobic respiration or, conversely, how the C-terminus helix conveys cytotoxicity. Collectively, this work reveals that Bax is more than an inducer of cell death but has complex activities yet to be determined.

ACKNOWLEDGMENTS

The completion of this work has involved many people. I first wish to acknowledge my advisor, Annette Khaled, Ph.D. Without her encouragement and ideas none of the presented work would have been possible. The five years I spent in her laboratory have been a wonderful experience. I have learned a lot not only about conducting research, writing papers, and presenting results, but also how to think as a scientist. For all of this, I thank her.

The members of my graduate committee, Alex Cole, Ph.D., Tony Zervos, Ph.D. and Suren Tatulian, Ph.D., also deserve special thanks and recognition for their advice and help during the process of my graduate training. I could not have advanced so quickly without their assistance and encouragement. I thank them for being there whenever I had a problem or need. I also want to thank Cristina Fernandez-Valle, Ph.D. for teaching me the basics of confocal microscopy on which so much of the work was based. I would like to thank Kathleen Nemec, Ph.D., and Michael Lee, PhD, for their advice, skills training and for being general sounding boards.

TABLE OF CONTENTS

LIST OF FIGURES.....	xii
LIST OF TABLES.....	xiv
CHAPTER 1: GENERAL INTRODUCTION.....	1
Apoptosis.....	1
Bcl-2 proteins in Metabolism.....	4
Bax in therapeutics	7
Computational modeling and Protein expression	8
Figures and Tables.....	11
CHAPTER 2: BAX SUPPORTS THE MITOCHONDRIAL NETWORK, PROMOTING BIOENERGETICS IN NON-APOPTOTIC CELLS	18
Introduction.....	18
Materials and methods	20
Cell Lines and Reagents.	20
Isolation of Primary Mouse Hepatocytes.	20
Plasmids, Mutagenesis, and Transfection.....	21
Glucose Deprivation.....	22

Measurement of Oxygen Consumption and Extracellular Acidification Rates.	22
Mitochondrial Staining: Fixed Imaging, Live Cell Imaging and Tissue Sectioning.	23
Sub-cellular Fractionation and Immunoblotting.	24
Proteinase K Digestion of Membrane Bound Proteins.	25
Measurement of ATP production and Mitochondrial Membrane Potential...	25
Measurement of Citrate Synthase Activity.	27
Inhibition by siRNA.	27
Measurement of Mitochondrial DNA.	28
Surface Plasmon Resonance (SPR) binding experiments.	28
Statistics.	29
Results	29
Mitochondrial Bioenergetics Requires Bax.	29
Bax Contributes to ATP production.	33
Interaction with BCL-2 Blocks Bax's Non-Apoptotic Activity.	37
Discussion	39
Figures and Tables	43

CHAPTER 3: EXPLOITING THE INHERENT CYTOTOXICITY OF THE ALPHA-9 HELIX OF BAX FOR USE AS A PEPTIDE DRUG FOR CANCER THERAPY	54
Introduction.....	54
Materials and Methods	56
Cell lines and CT20p.	56
Plasmids, Mutagenesis and Transfection.	57
Mitochondrial Translocation Assay and Immunoblotting.	58
Live-Cell Confocal Imaging.....	59
Treatments and Detection of Apoptotic Cells and Mitochondrial Membrane Potential by Flow Cytometry.	60
Synthesis of Polymeric NPs Encapsulating CT20p.	61
Synthesis of Aminated Polymeric NPs Encapsulating CT20p.	61
Calcein Release Experimental Protocol.	62
In Vivo Experiment.	63
Results	64
CT20p Enables Mitochondrial Membrane Binding and Permeabilization. ...	64
Delivery of the CT20p Using Polymeric NPs Kills Cancer Cells.	68
The Death-Inducing Activity of CT20p is Independent of Caspases and Resistant to Bcl-2, Causing Tumor Regression.	71

Discussion	74
Figures and Tables.....	79
CHAPTER 4: STABILIZATION OF THE TERTIARY STRUCTURE OF BAX IS DEPENDENT ON THE C-TERMINAL HELIX	87
Introduction.....	87
Materials and Methods	89
Generation of Bax Mutants in Silico.	89
Molecular Dynamics Simulations.....	90
Analysis of Simulations.....	91
Expression and Purification of the Full Length Bax Protein	91
SDS-PAGE and Western Blotting.....	92
Results	93
Energy Minimization and Validation of Force Fields.....	93
MD Simulations and Analysis of Protein Stability.	95
Protein Expression.	97
Discussion	97
Figures and Tables.....	99
CHAPTER 5: CONCLUSION	106
APPENDIX A: COPYRIGHT PERMISSION	110

APPENDIX B: IACUC APPROVAL LETTERS 112

REFERENCES..... 119

LIST OF FIGURES

Figure 1. Representative Members of the Bcl-2 Protein Family	12
Figure 2. Caspase Dependent Apoptotic Signaling Pathways.	13
Figure 3. The Electron Transport Chain.	14
Figure 4. Classes of Therapeutic Peptides.....	15
Figure 5. Schematic of pore types.....	16
Figure 6. Model for the membrane pore formed by the CT20p.	17
Figure 7: Treatment with the fusion inhibitor, Mdivi-1, did not alter MitoTracker staining.	45
Figure 8: Reduced metabolic activity in Bax deficient cells is not related to mitochondrial content or loss of viability.	46
Figure 9: Deficiency of Bax results in reduced intracellular ATP and oxygen consumption.	47
Figure 10: Cells deficient in Bax are susceptible to glucose deprivation.	48
Figure 11: Bax associates with mitochondria in non-apoptotic cells resulting in reduced citrate synthase activity.	49
Figure 12: Bax associates with mitochondria in non-apoptotic cells resulting in reduced citrate synthesis activity.	50
Figure 13: Liver hepatocytes from Bax deficient mice have with reduced metabolic activity, resulting in decrease ATP and oxygen consumption.	51
Figure 14 : Expression of full Length Bax restores mitochondrial association and ATP production in Bax deficient cells.	52
Figure 15: The interaction of Bax with BCL-2 inhibits the production of ATP in non- apoptotic cells.....	53
Figure 16 Lysines in CT20p, which is Based on the C-terminus of Bax, Contribute to Intracellular Localization.	80

Figure 17. CT20p causes the Release of Sequestered Contents from Mitochondrial-like Lipid Vesicles without Loss of Membrane Integrity.	81
Figure 18. CT20pe can be Encapsulated in NPs for Delivery to Cells.....	82
Figure 19. CT20p-NPs Kill Bax-containing or Bax-deficient HCT116 cells.....	83
Figure 20. CT20p-NPs Kill Breast Cancer Cells.....	84
Figure 21. Mechanism of Death Mediated by CT20p is Effector Caspase Independent and Resistant to Bcl-2.	85
Figure 22. CT20p Induces Tumor Cell Death in vivo.....	86
Figure 23. A Comparison of the Energy Minimization of Bax Variants.	99
Figure 24. Validation of the AMBER99SB-ILDN Force Field.....	100
Figure 25. Radius of Gyration Indicates Stability of the Structure in the System.....	101
Figure 26. Root Mean Square Deviation of the Structure as Compared to the Initial PDB File.....	102
Figure 27. Structural Changes as a Result of Increase in Temperature.....	103
Figure 28. RMSD of WT Bax and DCT at Each Temperature Step.....	104
Figure 29. Verification of the Presence of Bax from the Mammalian Expression System.	105

LIST OF TABLES

Table 1. Peptides and Small Molecules Currently in Development	11
Table 2. Level Of mtDNA Content in Bax ^{+/+} and Bax ^{-/-} HCT116 Cells	43
Table 3. Association of Membrane-bound Bax with Different Density Fractions Recovered after Differential Ultracentrifugation	44
Table 4. Comparison of CT20p with Anti-Microbial Peptides and Apoptosis-Inducing Peptides	79

LIST OF ABBREVIATIONS

AIF	Apoptosis Initiating Factor
AM	Aminated
AMP	Anti-microbial Peptide
ANT	Adenine nucleotide translocase
Apaf-1	Apoptotic Peptidase Activating Factor 1
ATP	Adenosine Triphosphate
BAD	Bcl-2 Associated Death Promoter
BAK	Bcl-2 Homologous Antagonist Killer
BAX	Bcl-2 Associated Protein X
BAX- Δ CT	Carboxy-Terminal Deleted Bax
BAX- Δ NT	Amine-Terminal Deleted Bax
BAX-FL	Full-Length Bax
BCL-2	B-cell Lymphoma-2
BCL _{XL}	B-cell Lymphoma Extra Large
BH	Bcl-2 Homology Domain
BID	BH3 Interacting Domain
Bif-1	Bax interacting factor-1
BIM	Bcl-2-like 11
BSA	Bovine Serum Albumin
Ca ²⁺	Calcium
CBD	Chitin Binding Domain
CDDP	Cisplatin
COOH	Carboxy
CPP	Cell Penetrating Peptide
CT	C-Terminus
CT20p	Peptide derived from the last 20 Residues of Bax
DCT	C-terminal Deleted Bax
DD	Destabilization Domain

DNA	Deoxyribonucleic Acid
DMEM	Dulbecco's Modified Eagle Medium
DMSO	Dimethylsulfoxide
Drp1	Dynamin-related Protein-1
DTNB	5-5'-dithiobis [2-nitrobenzoic acid]
$\Delta\Psi\mu$	Electrochemical Potential across the IMM
EB	Ethidium Bromide
ECAR	Extracellular Acidification Rate
EDC	1-ethyl-3-(3-dimethylamino-propyl)
EGFP	Enhanced Green Fluorescent Protein
EM	Energy Minimization
E_{pot}	Potential Energy
EPR	Enhanced Permeability and Retention
ER	Endoplasmic Reticulum
ETC	Electron Transport Chain
FADD	Fas-Associated Death Domain
FBS	Fetal Bovine Serum
GFP	Green Fluorescent Protein
GRP78	Binding Immunoglobulin Protein localized to the ER
FCCP	Carbonyl Cyanide 4-(trifluoromethoxy) phenylhydrazone
HBPE	Hyperbranched Polyester
HCl	Hydrochloric Acid
HCT116	Human Colon Carcinoma cell line
HRP	Horseradish Peroxidase
IEX	Ion Exchange Chromatography
IMM	Inner Mitochondrial Membrane
IR	Ionizing Radiation
IRES	Internal Ribosome Entry Site
k_a	Association Constant

k_d	Dissociation Constant
K_D	Equilibrium Constant
KO	Knock Out
LUVs	Large Unilamellar Vesicles
MCF-7	Michigan Cancer Foundation-7
MCL-1	Myeloid Cell Leukemia Sequence -1
MD	Molecular Dynamics
MDA-MB-231	M.D. Anderson Metastatic Breast Cancer Cell Line
Mfn-2	Mito-Fusin-2
mtDNA	Mitochondrial DNA
NAO	10-nonyl-Acridine Orange
nDNA	Nuclear DNA
NHS	<i>N</i> -hydroxysuccinimide
NMR	Nuclear Magnetic Resonance
NP	Nanoparticle
OCR	Oxygen Consumption Rate
OMM	Outer Mitochondrial Membrane
OXPPOS	Oxidative Phosphorylation
PARP	Poly (ADP-ribose) Polymerase
PBS	Phosphate Buffered Saline
PCR	Polymerase Chain Reaction
PDB	Protein Data Base
PEG	Polyethylene Glycol
PI	L- α phosphatidylinositol
PMSF	Phenylmethanesulfonylfluoride
POPC	palmitoyl-2-oleyl-sn-glycero-3-phosphatidylcholine
POPE	1-palmitoyl-2-oleyl-sn-glycero-3-phosphatidylethanolamine
POPG	1-palmitoyl-2-oleyl-sn-glycero-3-phosphatidylglycerol
PS	Phosphatidylserine

PTP	Permeability Transition Pore
RMSD	Root Mean Square Deviation
RNA	Ribonucleic Acid
ROS	Reactive Oxygen Species
SEC	Size Exclusion Chromatography
siRNA	Small Interfering RNA
SPR	Surface Plasmon Resonance
TCA	Tricarboxylic Acid Cycle
TNF	Tumor Necrosis Factor
TRADD	TNF Receptor Associated Death Domain
UV	Ultraviolet
VDAC	Voltage Dependent Anion Channel
WT	Wild Type
WTBax	Wild Type Bax
Z-VAD-fmk	Z-Val-Ala-Asp-fluoromethylketone

CHAPTER 1: GENERAL INTRODUCTION

At a cellular, tissue, and organism level, the balance between life and death is a highly complex system that operates on a very simple premise: it is better to die than to be wrong [1]. This is particularly true at the cellular level where the cell is forever deciding whether to skew its resources towards proliferation, differentiation or apoptosis. A substantial effort has been made to determine the specific initiators and mechanisms of, particularly, the intrinsic apoptotic pathway. This highly regulated and predictable series of events that result as the pathway propagates provides an excellent opportunity to determine the specific contribution of each player in the apoptotic cascade. Central to the intrinsic apoptotic pathway are the mitochondria and the proteins that interact with mitochondrial membranes. The understanding of the interplay between the pro- and anti-apoptotic proteins allows for a better design of activators or inhibitors to force the cell into a particular fate. This becomes highly desirable in disease states such as cancer, as any defects in the genetic or protein expression within the apoptotic machinery can push the cell into uncontrolled proliferation, immortality, and subsequent carcinogenesis [2].

Apoptosis

Maintaining the balance between life and death within a cell are the B-cell Lymphoma 2 (Bcl-2) family of proteins. This family, of which Bcl-2 is the founding member, is comprised of both pro- and anti- apoptotic members and shares a number of common features [3]. These features include, but are not limited to, helix-turn-helix tertiary structure and Bcl-2 homology (BH) functional domains [4] (Figure 1). These

characteristic features allow for both synergistic (ex. tBid – Bax) and antagonistic (ex. Bcl-2 – Bax) interactions, which then act as determinants of cell fate. Additionally, a majority of these proteins have the ability to target the mitochondrial membrane specifically, and contain trans-membrane domains [5]. The ability of these proteins to target the mitochondria with prejudice is integral to their function as homeostatic regulators or death inducers. Since mitochondria are the energy generators of the cell, in terms of aerobic respiration and adenosine triphosphate (ATP) production, maintenance of mitochondrial integrity is paramount for cell survival [6]. Under non-apoptotic conditions, the effects of the pro-apoptotic proteins are offset by the presence of anti-apoptotic Bcl-2 and Bcl_{XL} at the outer mitochondrial membrane. An imbalance of this interaction will push the cell toward either death (Bax > Bcl-2) or survival (Bax < Bcl-2) [7].

The caspase-mediated apoptotic process can be set into motion by either an extrinsic or intrinsic signal. In addition to these processes, a non-caspase mediated pathway involves the activation of Apoptosis Initiating Factor or AIF [8], [9]. The extrinsic process is activated by the engagement of death ligand, most commonly Tumor Necrosis Factor (TNF) or FasL receptors [8]. The resultant pathway involves intermediate proteins TNF receptor associated death domain (TRADD) and/or Fas associated death domain (FADD) in the activation of caspases 8 and 3. In a slightly more complex manner, the initiation of the intrinsic death pathway instigates a series of events that allow for the release of apoptotic peptidase activating factor 1 (apaf-1),

cytochrome c, and pro-caspase 9 [8]. The subsequent assembly of the apoptosome results in the activation of effector caspases that lead to cell death (Figure 2).

Central to the intrinsic pathway is the capability of the pro-apoptotic subset of Bcl-2 proteins (Bax, Bid, Bak, and Bad) to target the mitochondria. Bcl-2-associated protein X (Bax) contains within its primary sequence a mitochondrial targeting sequence that, when exposed, directs the protein to the outer mitochondrial membrane [10]. Once there, Bax acts as a direct competitor with Bcl-2. The identification of orthologs of the *BAX* gene throughout mammalian genomes indicates the evolutionary conservation of the protein is necessary for survival of the organism, even though no ortholog has been identified in *Caenorhabditis elegans* [11]. Differential tissue expression of Bax during embryogenesis promotes normal retinal, renal tube and kidney development. Conversely, Bax is down-regulated during the development of the nervous system [12–14].

Structurally, Bax retains the helical packing of other Bcl-2 family members, and of the four BH domains common to Bcl-2 proteins, Bax has three (BH1, 2, 3) [15] (Figure 1). Unlike Bcl-2 or Bcl_{XL}, which are both membrane bound, Bax exists in two conformations: 1) a soluble, monomeric, “inactive” form, and 2) a membrane-bound, oligomeric, “active” form [16]. The solved solution NMR structure yields some insight into how the protein is able to transition from the inactive to the active form. Bax is comprised of nine α -helices of which two ($\alpha 5$ and $\alpha 6$) are hydrophobic, and $\alpha 9$ is amphipathic, with these three helices containing the putative pore forming and membrane insertion domains of the protein [17]. As long as Bax remains cytosolic,

these domains are obscured from the environment and cannot interact with the mitochondrial membrane. Upon activation of the intrinsic apoptotic pathway, the protein undergoes a conformational change resulting in relaxation of the tertiary structure, exposing the domains and allowing for interaction with the membrane.

Though the exact mechanism of oligomerization is not clear, it is known that translocation of Bax from the cytosol to the outer mitochondrial membrane directly results in the release of apoptotic factor cytochrome c and activation of caspase 9 [18], [19]. The pore-forming capability of this oligomerization event also destabilizes the outer mitochondrial membrane causing a decrease in membrane potential, a release of Ca^{2+} , and resulting in a series of events such as mitochondrial fragmentation and phosphatidylserine (PS) flipping [20–22]. These events are predictable, measurable consequences of Bax activation. However, despite the fact that numerous studies have isolated, truncated, and mutated various domains of the protein, it remains to be determined which domains of Bax are necessary for it to execute its apoptotic function.

Bcl-2 proteins in Metabolism

The idea that the Bcl-2 family members can be compartmentalized into strictly pro- and anti-apoptotic roles is limiting to the scope in which these proteins act. Bad, for example, canonically characterized as a pro-apoptotic protein, acts as a shuttle for hexokinase 4 to the mitochondria under non-apoptotic conditions [23], [24]. Bcl_{XL} interacts with the F₁F_O ATP synthase to increase the efficiency of proton transport in the mitochondria of neurons [25]. Similarly, Bid has a critical role in the inflammatory response that is independent of its apoptotic function [26]. These, and other

observations, indicate that the cell can utilize the organelle targeting capability of Bcl-2 proteins to execute homeostatic functions. Similarly, cytochrome c, a component of the apoptosome, functions primarily as an electron shuttle between complex III (Coenzyme Q-Cyt c reductase) and complex IV (Cyt C oxidase) [27]. The ability of pro-apoptotic proteins to affect membrane permeability and even to associate with voltage channel component proteins indicates that any potential regulatory role is equally as important as the apoptotic activity.

The link between metabolism and cancer was first identified by Otto Warburg in what known as the Warburg effect [28]. The Warburg effect links a switch from oxidative phosphorylation to aerobic glycolysis with carcinogenesis. Since the mitochondria is, in essence, the power generator of the cell, the maintenance of oxidative phosphorylation (OXPHOS) is necessary to ensure that the cell has sufficient levels of ATP for cell homeostasis and growth [29]. OXPHOS is facilitated by a series of protein complexes housed in the inner mitochondrial membrane (IMM). These proteins shuttle electrons from donors to acceptors along a chemiosmotic gradient within the electron transport chain (ETC) (Figure 3). This gradient has both a pH and electrical component that is potentiated across the IMM, and acts as the driving force for the F_1F_0 ATP synthase that terminates the ETC. The status of the mitochondrial membrane potential ($\Delta\Psi\mu$) is indicative of viability of the cell and is maintained by a series of regulators at the OMM (as reviewed in [30]). The electrochemical potential across the IMM is 180 mV, which renders the matrix facing membrane negatively charged, is due in part to the presence of a lipid unique to the mitochondria, cardiolipin

[31]. Cardiolipin is unique in that it has two negative charges and is found acting as a proton trap in the IMM, surrounding the protein complexes in the ETC, and maintaining the impermeability of the IMM [32]. Increased electro-negativity of the OMM can be linked to an increased exposure of cardiolipin, an event that is an early indicator of apoptosis and a precursor to depolarization of the IMM [33]. While this is not the point of no return in the apoptotic cascade, the electro-negativity conferred by the exposed cardiolipin is sufficient to attract cationic proteins, particularly Bax with its cationic trans-membrane tail.

Protein complexes such as Voltage Dependent Anion Channels (VDAC) and ADP/ATP translocases like the adenine nucleotide translocators (ANTs) serve to maintain the overall integrity of the mitochondria by regulating ion and mitochondrial ATP flux, ultimately maintaining the $\Delta\Psi\mu$ [34]. The component proteins of these permeability transition pores (PTP) [35] contain known and putative binding partners of Bax. While Bax is predominantly cytosolic in its inactive form, it has been reported that even in non-apoptotic conditions, a fraction of the existing protein can be found associated with these candidate binding partners. Additionally, the transient negative charge on the OMM could act as an attractant for the positive charge localized within the trans-membrane region of Bax. The localized and transient interaction of Bax with the OMM and its resident proteins would account for a homeostatic, regulatory role for the protein.

Bax in therapeutics

The manipulation of Bcl-2 family proteins in the treatment of cancers has been studied for many years. Over-expression of Bcl-2 is common in a number of cancers, and often leads to resistance to traditional chemotherapies because of the overriding survival signal conveyed by the protein [36]. To combat this, oligonucleotide therapy targeting gene expression and small molecule inhibitors, such as ABT-737, targeting protein function [37–40] has been developed to mitigate the effects of over-expressed Bcl-2. Conversely, inducible activation of pro-apoptotic proteins, like Bax, would render a cancerous cell susceptible to a secondary treatment, if not kill the cell outright [41].

To this end, analysis of the structure and apoptotic function of Bax and its domains provides an insight into the derivation of novel small molecule therapeutics. The pore-forming capability of Bax is well documented, with helices 5,6 and 9 being putative membrane spanners [17]. There are a number of theories as to how the protein docks within the membrane, including an umbrella model [42], which involves unfolding of the protein once interfaced with mitochondrial membrane. However, an examination of the composition of the helices reveals that the $\alpha 9$ helix shares a striking similarities to anti-microbial peptides (AMPs); these peptides tend to be amphiphilic in nature with localized cationic residues and hydrophobic regions [43].

Peptides and small molecules provide a promising pool of candidates for potent cancer therapy. These peptides and small molecules are currently being developed, with some in clinical trials (Table 1) to either serve as targeting agents (RGD peptide) [44], cell permeabilizers (CPPs) [45], or cell penetrating peptides (TAT) [46] (Figure 4). The exploitation of a peptide derived from the mitochondrial localization region of Bax

would provide a novel peptide therapy for treatment of certain cancers. With the mitochondria, as the power generator of the cell, it is an ideal drug target. Additionally, contained within the mitochondrial matrix, and even bound to the IMM itself are factors that could push the cell into an apoptotic or even a necrotic fate. Targeting the organelle, itself, instead of a receptor or pathway makes it very difficult for the cell to engage a redundant mechanism, minimizing off-target effects.

A determination of the membrane disruption capabilities of the membrane targeting region would provide insight into the development novel therapeutic derived from Bax. The pore-forming capabilities of classical, cationic AMPs fall into two categories: barrel-stave and toroidal pores [47] (Figure 5). Previous studies examining the orientation and assembly of the Bax derived CT20p in model membranes by solid state NMR indicate that the peptide does indeed assemble in a membrane in an anti-parallel arrangement to form a pore (Tatulian, SA, et al. submitted) (Figure 6). Evaluation of the cytotoxic properties of this peptide also yields information on the ability of the protein as a whole to self-regulate in the absence of an apoptotic stimulus.

Computational modeling and Protein expression

Since the discovery of the *bcl-2* gene to convey immortality to pre-B cells in 1988 [48], a significant amount of research has been dedicated to the understanding of the interplay of the Bcl-2 family and the roles they play in promoting or inhibiting the progression of apoptosis. Surprisingly, insights into the functions and mechanisms of action are few and far between. Bax is a prime example of the difficulty in characterizing the fine details of the dynamic nature of these proteins. An examination

of the literature describing the functional domains places the “killer” or membrane interacting regions at the N-terminus [49], the $\alpha 5$ – $\alpha 6$ helices [50], or the C-terminus [51]. There is no true consensus on the regions that contribute to oligomerization, however, a BH3 binding groove can be targeted to activate the protein [52]. This is due in part to the relative difficulty of studying the protein in an isolated state. There is, to date, one solved NMR structure of the protein in its entirety, unbound to any other peptide, antibody or protein fragment [10]. This lone structure is the basis of *in silico* modeling that drives drug design geared to activation of the protein.

What is largely absent from the literature is the utilization of molecular dynamics *in silico* to assess the internal dynamics of Bax. The ability to measure a protein’s behavior after the application of a series of defined physical constraints provides valuable insight into the mechanisms of action of proteins of interest. Computational modeling allows for the generation of environments that simulate the behavior of a molecule, protein, or complex under a specified set of conditions. Analysis post simulation supplies information on the folding, mechanism of action, and interacting sites under those conditions.

Modeling of members of the Bcl-2 family allows for directed design of inhibitors of certain proteins. Most of the 30 identified family members have been solved either by NMR or by X-ray crystallography [53]. The highly conserved structural homology within the Bcl-2 family lends itself for comparative studies among the constituent proteins. For Bax to transition from the cytosol to the mitochondria, a relaxation of the structure is required to expose domains capable of interacting with a lipid membrane. This requires

some level of self-regulation by the protein, and measurements taken on the isolated model gives a step-wise look at the ordered reorganization, unfolding, or exposure of specific domains. Molecular dynamics simulations provide a high throughput means to determine the effects of mutations or deletions on the structure, energy and packing density on the protein.

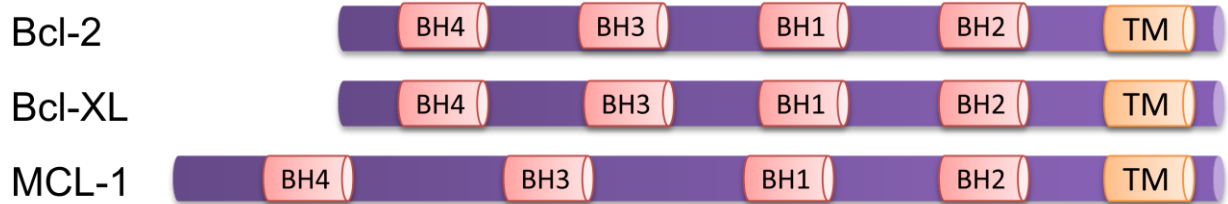
The work presented here takes an interdisciplinary approach to examine the structure and function of Bax and its constituent domains. An examination of the behavior of Bax in non-apoptotic conditions uncovered a previously undescribed role for Bax in the maintenance of the bioenergetics in the cell. Comparison of the primary sequence of the $\alpha 9$ -helix to known anti-microbial peptides led to isolation of the last 20 amino acid residues, and the discovery of a potent cytotoxic agent. These observations together prompted a series of computational simulations to help elucidate the regulatory regions that contribute the dual function of the full length protein.

Figures and Tables

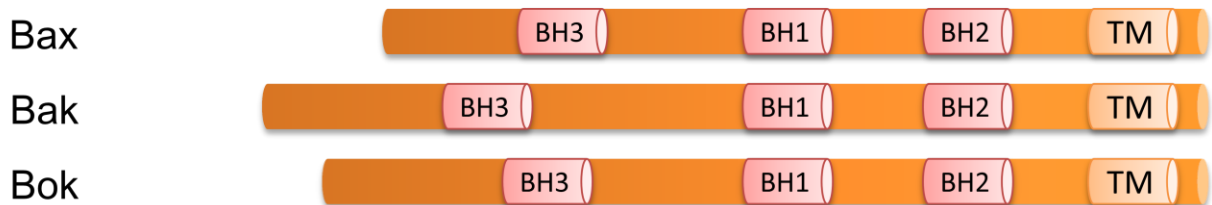
Table 1. Peptides and Small Molecules Currently in Development

PEPTIDE NAME	THERAPEUTIC USE	CLINICAL DEVELOPMENT PHASE	REFERENCES/ CLINICAL TRIAL SITE
Group I Peptides			
Cecropin A and B	Cancer: Leukemia Bladder	Pre-Clinical Pre-Clinical	Hui et al., 2002 Suttmann et al., 2008
Pleurocidin	Cancer: breast	Pre-Clinical	Hilchie et al., 2011
Magainin2	Cancer: Bladder Anti-microbial: Diabetic foot ulcers	Pre-Clinical Phase III	Lehmann et al., 2006 MarcoChem Corporation
β -defensin	Anti-microbial: Inflammatory Biomarker	Phase IV	Eastern Virginia Medical School/Merck
α 5- α 6 Bax peptide	Cancer: apoptosis	Pre-Clinical	Valero et al., 2010
BH3 domain	Cancer: apoptosis	Pre-Clinical	Walensky et al. 2004
KLAKLAK	Cancer: glioblastoma	Pre-Clinical	Agemy et al. 2011
Group II Peptides			
Tat	Cancer HIV: vaccine	Pre-Clinical Phase I, II	Istituto Superiore di Sanita
Group III Peptides			
RGD (Cilengitide, Delta 24- RGD, Delta 24-RGD 4C, RGD-K5)	Cancer: Brain Ovarian Head and Neck Prostate Lung Melanoma	Phase I Phase II Phase I Phase I and II Phase II Phase I and II Phase II	M.D. Anderson and others Erasmus Medical Center and others University of Alabama at Birmingham Merck, Chang Gung Memorial Hospital University of Michigan Cancer Center Merck, University Hospital Mannheim M.D. Anderson
NGR (NGR- hTNF)	Cancer: Ovarian Mesothelioma Lung Sarcoma Colon Hepatic	Phase II Phase II, III Phase II Phase II Phase II Phase II	MolMed S.p.A. MolMed S.p.A. MolMed S.p.A. MolMed S.p.A. MolMed S.p.A. MolMed S.p.A.

Anti-apoptotic



Pro-apoptotic



BH3-Only



Figure 1. Representative Members of the Bcl-2 Protein Family

The Bcl-2 family members divided into three subgroups: anti-apoptotic proteins which include Bcl-2, Bcl-XL, and MCL-1 among others, pro-apoptotic proteins Bax, Bak, and Bok, and BH3 only pro-apoptotic proteins which include Bim, Bad, and Bid.

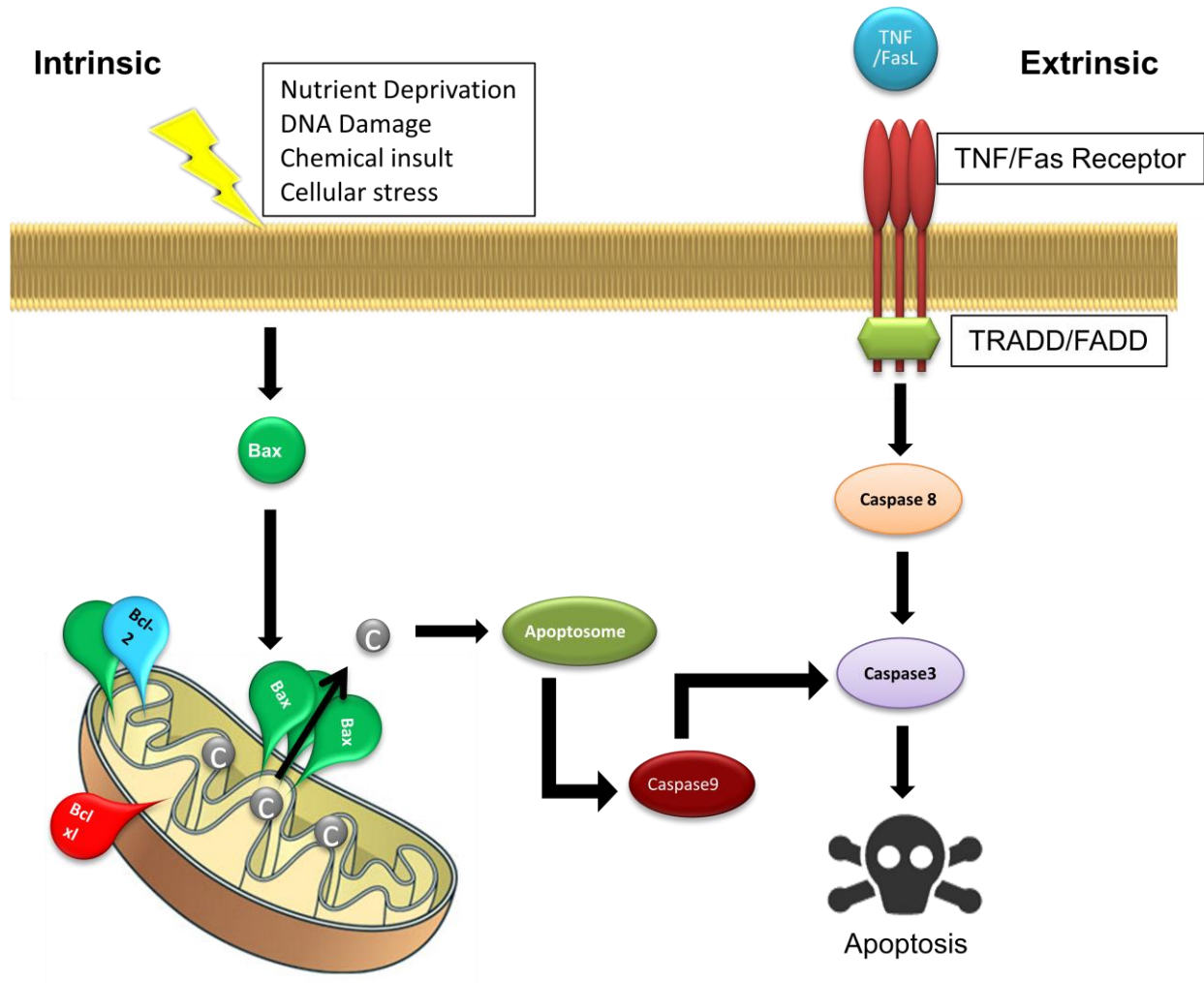


Figure 2. Caspase Dependent Apoptotic Signaling Pathways.

The apoptotic mechanism can be initiated in one of two ways: the intrinsic pathway, which engages the Bcl-2 family members and involves mitochondrial membrane disruption resulting in the release of apoptotic factors such as cytochrome C and pro- caspase 9. The second pathway is the Extrinsic pathway which involves activation of death receptors on the cell surface by their respective ligands. The activation of effector caspases leads to controlled cell death characteristic of apoptosis.

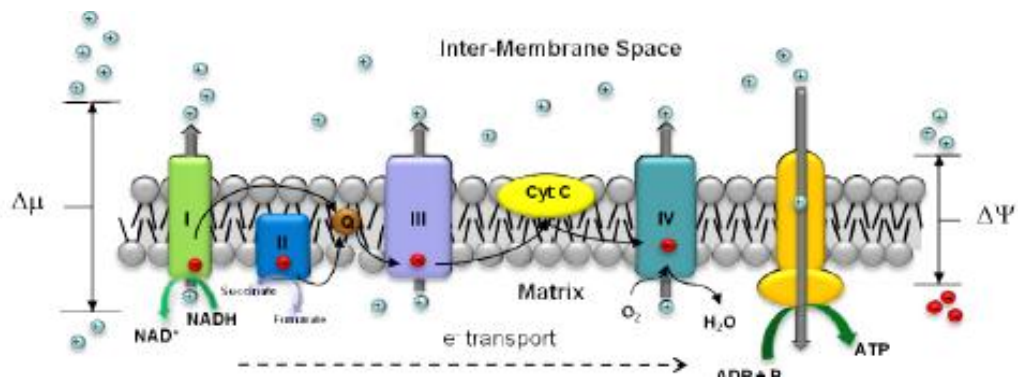


Figure 3. The Electron Transport Chain.

The electron transport chain operates on the combination of a chemiosmotic gradient and an electric potential. The five component complexes reside in the IMM and use the transfer of electrons to pump protons into the inner membrane space. The proton gradient drives the F_0F_1 ATPase to generate ATP from ADP.

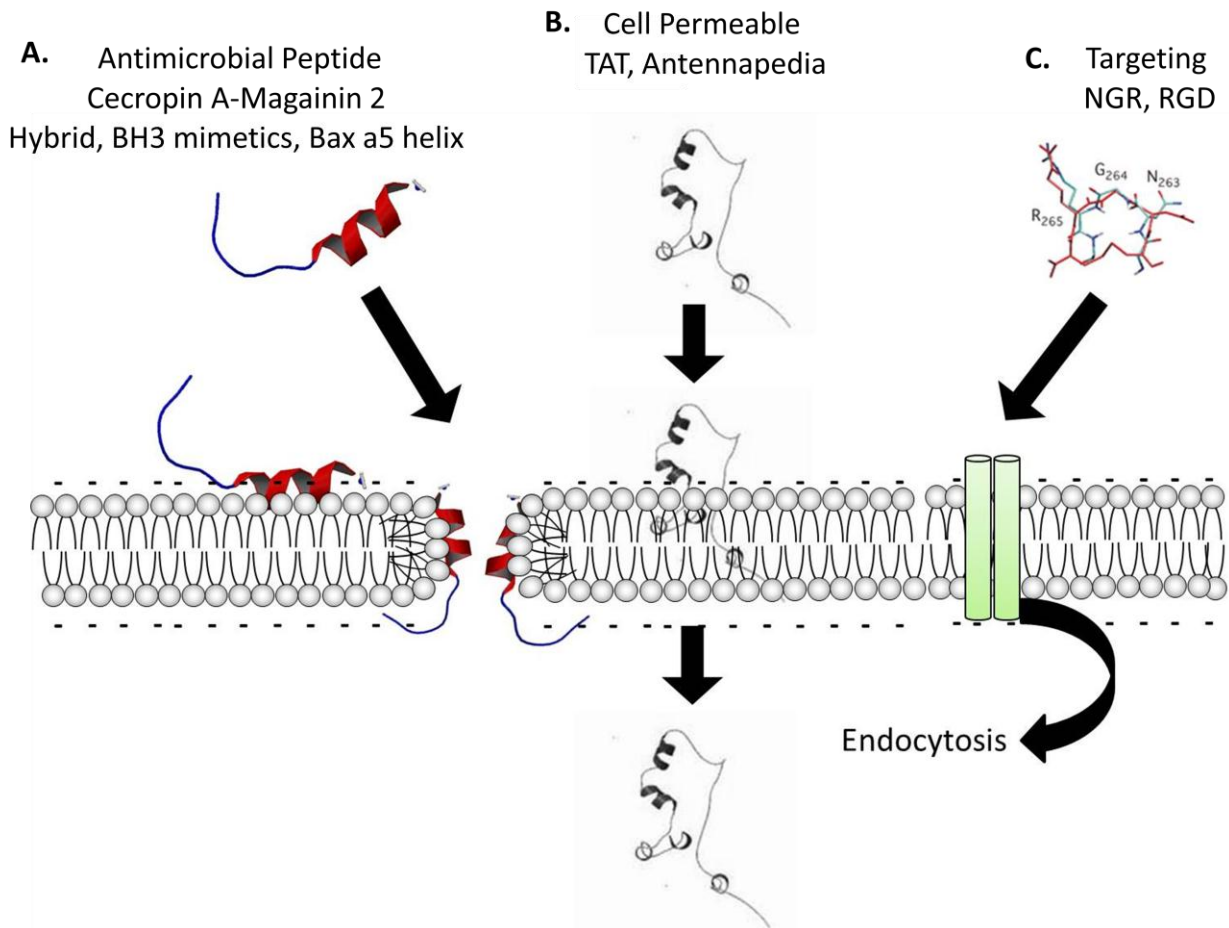


Figure 4. Classes of Therapeutic Peptides.

Current therapeutic peptides can be classified into three major divisions. A) Antimicrobial peptides (i.e. magainins or cecropins) or “pore forming” peptides (i.e. derived from the Bcl-2 family of apoptosis mediators) are targeted to characteristics of certain membranes and typically incorporate into the membrane to form toroidal pores, affecting both membrane stability and membrane potential. B) Cell permeable peptides, for example the Tat peptide derived from HIV, are usually arginine rich and inert to the cell. They do not require an endocytotic mechanism to incorporate in the cell, and are often tethered to another more active compound or peptide that, making this a “Trojan horse” class. C) Targeting peptides, such as RGD or NGR peptides, are specific for a plasma membrane component overexpressed by the tumor vasculature. These peptides are typically used to target a secondary chemotherapy agent or biological preferentially to tumors.

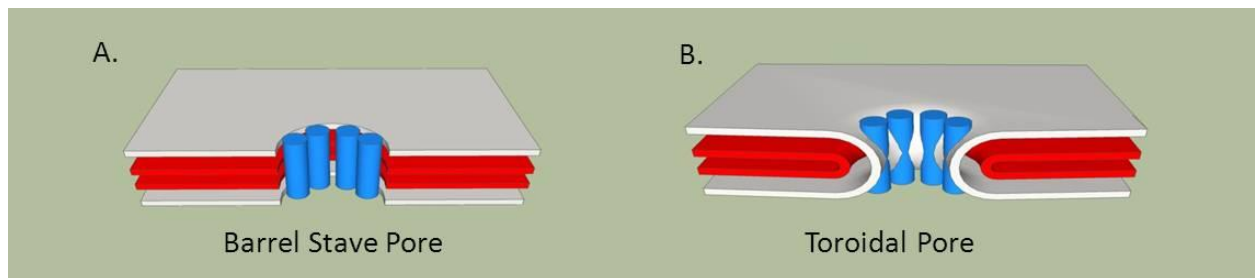


Figure 5. Schematic of pore types.

The models of the (A) barrel-stave and (B) toroidal pores were generated using SketchUp (Google). The gray layer represents the outer membrane, the red the inner membrane. The blue cylinders are peptide monomers.

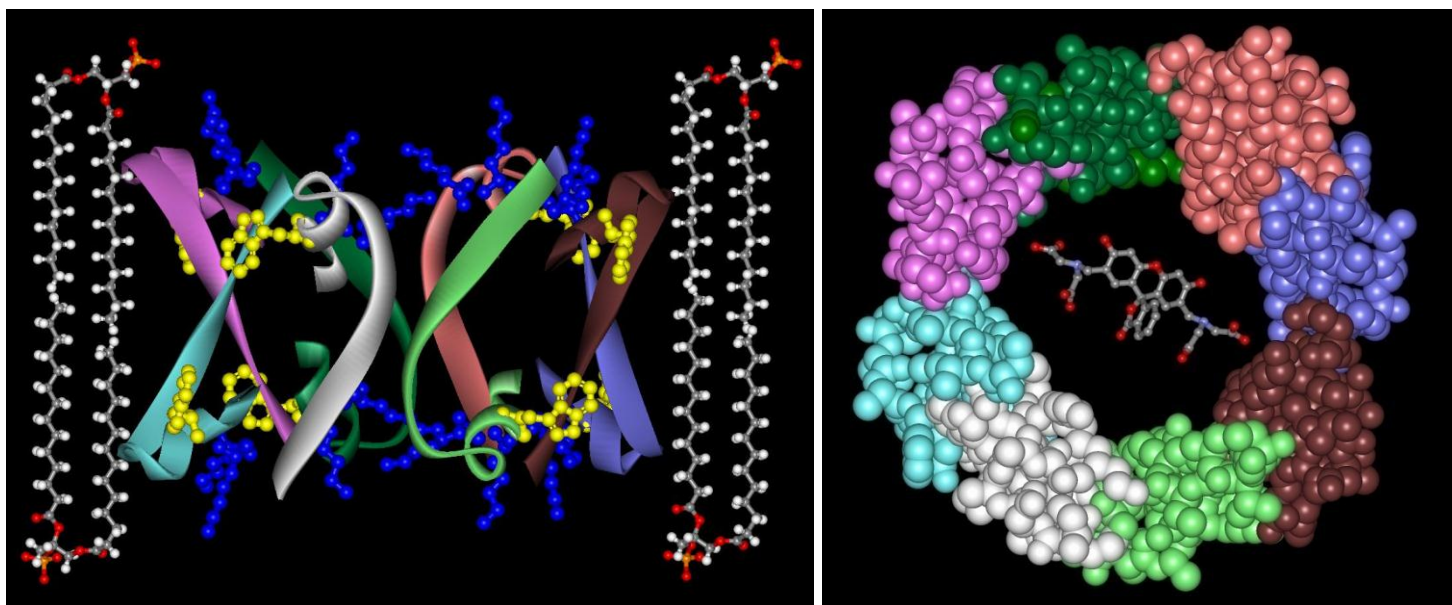


Figure 6. Model for the membrane pore formed by the CT20p.

Left: Peptide molecules are shown in ribbon format, colored according to peptide monomer. The secondary structure, orientation of strands and helices, and tryptophan insertion into the membrane are based on polarized ATR-FTIR and fluorescence quenching data. Right: Top view of the pore formed by CT20p is shown in a CPK format, colored according to peptide monomer. A calcein molecule is shown within the pore in a ball and stick format.

(Figure from Tatulian et al. Submitted manuscript)

CHAPTER 2: BAX SUPPORTS THE MITOCHONDRIAL NETWORK, PROMOTING BIOENERGETICS IN NON-APOPTOTIC CELLS

Introduction

An understanding of the apoptotic process has revealed that many of the important mediators, such as cytochrome c, can have dual roles: a non-apoptotic function and an apoptotic function [27]. The non-apoptotic roles of such proteins can range from contributing to energy production [27] to maintaining pH homeostasis [54]. During apoptosis, these proteins' housekeeping functions are subverted committing the cell to a death program. When first discovered, the members of the B-Cell Lymphoma (BCL-2) family of apoptotic modulators were presented as regulators of cell death [55], and the detrimental effects upon their deletion were attributed to loss of their apoptotic activity [56], [57]. While these proteins remain critical effectors of apoptosis, recent findings suggest that functional duality may also exist for multiple BCL-2 proteins.

Conventionally, the Bcl-2 family is segregated into two sub-groups: pro- and anti-apoptotic proteins. Each of the proteins in this family shares at least one and up to four Bcl-2 homology domains (BH1-4) [58], [59]. The anti-apoptotic group includes such proteins as Bcl-2, Bcl-_{XL} and MCL-1. Pro-apoptotic proteins include the multi-domain proteins, Bax and BAK, and the BH3-only proteins Bim, Bad, and Bid [15]. The solved NMR structure of Bax revealed a globular structure with nine α -helices [10]. Residues from the α 2, α 3, α 4, and α 5 helices, which encompass part of the protein's BH3 domain, arrange to form a prominent hydrophobic groove. In its cytosolic state the C-terminal α 9 helix of Bax, a putative trans-membrane domain, occupies this hydrophobic

groove [10]. Although the apoptotic roles of these Bcl-2 family members are the focus of much research, only a small number of non-apoptotic functions have been described. The BH3-only protein, Bad, was reported to complex with hexokinase 4 in order to regulate intracellular glucose metabolism in non-apoptotic hepatocytes [23]. Bcl-2 was shown to modulate cell cycle progression [60], [61]. Bax was found to affect the production of reactive oxygen species (ROS) by the mitochondria in non-apoptotic neurons [62], and the absence of Bax and Bak in T cells altered Ca²⁺ release resulting in a defect in antigen-specific proliferation [63]. These findings are intriguing and suggest that possible non-apoptotic activities of the Bcl-2 family merit further examination.

Current studies on the apoptotic activity of Bax revealed many interesting features that enable the protein to transition from a soluble, cytosolic form to a membrane-bound form. But do these same features enable Bax to have a non-apoptotic function? While Bax is known as a tumor suppressor, it is mutated but rarely completely ablated in certain types of tumors [64], suggesting that the complete loss of all function could be detrimental. As an example, HCT-116 colorectal cells were treated with a mutagen to produce cells deficient in Bax with the result that only 4% of the cells had two mutant *BAX* alleles (-/-), while 94% mutated one allele (+/-) [65]. Studies of Bax deficient mice revealed conflicting results, the loss of Bax produced either hyperplasia or hypoplasia in a tissue-specific manner [66]. These data indicate that Bax may have an unrecognized activity in healthy, normal cells. To study this, we examined mitochondrial bioenergetics in Bax-containing (Bax+/+) and Bax-deficient (Bax-/-) HCT-

116 cells as well as hepatocytes from Bax-deficient or wild-type mice. We found that in Bax^{-/-} cells intracellular ATP and aerobic respiration was significantly reduced, while glycolysis was increased. We inferred that a small amount of mitochondrial-associated Bax was needed to support cellular respiration. We thus describe a novel non-apoptotic activity of Bax that sustains mitochondrial metabolism and could mitigate the complete loss of the protein by a tumor cell.

Materials and methods

Cell Lines and Reagents.

Bax^{+/+} and Bax^{-/-} HCT-116 colorectal cancer cell lines (a kind gift from Dr. Bert Vogelstein, John Hopkins University) were grown and maintained in McCoy's 5A Medium (Gibco), 10% Fetal Bovine Serum (FBS) and 1% Penicillin-Streptomycin. FCCP (carbonyl cyanide-p-trifluoro-methoxyphenylhydrazone) (Sigma) was used at a concentration of 5 μ M as described below. This was determined to be the optimal concentration after performing a titration experiment (FCCP 0-25 μ M) and measuring effects on cell viability and ATP production as described below.

Isolation of Primary Mouse Hepatocytes.

Hepatocytes were isolated from the livers of adult Bax knock-out (KO) and wild type (WT) C57BL6 mice (Jackson Labs). The livers were perfused with Ca²⁺ free Krebs buffer by inserting a cannula into the hepatic portal vein, severing the inferior vena cava and injecting buffer to flush red blood cells from the liver. The buffer was injected at a constant flow rate of 700 μ L/min for 10 minutes using a syringe pump (ColeParmer).

After 10 minutes perfusion, the caudate lobe was removed for sectioning and the livers were then perfused with PBS/ 5% collagenase (MPBiomedicals) for 10 minutes or until the tissue became spongy. The isolated tissues were then run through 0.2 μm cell strainer (BD Biosciences) with ice cold Krebs buffer and residual red blood cells eliminated by osmotic lysis. The cells were then washed 3 times in Krebs buffer to remove any residual collagenase. Isolated hepatocytes were re-suspended in DMEM, 10% FBS, 1% pen-strep and assayed immediately.

Plasmids, Mutagenesis, and Transfection.

PCR-directed deletion of the C-terminus of Bax to generate the C-terminal truncated form of Bax (Bax- Δ CT) was performed using untagged primer sets and was confirmed by sequencing. Bax was PCR amplified from the template, pEGFP-Bax (a gift from Dr. Richard Youle, NINDS, NIH). To examine the transient expression of both the full length (Bax-FL) and Bax- Δ CT recombinant Bax constructs, bi-cistronic ProteoTuner vectors (CloneTech) containing Bax insert and green fluorescent protein (GFP) separated by an internal ribosome entry site (IRES) were transfected into Bax-/- HCT-116 cells. Expression of the Bax construct was induced upon the addition of Shield (CloneTech) at a concentration of 1 μM . The plasmid DNA was delivered at a concentration of 1 $\mu\text{g}/\text{mL}$ using the TransIT-LT1 transfection reagent (Mirus) following manufacturer's protocol. Transfection efficiency was determined microscopically by visualizing GFP expression after 18 hours, and ranged from 50-70%. Experiments were performed within defined timeframes to ensure optimal cell viability, prior to any induction of apoptosis.

Glucose Deprivation.

Bax^{+/+} and Bax^{-/-} HCT-116 cells were cultured in RPMI, without glucose, containing 10% FBS, 1% Penicillin-Streptomycin. FCCP (carbonyl cyanide-p-trifluoromethoxyphenylhydrazone) (Sigma) was used at a concentration of 5 μ M. DIC images for visualization of the effects of glucose deprivation were obtained with a Nikon Eclipse TE200 microscope using a 20x PH1 objective. The images are representative of 2 separate experiments.

Measurement of Oxygen Consumption and Extracellular Acidification Rates.

Bax^{+/+} and Bax^{-/-} HCT-116 cells, as well as isolated hepatocytes, were cultured in a BD Oxygen Biosensor plate at a concentration of 50,000 cells per well. The biosensor plate contained an oxygen-sensitive dye embedded in a gas-permeable matrix. Based on the properties of this dye, oxygen quenches the ability of the dye to fluoresce. The dissolved oxygen in the media is depleted by the cells metabolizing in the well, resulting in an increase in fluorescence. This allows a correlation of the rate of oxygen consumption to be made. The plate was read at 37°C on an EnVision plate reader (PerkinElmer) using ex/em wavelengths of 485/630nm. Fluorescence intensity was measured every hour for 24 hours. For comparisons of Oxygen consumption rates (OCR) and extracellular acidification rates (ECAR), Bax^{+/+} and Bax^{-/-} HCT-116 cells were seeded at 40,000 cells/well in a 24 well Seahorse cell culture plate. Full-length and Δ CT Bax constructs were transfected into Bax^{-/-} cells for measurement as well. The transfected cells were treated with shield 3 hours prior to reading to induce expression

of the protein. Measurements were taken on the Seahorse XF24 plate reader (Seahorse Bioscience). Values were normalized as changes relative to the initial reading.

Mitochondrial Staining: Fixed Imaging, Live Cell Imaging and Tissue Sectioning.

For fixed cells, Bax^{+/+} HCT-116 cells were plated onto coverslips coated with 10 μ g/mL laminin (Invitrogen). Cells were plated at a density of 50,000 cells/well and were fixed by methanol fixation. The cells were then probed with anti-Bax (N-20; Santa Cruz) and anti-HSP60 (H-300; Santa Cruz) antibodies, followed by FITC and CY3 secondary antibodies. Images were scanned using the LSM 510 (Zeiss) with a 100x/1.4 plan-apochromat objective. The scanned image was processed using the Zen 2009 software (Zeiss). For live cell imaging, Bax^{+/+} and Bax^{-/-} HCT-116 cells were grown and plated in 24-well glass bottom dishes (MatTek) that had been pre-treated with 1N HCl and coated with 10 μ g/mL laminin. The cells were plated at 10,000 cells per well and allowed to grow over night. Bax-FL or Bax- Δ CT constructs were transfected using the TransIT-LT1 transfection reagent (Mirus) and expressed as previously described. At 18 hours post-transfection, cells were incubated with 1 μ M MitoTracker Red 580 or 5 μ M 10-Nonyl Acridine Orange (NAO) (Molecular Probes) in McCoy's complete media for 30 minutes prior to imaging. Treatments with 5 μ M FCCP were done 15 minutes prior to imaging. For cells treated with Mdivi 1 (Biomol International), an inhibitor of DRP1 and mitochondrial fission, the cells were treated with a

5 μ M concentration in McCoy's complete media for 4 hours prior to the addition of MitoTracker.

The caudate lobes of Bax knock-out and C57BL6 mice were frozen and sectioned using a Leica CM 1850 cryostat. Tissues were cut into 12 μ m sections. The sections were rehydrated with PBS then stained with either 1 μ M MitoTracker Red or 5 μ M NAO.

Fluorescent images were acquired with the UltraView spinning disc confocal system (PerkinElmer) with AxioObserver.Z1 (Carl Zeiss) stand, and a Plan-Apochromat 63x/1.4 Oil DIC objective. Z-stack projections of the scanned images were generated and modified within the Volocity image processing program (PerkinElmer).

Sub-cellular Fractionation and Immunoblotting.

Bax^{+/+} and Bax^{-/-} HCT-116 cells were plated in 75cm² flasks and grown to 70-80% confluence. Cells were transiently transfected with the Bax^{-FL} or Bax^{- Δ CT} constructs and protein expressed as previously described. At 18 hours post transfection, the cells were lifted and pelleted. The pellets were re-suspended and lysed according to the protocol from the Mitochondrial Enrichment Kit (Pierce). Note that a low speed centrifugation step in the mitochondrial enrichment process ensures that only intact and non-fragmented mitochondria are isolated. The enriched mitochondria were layered on an iodixanol gradient (6%, 10%, 15%, 20%, 23%, and 27%) and subjected to ultracentrifugation using an Optima L-100XP Ultracentrifuge for 2 hours at 145,000 rcf in a SW55.1 swing bucket rotor (Beckman Coulter). After centrifugation, each sample was unloaded in 500 μ L fractions using a fraction recovery

system (Beckman Coulter), and washed in ice cold PBS twice (18,000 rcf, 30 minutes) to remove residual iodixanol. The pellets from each of these fractions were re-suspended in 1x loading buffer and run on 8-16% Tris-glycine gradient gels (Invitrogen). The gels were transferred to PVDF membranes and probed with primary antibodies to Bax (N-20; Santa Cruz), Prohibitin (ABCAM), and GRP78 (Santa Cruz), followed by incubation with the appropriate HRP conjugated secondary antibodies (Santa Cruz, Cell Signaling) and developed by chemiluminescence (Pierce).

Proteinase K Digestion of Membrane Bound Proteins.

Bax^{+/+} and Bax^{-/-} HCT-116 mitochondria were isolated as above. The mitochondria were then treated with Proteinase K (Sigma) (10 µg/ml) for 5, 10, 15 or 20 minutes in order for the outer mitochondrial membrane associated proteins to be digested. The reaction was terminated with phenylmethylsulfonyl fluoride (PMSF) [67]. The mitochondria were then washed with isotonic buffer, pelleted, re-suspended in 1X sample buffer, and run on 12% poly-acrylamide gels in parallel with untreated mitochondria. The gels were then transferred to PVDF membranes which were then probed with anti-Bax (N-20; Santa Cruz), as well as anti-BclXL (2762, Cell Signaling) primary antibodies, followed by incubation with anti-mouse or anti-rabbit IRDye 800CW secondary antibodies (Licor). The membranes were imaged using the Licor Odyssey Infrared Imaging system. Densitometry measurements were made using Image J.

Measurement of ATP production and Mitochondrial Membrane Potential.

Cells were seeded and treated in 24 well plates overnight. The cells were then lifted, counted and seeded in black 96 well flat-bottom plates at a density of 4,000-

5,000 cells/well. To uncouple oxidative phosphorylation, 5 μ M FCCP was added to the cells two hours prior to analysis of ATP concentration. ATP levels were quantified using the ATPLite 1-Step assay kit (PerkinElmer). Luciferase activity, reported as Relative Luminescence Units (RLU), was measured on an EnVision (PerkinElmer) plate reader. The luminescence was normalized to the number of cells/well. Additionally, a standard curve of known ATP concentrations was established to ensure that the experimental values were within the detectable range of the assay. Background signal was corrected for by subtracting the RLU values of an empty plate. In addition, as the fluorescence of MitoTracker Red 580 (Invitrogen) is a result of oxidation of the compound within the mitochondrial matrix, changes in MitoTracker fluorescence intensity was used to assess the qualitative and quantitative efficiency of the electrochemical potential (the relative oxidative capability of actively respiring mitochondria) [68].

Measurements of mitochondrial content, membrane potential, and viability were done by staining the cells with both ethidium bromide (Fisher Scientific) and NAO [69]. Briefly, 500,000 cells/sample were stained with 25ng/mL NAO and 40ng/mL ethidium bromide for 10 minutes. The cells were then washed 3 times with 0.1% BSA in PBS at 4°C for 10 minutes at 1000 rcf. The cells were read using the C6 flow cytometer (Accuri) using the FL1 and FL3 channels. Data was analyzed using FCSExpress (DeNovo).

Measurement of Citrate Synthase Activity.

Isolated mitochondria from Bax^{+/+} and Bax^{-/-} HCT-116 cells, as well as primary hepatocytes from Bax KO and C57BL6 mice were assayed for citrate synthase activity.

The citrate synthase enzyme catalyzes the reaction:



The rate of TNB formation is linear and has a measurable absorbance at 412nm. The rate of TNB generation ($\mu\text{Mol/ml/min}$) was measured by spectrophotometry (Beckman Coulter SD8000) for 200 seconds. Mitochondrial samples were run in Tris buffer to determine inner mitochondrial membrane integrity (reported as % ruptured mitochondria), or Tris buffer with Triton X-100 to determine citrate synthase activity.

Inhibition by siRNA.

Bax containing HCT-116 or lung cancer cells were seeded at a density of 200,000 cells/well in 6 well plates. After 24 hours, the cells were treated with $1\mu\text{M}$ Bax SMART pool siRNA (Dharmacon) using the Accell delivery reagent (Dharmacon) for 72 hours, following the manufacturer's protocol. Briefly, SMART pool siRNA combines four different siRNAs to reduce off-target effects, negating the need to test scrambled or control Bax siRNA sequences; however as a control a non-targeting siRNA was used to treat the cells, showing no measurable effect as compared to the Accell reagent alone. Delivery efficiency and siRNA non-targets effects were previously tested using Accell fluorescent (Cy3) non-targeting control siRNA (Dharmacon).

Measurement of Mitochondrial DNA.

DNA was isolated from Bax^{+/+} and Bax^{-/-} HCT116 cells using TRIZOL Reagent (Invitrogen) followed by ethanol precipitation. Re-suspended DNA pellets were analyzed for nuclear DNA (nDNA) and mitochondrial DNA (mtDNA) content. Primers for the detection of the nuclear housekeeping gene β -actin and for the mitochondrial DNA encoded ATPase (MTATP) 8 gene were as follows: β -actin (forward): 5'-GAA ATC GTG CGT GAC ATC AAAG; (reverse): 5'-TGT AGT TTC ATG GAT GCC-ACAG. MTATP (forward): 5'-AAT ATT AAA CAC AAA CTA CCA CCT ACC; (reverse): 5'-TGG TTC TCA GGG TTT GTT ATA [70]. The PCR was carried out in a 7500 Fast real-time PCR system (Applied Biosystems). All reactions were carried out in 20 μ l of total reaction volume containing 1 μ g/ μ l total DNA, appropriate primers and Fast SYBR Green Master Mix (Applied Biosystems). Each reaction underwent a 30s 90°C denaturation followed by 40 cycles of 30s at 60°C then 3s at 95°C. All samples were analyzed in triplicate. The relative amount of mtDNA (normalized to nuclear content) is represented as $2^{\Delta Ct}$, calculated using the following equation:

$$\Delta Ct = (Ct_{mtDNA} / Ct_{nDNA}) - (Ct_{nDNA} / Ct_{nDNA}),$$

where Ct is the cycle threshold for each condition.

Surface Plasmon Resonance (SPR) binding experiments.

Recombinant BCL-2, Bax-FL and Bax- Δ CT were generated using the Human *In Vitro* Protein Expression Kit for DNA Templates (Pierce). A SR7000DC (Reichert) dual channel SPR and SR7000 gold sensor slide (Reichert) with a surface composition of 10% COOH-(PEG)6-C11-SH, 90% OH-(PEG)3-C11-SH were used to test the binding

affinities of Bax^{-FL} and Bax^{-ΔCT} to BCL-2. Either Bax^{-FL} or Bax^{-ΔCT} was covalently linked to the sensor slide at a concentration of 1.4 μg/mL at a flow rate of 25 μL/min. The recombinant BCL-2 was then passed over the bound Bax derivatives at 5 serially diluted concentrations (1.56, 0.78, 0.39, 0.195, and 0.0975 mg/ml) at a flow rate of 25 μL/min. Kinetic information was calculated using the Scrubber2 program (BioLogic Software).

Statistics.

Statistical analysis and experimental significance was determined using Prism5 for Windows, Version 5.02 (GraphPad).

Results

Mitochondrial Bioenergetics Requires Bax.

To determine whether Bax has a previously unrecognized non-apoptotic activity, we examined mitochondrial structure, function and bioenergetics in Bax^{+/+} and Bax^{-/-} HCT-116 colon cancer cells. MitoTracker Red 580 fluorescence intensity was used as an indicator of oxidative capacity and to visualize actively respiring mitochondria [68]. Live-cell imaging was performed to ensure that fixatives would not disrupt MitoTracker uptake. In Figure 8A, when Bax is present, we observed respiring mitochondria that appeared elongated and tubular in shape with a loosely dispersed branching network (Figure 8A). In contrast, when imaging of the Bax^{-/-} cells, we observed that, in the absence of Bax, respiring mitochondria were numerous but appeared less elongated (Figure 8B). These observed differences in functional morphology upon MitoTracker staining were not due alterations in the fission/fusion process. Treatment with Mdivi 1, a

chemical inhibitor of DRP1 that prevents fission by blocking the early stages of DRP1 assembly, resulted in uniform changes in MitoTracker fluorescence that were independent of Bax's presence in the cell (Figure 7).

To determine whether loss of Bax changed mitochondrial density, accounting for the differences observed in MitoTracker staining (Figures 8A, 8B), we probed Bax^{+/+} and Bax^{-/-} HCT-116 cells with N-nonyl acridine orange (NAO). NAO accumulates in mitochondria by binding to negatively charged phospholipids, specifically, cardiolipin [69], [71]. Hence, NAO accumulation is not dependent on mitochondrial respiration and would directly show mitochondrial content. Seen in Figures 8A and 8B, NAO incorporation in mitochondria was similar in both Bax^{+/+} and Bax^{-/-} HCT-116 cells. This was confirmed by the measurement of total NAO fluorescence in each cell population (Histogram, Fig. 8C). Hence, total mitochondrial density or content was independent of Bax expression. To confirm results from NAO staining, we performed a quantitative experiment, measuring total mitochondrial DNA (mtDNA) relative to nuclear DNA (nDNA). These results are shown in Table 2. We found no detectable differences in mtDNA content between Bax^{+/+} and Bax^{-/-} HCT-116 cells, with *p* values that were not significant. In total these results suggest that the observed morphological differences detected by MitoTracker staining (Figure 8) were due more to a functional defect rather than decreased mitochondrial content. To demonstrate that Bax^{+/+} and Bax^{-/-} HCT-116 cells were equally viable, we stained cells with NAO and ethidium bromide (EB). EB stains DNA only when the cell membrane is ruptured, as it is in apoptotic cells in culture. Representative data displayed in Figure 8D revealed no significant Bax⁻-dependent

differences in overall viability. Approximately only 2-4% of the Bax^{+/+} and Bax^{-/-} HCT-116 cells were found to be apoptotic, or double-stained for both NAO and EB, and about 30% of the cells were viable (negative EB staining) but had low NAO fluorescence that was unrelated to Bax expression. The viability of cell lines used in all experiments reported herein was consistent with the data shown in Figure 8D.

To explore a possible functional defect upon Bax loss that was revealed by MitoTracker staining, we examined the electrochemical properties of the mitochondria in the two HCT-116 Bax variants using the uncoupling agent, FCCP. FCCP is a hydrophobic compound that carries protons across the inner mitochondrial membrane (IMM), releasing these protons into the matrix and allowing for the dissipation of the chemiosmotic gradient. A titration of FCCP was previously performed to determine the optimal concentration of FCCP for use, that is, caused the least effect on cell viability and the most effect on ATP production (data not shown). When treated with FCCP, Bax^{+/+} mitochondria displayed a stronger intensity of MitoTracker fluorescence compared to untreated cells (Figure 9A, 9C). This was not observed in Bax^{-/-} cells (Figure 9B, 9C). Although relaxation of MitoTracker fluorescence quenching has been reported with FCCP, we do not think this artifact is the reason for the observation made with Bax^{+/+} cells, since the increase in MitoTracker fluorescence was not also observed in Bax^{-/-} cells. Quantification of the effect of FCCP treatment revealed a two fold increase in MitoTracker fluorescence in Bax^{+/+} cells compared to untreated cells that was not observed with Bax^{-/-} cells (Figure 9C). We propose that, in Bax^{+/+} cells, the FCCP-mediated uncoupling of the electron transport system results in the rapid oxidation of

matrix substrates, such as MitoTracker Red 580, which can be detected as an increase in MitoTracker fluorescence [69]. This does not occur in Bax^{-/-} cells, suggesting that loss of Bax may result in a defect in mitochondrial oxidative capacity.

Bax^{-/-} cells also had significantly decreased levels of intracellular ATP as compared to Bax^{+/+} cells (Figure 9D). Furthermore, FCCP treatment resulted in a marked drop in ATP levels in Bax^{+/+} cells, but not in Bax^{-/-} cells (Figure 9D). Note that a previous titration of FCCP concentrations correlated with ATP amounts detected, indicating that we were primarily assessing changes in ATP production (data not shown). To determine whether the loss of ATP in Bax^{-/-} cells was due to abnormal bioenergetics, we measured glycolysis and oxygen consumption using an XF analyzer. Metabolic activity in Bax^{+/+} and Bax^{-/-} HCT-116 cells was assessed by plotting the oxygen consumption rate (OCR), a measure of mitochondrial respiration, against the extracellular acidification rate (ECAR), an indicator of glycolysis. Comparing changes that occur in aerobic and glycolytic metabolism, in Figure 9E, revealed that Bax^{+/+} cells had increased oxygen consumption (OCR) and decreased glycolytic activity (ECAR) relative to Bax^{-/-} cells; hence Bax^{-/-} cells were more dependent on glycolysis for their energetic needs. A separate measure of oxygen consumption, using an alternative method, confirmed these findings (Figure 9F). In support, we had previously observed that Bax^{-/-} cells were more susceptible to glucose deprivation, acquiring a shrunken morphology with decreased cytosolic content as compared to Bax^{+/+} cells (Figure 10). From our experimental findings, we concluded that the decreased levels of ATP observed in Bax^{-/-} cells was likely due to depressed respiration, indicating that cells

lacking Bax had a significant defect in oxidative phosphorylation that was in part compensated by glycolytic energy production.

Bax Contributes to ATP production.

Having identified a non-apoptotic function for Bax in the regulation of mitochondrial metabolism, we determined whether Bax could localize to the mitochondria in the absence of induced apoptosis. We performed an immunofluorescence experiment, using Bax^{+/+} HCT-116 cells, and were able to detect partial co-localization of Bax with mitochondria (HSP-60 used as a mitochondrial marker) (Figure 11A). To better quantitate the interaction of Bax with mitochondria under standard growth conditions, ultra centrifugation of enriched mitochondria was performed to examine the localization of Bax. Note that lysates were prepared from cells that were viable (Figure 8D), and the isolation procedure ensured that only intact mitochondria were used. The enriched mitochondrial lysate was layered on an iodixanol gradient and subjected to ultracentrifugation as described in Methods. Separation of organelles was based on density, which is defined as a function of the protein-lipid ratio of the organelle membranes. Western blot analysis of the gradient fractions for Prohibitin (mitochondrial content) (Figure 11B) showed that the distribution of the mitochondria between Bax^{+/+} and Bax^{-/-} HCT-116 cells was comparable (across the 20-23% fractions). While no Bax was detected in Bax^{-/-} cells, approximately 7% of the total endogenous Bax detected in the non-apoptotic Bax^{+/+} cells was associated with the mitochondrial fractions (Figure 11B, Table 3). Using the appropriate loading controls, the percentage of Bax localized to the mitochondria was determined by densitometry,

calculating the relative band intensity in each lane compared to the amount of Bax detected in a western blot of whole cell lysates (data not shown). This finding suggested that the amount of mitochondria-associated Bax that supports energy production is considerably less than the amount that is required for the Bax mediated perpetuation of the apoptotic cascade.

It remained to be determined whether Bax was loosely associated with mitochondria (i.e. bound to the outer mitochondrial membrane (OMM)) or whether it was sequestered within an inner membrane compartment (i.e. IMM). Enriched mitochondrial lysates, as those used for the ultracentrifugation experiment, were treated with Proteinase K for as few as 5 and up to 20 minutes. Digested lysates were analyzed by SDS-PAGE and immunoblotted with antibodies to detect Bax, and, as a control, BCL_{XL}. BCL-XL is mainly an OMM localized protein and is sensitive to protease digestion. We found that treatment with Proteinase K resulted in 50-60% lysis of Bax, compared to BCL_{XL}, in which 77-100% of the protein was lysed (Figure 11C). Although in the same sample there was less BCL_{XL} protein detected compared to Bax, an increase in the amount of BCL_{XL} digested occurred over time, while Bax was mostly digested within the first 5 minutes. These results suggest that a significant amount of Bax was sequestered within the mitochondria and not accessible to protease treatment. Hence, Bax has both outer and inner mitochondrial localization, supporting its proposed role mediating mitochondrial respiration. The argument that Bax could be directly regulating mitochondrial metabolism was further demonstrated by measurements of citrate synthase activity. Citrate synthase, which is localized to the mitochondrial matrix, is one

of the primary enzymes of the TCA cycle. We found that Bax^{-/-} cells had reduced levels of citrate synthase activity in comparison to Bax^{+/+} cells (Figure 11D). It is important to note that background levels of citrate synthase released from ruptured mitochondria were not significantly different in the Bax variants (Figure 11D).

To confirm that loss of Bax is sufficient to inhibit ATP production, and is not due to a defect inherent to Bax^{-/-} cells, Bax^{+/+} HCT-116 cells were treated with SMARTPool Bax siRNA. Previously, using Cy3-tagged non-specific control siRNA, we established uptake efficiency and the absence of non-target effects in HCT-116 cells (data not shown). After Bax siRNA treatment, cells were lysed and protein lysates analyzed by western blot for inhibition of Bax expression and measured for ATP production. Bax protein expression was reduced approximately 50% when treated with Bax siRNA, as shown in a representative blot (Figure 12A). This correlated to a reduction in ATP as well, indicating that the amount of available Bax dictated the effect on the ATP produced (Figure 12B). We repeated this experiment using a lung cancer epithelial line, which is highly dependent on oxidative phosphorylation, to ensure that this phenomenon was not isolated to HCT-116 cells. Western blot and ATP analysis of these lung cancer cells showed that a reduction in Bax expression correlated with the measured decrease in ATP levels (Figures. 12A, B).

The work presented indicated that cell lines lacking Bax had reduced ATP production due to depressed respiration. To show that these results were not due to cell line or culture artifacts, we examined mitochondrial metabolism in primary hepatocytes freshly isolated from Bax KO mice. We observed that livers from Bax KO

mice were slightly enlarged compared to aged WT mice. Staining liver sections from Bax KO and WT mice with MitoTracker and NAO revealed findings very similar to those observed with HCT-116 cells (in Figure 8). MitoTracker fluorescence was dim in liver sections from Bax KO mice as compared to WT mice, while NAO staining was comparable (Figure 13A, 13B). Hence there appeared to be diminished mitochondrial respiration in Bax KO liver cells. This was confirmed by measuring oxygen consumption of Bax KO hepatocytes compared to WT hepatocytes (Figure 13C). ATP production was likewise reduced in Bax KO hepatocytes (Figure 13D) as well as citrate synthase activity (Figure 13E). While, due to the limitations of cell numbers, biochemical assay results were less striking using freshly isolated hepatocytes, the differences between Bax KO and WT cells are statistically significant and follow similar patterns as those demonstrated with HCT-116 cells.

Having found that inhibition of Bax replicated the loss of respiration seen in cells that were genetically ablated (Figures. 12 and 13); we next determined whether restoring Bax to deficient cells would rescue mitochondrial metabolic activity. Over-expression of full-length Bax (Bax -FL) in Bax^{-/-} cells resulted in recovery of respiring mitochondria morphology (as seen in Bax^{+/+} cells in Figure 8A) observed upon MitoTracker staining (Figure 14A). Western blot analysis of density gradients showed that ~2.5% of the total expressed protein associated with mitochondrial fractions (Table 3, Figure 14B). As a result, we observed a three-fold increase in ATP production upon the expression of Bax -FL that was inhibited by treatment with FCCP (Figure 14E). This indicated that Bax -FL could rescue ATP production through oxidative phosphorylation.

ECAR/OCR measurements confirmed that expression of Bax -FL could increase oxygen consumption, while reducing glycolytic activity, indicating that Bax was a critical regulator of these activities (Figure 14F).

Over-expression of C-terminal truncated Bax (Bax - Δ CT) in Bax ^{-/-} cells was performed to determine the contribution of the C-terminal helix of Bax to mitochondrial bioenergetics. Expression of Bax - Δ CT did not restore the respiring mitochondrial morphology seen in the presence of Bax (Figure 14C). This activity of Bax appears to require the C-terminal domain. Predictably, the removal of this C-terminal helix resulted in a scattered localization of Bax - Δ CT, as exhibited by the altered banding pattern in the gradient fractions (Figure 14D). Even though mitochondrial targeting was deregulated in this mutant, some Bax - Δ CT was found in the mitochondrial fractions (~9%, Table 3, Figure 14D), and, surprisingly, was sufficient to restore ATP production as effectively as Bax -FL (Figure 14E). Moreover, measurements ECAR/OCR showed that expression of Bax - Δ CT was just as effective in restoring metabolic balance in Bax ^{-/-} cells as Bax -FL (Figure 14F). The differences between Bax ^{-/-} cells and Bax ^{-/-} cells expressing Bax -FL or Bax - Δ CT were statistically significant. These results suggest that there are multiple regulatory domains of Bax, such as the C-terminal helix or the BH3 domain, which can operate independently of each other to affect the function of mitochondria.

Interaction with BCL-2 Blocks Bax's Non-Apoptotic Activity.

Bax's known antagonist is the anti-apoptotic protein, BCL-2, which resides anchored in the outer mitochondrial membrane [72]. Bax and BCL-2 exist in a balance

– each countering the other’s activity [73]. This balance is likely dependent on interactions mediated through each of the proteins’ BH3 domains [74]. Since expression of Bax Δ CT could rescue mitochondrial respiration and ATP synthesis, we postulated that this activity was being mediated through Bax’s BH3 domain, which could be inhibited by binding to BCL-2. To test this, the binding capabilities of the Bax constructs with BCL-2 were first measured by SPR. Recombinant Bax -FL or Bax Δ CT proteins were generated and covalently linked by amine coupling to gold SPR sensor plates. The recombinant BCL-2 protein was then passed over the bound Bax constructs. Binding kinetics was determined by calculating the association constant (k_a) and dissociation constant (k_d) of serially diluted BCL-2 binding to immobilized Bax. The binding profile of BCL-2 to both Bax proteins was similar, but based on the kinetics, BCL-2 bound with twice the affinity to Bax Δ CT when compared to Bax -FL (Figures. 15 A, B). This disparity in binding affinities was exemplified by the two fold difference in the calculated equilibrium constant (K_D) between Bax -FL and Bax Δ CT. This outcome is likely due to a greater exposure of a BCL-2 interacting domain in Bax Δ CT resulting from removal of the C-terminus of the Bax protein.

Over-expression of BCL-2 in Bax $^{+/+}$ cells resulted in decreased mitochondrial ATP production (Figure 15 C), indicating that BCL-2 was impeding the normal function of Bax in mitochondria. This reduction was equivalent to the reduction observed upon FCCP treatment of Bax $^{+/+}$ cells. Adding FCCP to the BCL-2 over-expressed cells further amplified the reduction of ATP (Figure 15 C). Because of the effects of binding to BCL-2 that are observed in both the Bax -FL and Bax Δ CT mutant (Figures. 15 A, B),

it can be inferred that BCL-2 also acts as an antagonist to Bax's activity in promoting bioenergetics. Since Bax still binds BCL-2 in the absence of the C-terminus, it is possible that a regulatory region, likely the BH3 domain, for this interaction becomes more accessible upon deletion of the C-terminal helix, and that this domain could associate with other mitochondrial membrane proteins to support ATP synthesis.

Discussion

Our findings suggest that Bax has an essential, non-apoptotic, homeostatic activity. Although the major portion of Bax in non-apoptotic cells resides in a soluble, cytosolic form [10], we and others [75] have observed that under normal conditions, Bax can also associate with mitochondria. Herein, we report that Bax has a supporting role in mitochondrial energy production. Cells deficient in Bax had decreased mitochondrial oxidative capacity and reduced levels of intracellular ATP. Such cells were dependent on energy produced through glycolytic activity. The localization of a small fraction of Bax to outer and inner mitochondrial compartments could enable ATP production through respiration, a process reversed when Bax was inhibited by specific siRNAs or genetically ablated such as in knockout mice. By introducing Bax -FL into cells lacking endogenous Bax, we were able to restore mitochondrial respiration and increase the amount of ATP. Expression of a Bax mutant lacking the C-terminal $\alpha 9$ helix also restored aerobic metabolism and ATP production, indicating that Bax was required for mitochondrial bioenergetics in manner that is independent of the C-terminal trans-membrane helix. Co-expression of Bax with BCL-2

resulted in reduced ATP detection, suggesting perhaps that the interaction of Bax with a mitochondrial protein(s) (inhibited by BCL-2) was required for regulation of ATP levels.

In the current model of apoptosis, the cytosolic, monomeric (inactive) form of Bax must undergo significant conformational changes (activation), which enable transitioning to mitochondria [3]. We may infer from our results that, under non-apoptotic conditions, equilibrium could exist between the two conformations, inactive and active. A small amount of “active” Bax could associate with healthy mitochondria, contributing to the regulation of functional architecture and bioenergetics, but at a concentration well under that needed to induce apoptosis. This leads to the idea that the movement of Bax to mitochondria under non-lethal conditions could be restricted by the lipid and protein composition of the organelle membrane [76], [77]. Apoptosis induces changes in mitochondria that could help recruit Bax, while, in the absence of apoptosis the outer mitochondrial membrane environment is less likely to support the translocation of Bax. In healthy mitochondria, a few Bax monomers or dimers may insert into mitochondrial membranes to form small pores, but this process needs to be tightly regulated. It is more feasible that Bax interacts with existing mitochondrial proteins. This idea is supported by our findings that a portion of Bax was sequestered within the mitochondria, perhaps interacting with an IMM protein. Hence, the amount of Bax associated with mitochondria in non-apoptotic cells would be constrained by the availability of the binding partner(s), a process we demonstrated by the inhibition of ATP production with co-expression of a known inhibitor (BCL-2) with the Bax constructs.

A review of current literature reveals a number of possible mitochondrial binding partners for Bax, although most were discovered in the context of an apoptotic scenario. Examples include the adenine nucleotide translocator (ANT) [78] and the voltage-dependent anion channel (VDAC). VDAC could serve as a mitochondrial receptor for Bax [79]. In addition to ANT and VDAC, many other proteins are known to interact with Bax, including factors that mediate changes in the mitochondrial network such as fission or fusion proteins like Drp1 [80], Mfn-2 [81] or endophilin B1 (Bif-1) [82] as well as other regulatory proteins such as cyclophilin D or Ku70 (reviewed in [83]). Although this may seem speculative, the excess of circumstantial evidence for the interaction of Bax with healthy mitochondria highlights the need for further study to determine whether some of these proteins act to facilitate Bax's role in mitochondrial bioenergetics.

In a recent proteome-wide quantification of proteins that are differentially expressed between Bax -containing and Bax -deficient HCT-116 cells [84], a number of mitochondrial proteins were found to be down regulated upon loss of Bax, including VDAC. Significantly, two essential enzymes for glucose metabolism and ATP production were also decreased in Bax -deficient cells: Glucose-6-phosphate isomerase was reduced over 10-fold and citrate synthase was reduced over 7 -fold. This supports our own observation of reduced citrate synthase activity in the absence of Bax. Loss of critical metabolic components exacerbates the inability of Bax -deficient cells to produce energy from glucose. That the reintroduction of Bax into these cells dramatically increased respiration and ATP production, as we showed, strongly supports the concept that Bax plays an important homeostatic role supporting growth and metabolism. Given

the decisive role of Bax in apoptosis, it would seem that the mutation rate in cancerous cells would be equivalent to p53, yet this is not observed. There are only a handful of documented cases in which there is a complete mutational inactivation (or deletion) of Bax, one of which is in colorectal cancer [85]. More commonly, only mutations that restrict the pro-apoptotic activity of Bax are seen [64]. However, the nature of cancerous cells is one of perpetual proliferation at high energy costs, thereby demanding a constant generation of ATP. Cancerous cells are known to generate their energy through glycolysis rather than oxidative phosphorylation – a phenomenon known as the Warburg effect [86]. It is possible that a partial deletion of Bax, or over expression of BCL-2 as occurs in many cancers, would favor the glycolytic pathway. This indicates that, perhaps due to its non-apoptotic function in maintaining energy production, the total inactivation of Bax in cancer would be rare, while retention of partial activity would more likely support the growth and metabolic needs of malignant cells

Figures and Tables

Table 2. Level Of mtDNA Content in Bax^{+/+} and Bax^{-/-} HCT116 Cells

. Level of mtDNA content in Bax^{+/+} and Bax^{-/-} HCT116 cells			
	HCT 116 Bax^{+/+}	HCT116 Bax^{-/-}	P Value
ΔCt	-0.355	-0.318	0.4044
$2^{\Delta\text{Ct}}$	0.782	0.802	0.4047
mtDNA/nDNA	r = 0.644	r = 0.681	0.1967

*P values were determined using Unpaired t test with Welch's correction
Values are averages of 3 experiments*

Table 3. Association of Membrane-bound Bax with Different Density Fractions Recovered after Differential Ultracentrifugation

Association of Membrane-bound Bax with Different Density Fractions Recovered after Differential Ultracentrifugation*			
Bax construct	Total protein	Membrane associated protein	
	Membrane-associated (%)	Non-mitochondrial peak fractions (%)	Mitochondrial peak fractions (%)
Endogenous Bax (+/+)	7.21	47	53
Bax (-/-)	0	0	0
Full Length	2.73	0.9	91
ΔCT	9.46	67	33

**Data shown was determined by quantification of the mean pixel intensity of the BAX and prohibitin bands from blots shown Figures 3B, and 5B, 5D, and are representative of three independent experiments.*

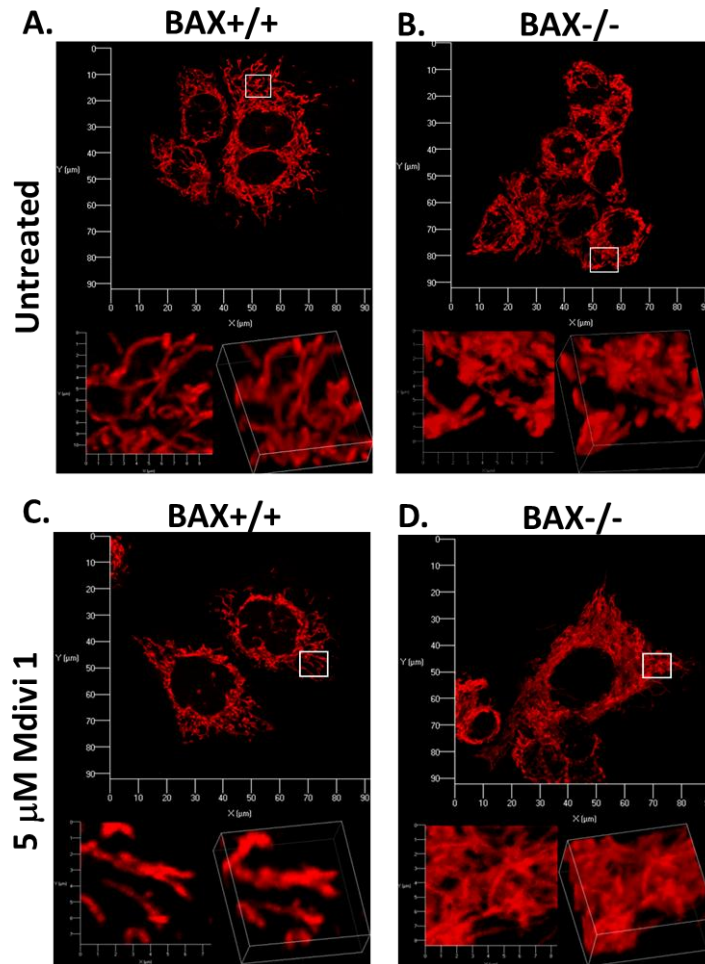


Figure 7: Treatment with the fusion inhibitor, Mdivi-1, did not alter MitoTracker staining.

Bax^{+/+} HCT 116 cells (A) and Bax^{-/-} HCT 116 cells (B) MitoTracker incorporation allows for qualitative analysis of the shape, distribution and oxidative capacity of the mitochondria. Inhibition of fission machinery by Mdivi-1 was followed by incorporation of MitoTracker. Bax^{+/+} (C) and Bax^{-/-} (D) HCT 116 cells were treated with 5 μM Mdivi-1 for 2 hours prior to imaging.

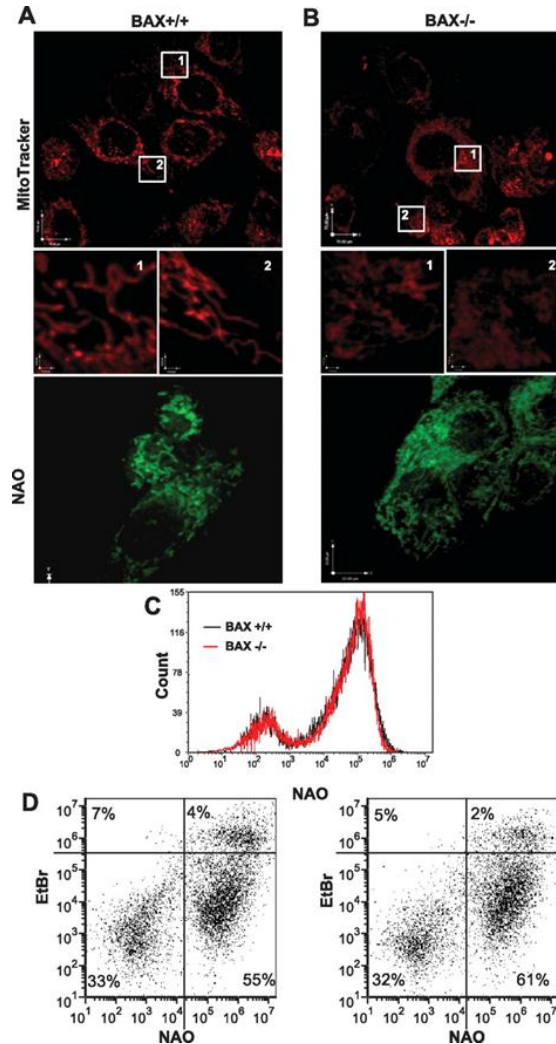


Figure 8: Reduced metabolic activity in Bax deficient cells is not related to mitochondrial content or loss of viability.

Bax^{+/+} HCT-116 cells (A) and Bax^{-/-} HCT-116 cells (B) were cultured on MatTek 24-well glass bottom plates coated with laminin to 70-80% confluence. The cells were treated with MitoTracker Red 580 or NAO prior to imaging as described in Methods. Live cell images were obtained using the UltraView (PerkinElmer) spinning disc confocal system. The stand was a Zeiss AxioObserver Z.1 with a Plan-Apochromat 63x/1.4 Oil DIC objective with a resolution of 0.124 μ m. Post-acquisition processing was done using Velocity software (PerkinElmer). Images are representative of three replicates per condition. Insets are 10X magnification of the two highlighted areas in each field. (C, D) To assess mitochondrial density (C) and viability (D), 500,000 cells/sample were stained with NAO (C) or NAO and ethidium bromide (EtBr) (D) for 10 minutes. Fluorescence output was read using the FL1 and FL3 channels on a C6 flow cytometer (Accuri). Each experiment was performed in triplicate for each cell line variant. Representative data are shown. The data plotted in histogram and dot plots was analyzed using FCSEXPRESS (DeNovo) software.

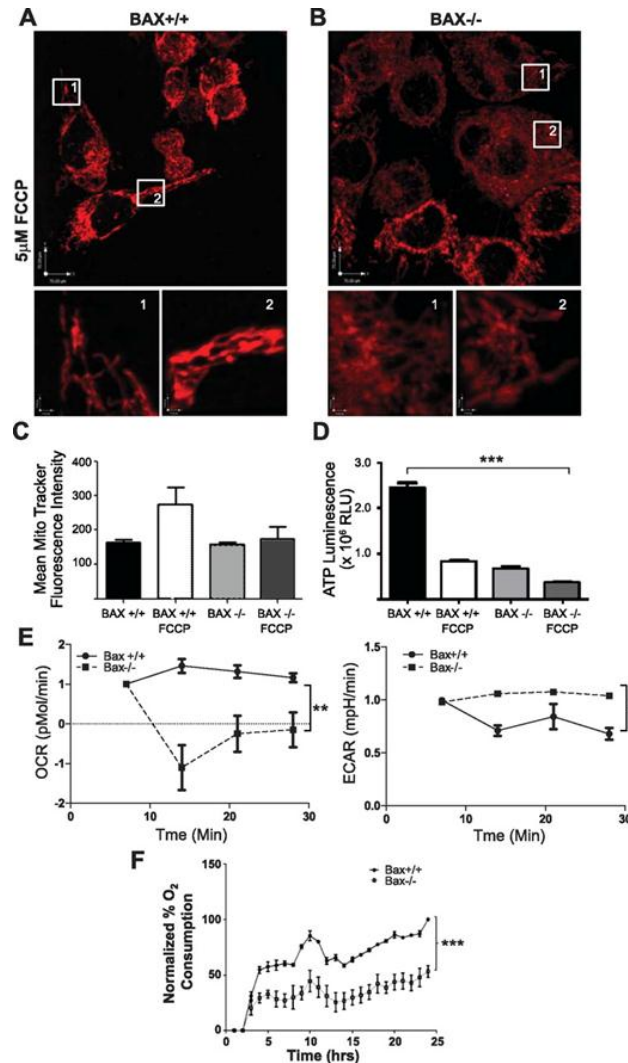


Figure 9: Deficiency of Bax results in reduced intracellular ATP and oxygen consumption.

Bax^{+/+} HCT-116 cells (A) and Bax^{-/-} HCT-116 cells (B) were cultured on MatTek 24-well glass bottom plates coated with laminin to 70-80% confluence. Cells were treated with FCCP in McCoy's complete media for two hours prior to imaging. Live cell images were obtained using the UltraView (PerkinElmer) spinning disc confocal system. The stand was a Zeiss AxioObserver Z.1 with a Plan-Apochromat 63x/1.4 Oil DIC objective with a resolution of 0.124 μ m. Insets are 10X magnification of the two highlighted areas in each field. Post-acquisition processing was done using Velocity software (PerkinElmer). Images are representative of three separate experiments with two replicates per condition. (C) Calculation of MitoTracker fluorescence intensity was done with Velocity software by averaging the mean intensity of the voxels in each fluorescent cell. (D) ATP concentration was assessed by measuring the activity of Luciferase as relative luminescence units (RLU). (E) OCR and ECAR data obtained from the Seahorse XF24 Analyzer was calculated based on the oxygen consumption and acidification rates of 40,000 cells per well. The values were pooled from three separate experiments and normalized to changes from the initial rate, n=9. (F) Oxygen consumption in both Bax^{+/+} and Bax^{-/-} cells was measured over time as a function of increased fluorescence. Fluorescence, oxygen biosensor, and ATP data are representative of n=6. The values for the ATP, OCR and ECAR assays were normalized to cell number per well, and statistics were done using One-way ANOVA with Dunnett's post-test analysis. P<0.05 (*), P<0.01(**) and P<0.001 (***)

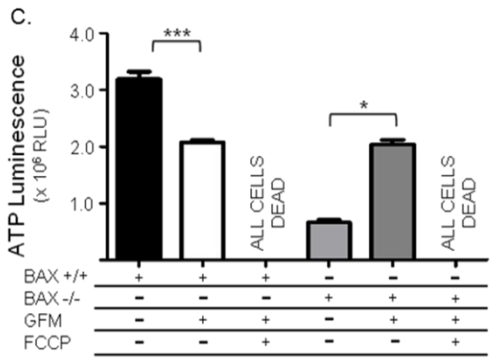
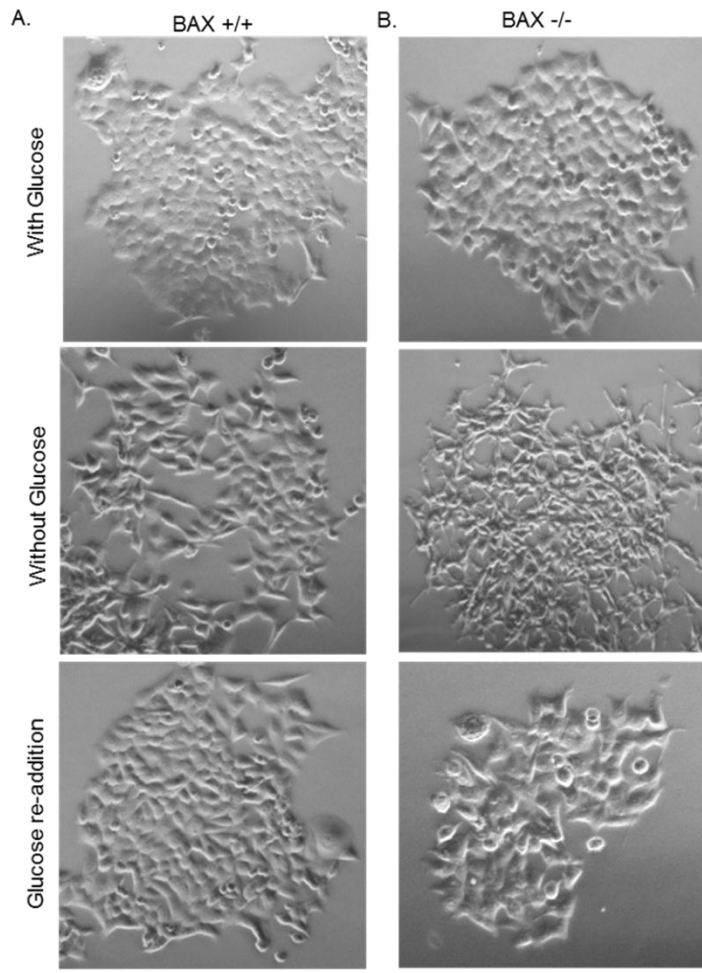


Figure 10: Cells deficient in Bax are susceptible to glucose deprivation.

The effect of glucose withdrawal on Bax^{+/+} HCT-116 cells (A) and Bax^{-/-} HCT-116 cells (B) was determined by assessing cellular morphology using DIC imaging at 20x magnification, with the small scale used to acquire images in each field. To deprive glucose, cells were cultured in complete RPMI media without D-Glucose (GFM) for 24 hours. The effects of glucose re-addition were assessed after culturing the cells for 4 hours with 25% glucose containing RPMI. Images are representative of three experiments.

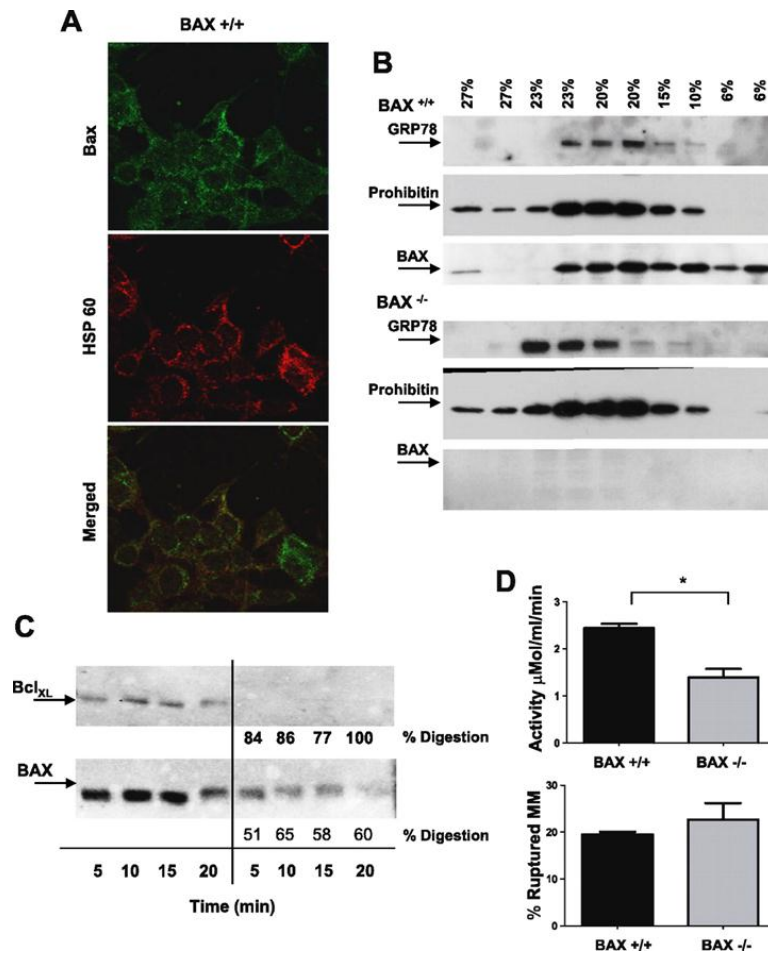


Figure 11: Bax associates with mitochondria in non-apoptotic cells resulting in reduced citrate synthase activity.

(A) Bax^{+/+} HCT-116 cells were fixed and stained with the indicated fluorochrome-conjugated antibody as described in Methods. Confocal microscopy of cells shows endogenous Bax, in green, the mitochondrial protein, HSP60, in red, and in the merged field, yellow regions indicate co-localization of Bax with HSP60. Images were acquired with LSM 510 using 100x/1.4 Oil DIC objective and are representative of ten different images scanned from three separate experiments. (B) Enriched mitochondrial lysates of membrane-bound proteins were prepared from Bax^{+/+} and Bax^{-/-} HCT-116 cells and subject to differential ultracentrifugation as described in Methods. Gradient fractions collected were analyzed by SDS-PAGE and membranes immunoblotted for the presence of Bax, Prohibitin (mitochondria), and GRP78 (ER). Each blot shown is representative of three independent experiments. (C) Western blot analysis of mitochondria isolated from Bax^{+/+} cells shows the effects of Proteinase K digestion on mitochondrial membrane proteins over time. The extent of the digestion was calculated based on the percent change in densitometry between the treated and untreated samples. (D) The assessment of citrate synthase activity was determined by the rate of formation of thionitrobenzoic acid (TNB) as described in Methods. The rate of activity is shown as $\mu\text{Mol/ml/min}$. Background levels of citrate synthase activity in spontaneously ruptured mitochondria are included as controls. The data encompasses two separate experiments for a total of n=4 per sample. Statistics were calculated using unpaired Students t-test. P<0.05 (*).

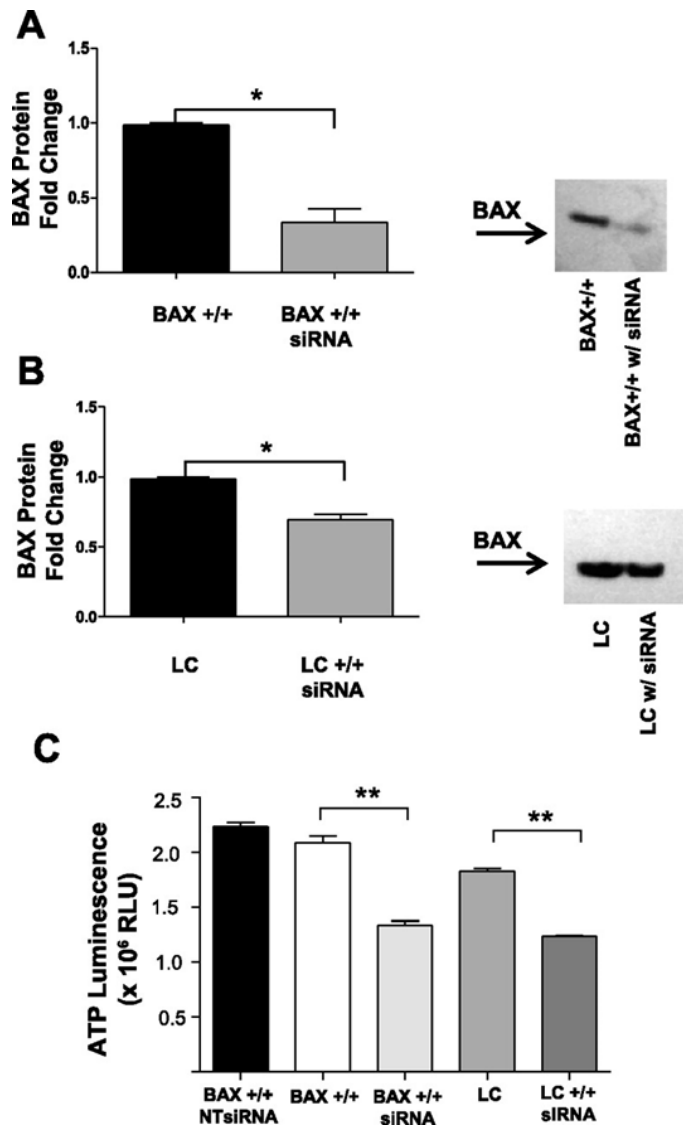


Figure 12: Bax associates with mitochondria in non-apoptotic cells resulting in reduced citrate synthesis activity.

Bax +/+ HCT-116 or lung cancer cells (LC) were seeded at a density of 200,000 cells/well in 6-well plates. After 24 hours, Bax SMARTpool siRNA (Dharmacon) or non-targeting siRNA was delivered using the Accell reagent (Dharmacon). Cells were analyzed 72 hours later. Controls cells received the Accell reagent alone. No significant differences were previously observed between Accell reagent alone and Accell reagent with non-targeting siRNA. (A) Cells treated with Accell reagent alone or Accell reagent with Bax siRNA were lysed for western blot analysis of Bax. Densitometry readings, indicative of fold changes in Bax expression, are shown. Images are representative of triplicate experiments. Calculations are based on multiple samples (n=4). Samples were normalized to cells without Bax siRNA. (B) For ATP assay, cells were counted and plated at a density of 4000 cells/well. Treatments included Accell reagent alone and Accell reagent with non-targeting siRNA (NTsiRNA) or Bax siRNA (siRNA). ATP assays were done in triplicate. Statistical analysis was performed with using One-way ANOVA test for equal variances. P<0.01(**).

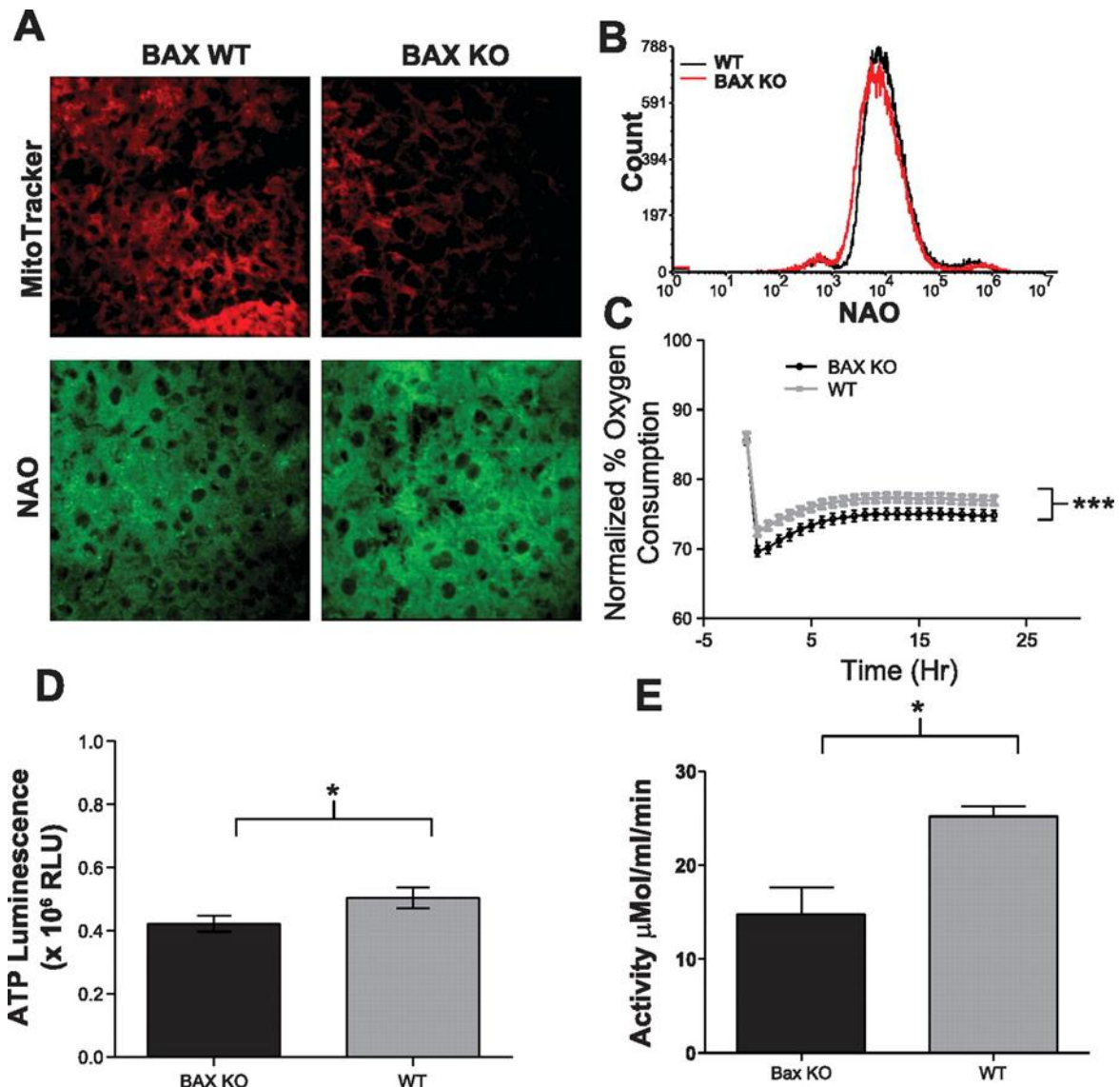


Figure 13: Liver hepatocytes from Bax deficient mice have with reduced metabolic activity, resulting in decrease ATP and oxygen consumption.

Sections of the caudate lobe of the liver (A) from Bax KO and C57BL6 mice were stained with MitoTracker Red or NAO. (B) Isolated hepatocytes from these mice were stained with NAO and measured by flow cytometry to determine mitochondrial content. Data is representative of 3 replicates and n=2 for each group. (C) Oxygen consumption of 50,000 isolated hepatocytes per well was measured over 24 hours. The data is representative of two experiments each with 46 replicates per group. (D) ATP content was measured in isolated hepatocytes. Luminescence was normalized to 5,000 cells per well and each of three experiments consisted of 42 replicates per condition. (E) Citrate synthase activity was examined in isolated mitochondria by measuring the absorbance of TNB over time. ATP and citrate synthase assay analysis was done using One-way ANOVA with Dunnett's post-test analysis. $P < 0.001$ (***) and $P < 0.05$ (*).

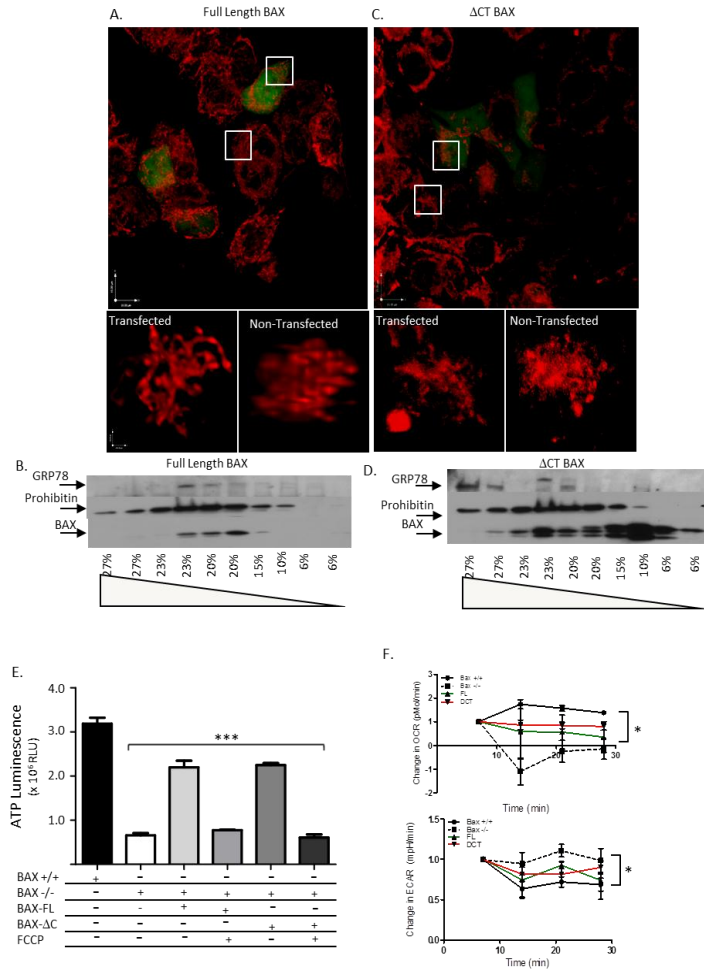


Figure 14 : Expression of full Length Bax restores mitochondrial association and ATP production in Bax deficient cells.

Bax^{-/-} HCT-116 cells were transfected with a ProteoTuner bi-cistronic vector expressing either Full Length (FL) BAX (A, B) or BAX-ΔCT(C, D) and GFP. (A, C) Cells were grown on MatTek plates as described in Methods, and transiently transfected (efficiency 60-70%). Shield was added to induce expression. Transfected cells were imaged based on GFP expression, and MitoTracker Red was used for mitochondria visualization. Live cell images were obtained using the UltraView (PerkinElmer) spinning disc confocal system. The stand was a Zeiss AxioObserver Z.1 with a Plan-Apochromat 63x/1.4 Oil DIC objective with a resolution of 0.124 μm. Insets were acquired at 10X magnification. Post-acquisition processing was done using Velocity software (PerkinElmer). (B, D) BAX^{-/-} HCT-116 cells were transfected with either BAX-FL or BAX-ΔCT as described above. Mitochondrial enriched lysates were subjected to differential ultracentrifugation and SDS-PAGE as described in Methods. Membranes were probed with antibodies for BAX, prohibitin (mitochondria) and GRP78 (ER). Images are representative of three independent experiments. (E) BAX^{+/+} HCT-116 cells, BAX^{-/-} HCT-116 cells, and BAX^{-/-} HCT-116 cells transiently transfected with BAX-FL or BAX-ΔCT (ΔC) were treated with and without FCCP and analyzed for changes in ATP levels as described in Methods. (F) BAX^{+/+} HCT-116 cells, BAX^{-/-} HCT-116 cells, and BAX^{-/-} HCT-116 cells, transiently transfected with BAX-FL (FL) or BAX-ΔCT (ΔCT or DCT,) were analyzed for changes in OCR and ECAR as in Methods. One-way ANOVA was used for statistical analysis. Microscopy and ATP data is representative of two experiments each with three replicates. OCR and ECAR data are representative of two experiments with a total of six replicates. Statistical results for OCR and ECAR assays are p<0.05 (*) for BAX^{-/-} vs. BAX-FL and BAX^{-/-} vs. BAX-ΔCT. For the ATP assay p<0.001 (***).

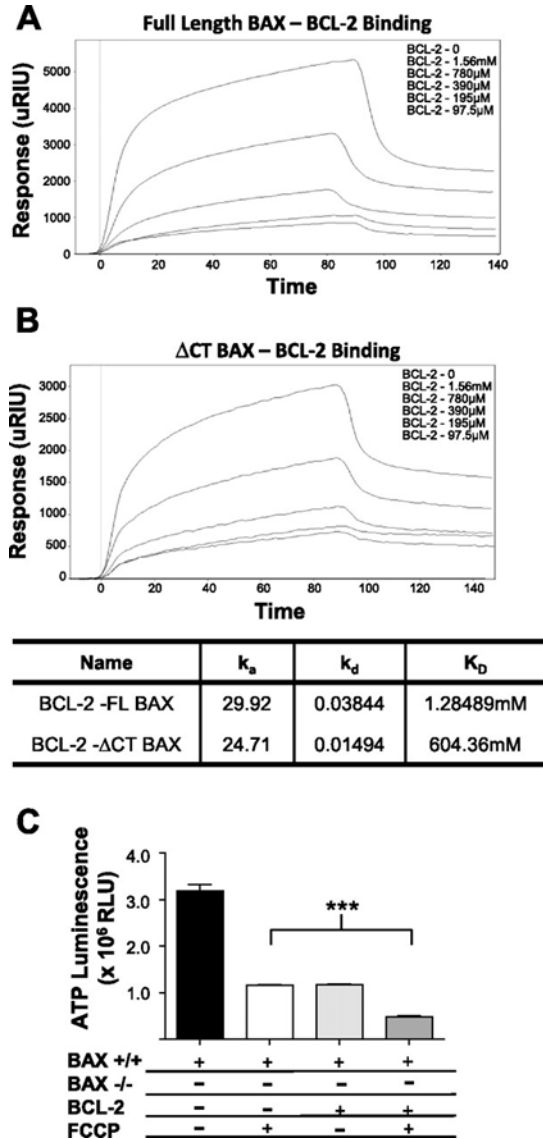


Figure 15: The interaction of Bax with BCL-2 inhibits the production of ATP in non-apoptotic cells

SPR analysis of the binding of full-length Bax -FL (A) or Bax -ΔCT (B) recombinant proteins with BCL-2 was done by amine-coupling Bax to the sensor chip and then flowing BCL-2 over the immobilized Bax proteins. Response is measured in micro-Refractive Index Units (μ RIU), and the equilibrium constants (K_D) for each Bax construct were calculated from the observed association and dissociation constants (k_a and k_d) (Table). (C) Bax ^{+/+} HCT-116 cells, Bax ^{-/-} HCT-116 cells, and Bax ^{-/-} HCT-116 cells transiently transfected with Bax -FL or Bax -ΔCT (for 18 hours) were treated with and without FCCP and analyzed for changes in ATP levels as described in Methods. One-way ANOVA was used for statistical analysis. $P < 0.001$ (***)

CHAPTER 3: EXPLOITING THE INHERENT CYTOTOXICITY OF THE ALPHA-9 HELIX OF BAX FOR USE AS A PEPTIDE DRUG FOR CANCER THERAPY

Introduction

It is generally recognized that cell death can occur through diverse mechanisms, including apoptosis, programmed necrosis, autophagy or mitotic catastrophe. Most studied is the apoptotic pathway that is triggered by extracellular and intracellular cues and is governed by the relative ratios of pro- (i.e.: Bad, Bax, Bim, Bak) to anti-apoptotic (i.e.: Bcl-2, Bcl-XL) members of the Bcl-2 family of proteins. Tumors expressing high levels of anti-apoptotic proteins, such as Bcl-2, Mcl-1 or Bcl-xl, are often resistant to the effects of chemotherapeutics [39]. This is accomplished, in part, by inhibition of the pro-apoptotic Bcl-2 family members, such as Bax, first identified as a protein that interacts with Bcl-2 [73]. A third group of Bcl-2 proteins, identified as the BH3-only proteins such Bid, Bim or Bad, tip the balance between anti- and pro-apoptotic members and serve as molecular tie breakers favoring cell death [87]. Comparably, less is known about the mechanisms that activate programmed necrosis, autophagy and mitotic catastrophe; however the Bcl-2 family members may play a role in these processes [88].

To kill cancer cells, conventional chemotherapeutic agents typically rely on an intact apoptotic signaling pathway induced by cellular insults like ionizing radiation (IR), ultraviolet (UV) radiation, or reactive oxygen species (ROS) that can cause DNA damage. Resistance to chemotherapeutic agents may result from mutation, duplication, or elimination of gene products that are involved in the initiation and/or execution

apoptosis. As an example, DNA alkylating agents become ineffective in tumor cells in which p53 is mutated, resulting in transcriptional loss of Bad and Bax and impairment of the apoptotic program [89]. Due to the prevalence of tumors harboring p53 mutations, recent efforts have focused on directly targeting Bcl-2 family members. Whether acting directly or indirectly on the Bcl-2 proteins, most chemotherapeutic agents cause cytochrome C to be released from mitochondria leading to activation of effector caspases [90]. Thus, given the central role that mitochondria play in life and death, this organelle is a logical target for direct intervention with small molecules or peptides.

Small molecules are easy to synthesize and have long half-lives. However, *in vivo* efficacy is hard to predict given their extra-physiologic structures that could produce off target effects [91]. As a result, a number of small molecule cancer therapeutic agents have exhibited significant toxicity when translated for human use [92]. Several small molecule BH3 mimetics, including ABT-737 and navitoclax, are currently being investigated at varying levels of phases of pre-clinical and clinical trials[40], [93]. Despite their selective affinity for specific anti-apoptotic proteins, these compounds appear to be subject to the same constraints that affect other small molecule therapeutics: off-target cytotoxicity [38].

As an alternative approach to the use of small molecules, anticancer peptide therapy focuses on the development of therapeutic peptides to kill cancer cells [94]. This approach has significant advantages over small molecules, including ease of design and synthesis. A vast knowledgebase of normal protein function facilitates the intelligent design of peptides that can specifically target a protein of interest. This study

describes the rational development of a cytotoxic peptide that promotes non-apoptotic cell death. Guided by primary sequence similarities of the pro-apoptotic protein Bax to anti-microbial peptides and the evolutionary relationship of mitochondria to bacteria, we examined the suitability of a peptide modeled after the C-terminus of Bax (CT20p) as a selective mitochondrial pore forming therapeutic. Biophysical studies previously revealed that CT20p could form a pore that permits the passage of small molecules (Garg et al and Tatulian et al, submitted). The purpose of the present study is to determine whether an inherent property of CT20p is the capacity to induce cell death that is non-apoptotic and could result in direct demise of cancer cells. To introduce CT20p in vehicle that could be modified for tumor-targeting, the peptide was encapsulated in polymeric nanoparticles (NPs). Polymeric NPs are inert particles that have the inherent capacity to incorporate drugs, dyes or tumor-targeting ligands, and, thereby, provide an ideal carrier for CT20p. Data presented herein supports the development of CT20p-NPs as a novel cytotoxic that can be used alone or in combination therapies for the treatment of cancer.

Materials and Methods

Cell lines and CT20p.

The Flp-In T-REx-293 cell line (Invitrogen) stably expresses the *lacZ*-Zeocin fusion gene and Tet repressor. The 293 line was maintained in DMEM, 10% fetal bovine serum (FBS) (tetracycline-reduced), 2 mM L-glutamine and 1% Penicillin-Streptomycin. The HCT-116 Bax^{-/-} and Bax^{+/+} colorectal cancer cell lines [65] (gift from

Dr. Bert Vogelstein, John Hopkins University) were maintained in McCoy's 5A media, 10% FBS and 1% Penicillin-Streptomycin. The breast cancer cell lines, MCF-7 and MCB-MD-231 (ATCC), were maintained in DMEM, 10% FBS, and 1% Penicillin-Streptomycin. MCF-7 cells were supplemented with 1% L-Glutamine every 15 day. Early passages of all cell lines were frozen as stocks at time of receipt. Cell lines were used at less than 10 passages from stocks. CT20p (Ac-VTIFVAGVLTASLTI WKKMG-NH2) (Biopeptide Co., Inc.) was commercially synthesized at >98% purity.

Plasmids, Mutagenesis and Transfection.

For inducible expression of full-length Bax, we employed the Flp-In T-REx System (Invitrogen) following manufacturer's protocol. Briefly, PCR-directed mutagenesis of K189/K190 was performed using HA-tagged primer sets. Bax constructs were amplified from pEGFP-Bax (gift from Dr. Richard Youle, NINDS, NIH), digested with EcoRV and cloned into the plasmid pcDNA5/ FRT/TO which undergoes DNA recombination at the Flp Recombination Target (FRT) site when co-expressed with the Flp recombinase pOG44 plasmid. Constructs were confirmed by sequencing; Fugene transfection reagent (Roche) was used to co-transfect plasmids at a ratio of 9:1. Stable Flp-In T-REx expression cell lines were selected for Blasticidin resistance (10µg/ml), Hygromycin resistance (100µg/ml) and Zeocin sensitivity (200µg/ml). Bax expression was induced with 1µg/ml tetracycline. Cells were assayed after 24 hours of induction.

To generate the Destabilization Domain (DD)-tagged Bax C-terminal (CT) constructs (amino acids 173-192) with K189K190 (wild-type) or EE, LL, and RR mutations, primers were annealed and ligated into the ProteoTuner vector (Clontech)

digested by *EcoRI* and *BamHI*. Generation of DD-tagged, full-length WT Bax was previously described [95]. The ProteoTuner IRES2 system (Clontech) also had the marker protein GFP downstream to the internal ribosome entry sequence (IRES) and was translated independently of the DD-tagged protein. Cells were transiently transfected using the TransIT-LT1 transfection reagent (Mirus) for 24 hours and microscopically assayed for GFP expression. Expression of DD-tagged proteins was induced for 4-5 hours by adding 500nM of Shield (Clontech).

MDA-MB-231 cells were transiently transfected with pcDNA-Bcl2 (gift from Dr. Wenqing Li, NCI-Frederick) (or as control pEGFP (Clontech)) using the TransIT-LT1 transfection reagent (Mirus). To assess transfection efficiency, cells assayed microscopically for EGFP expression. To assess Bcl-2 expression, cells lysates were immunoblotted as described below.

Mitochondrial Translocation Assay and Immunoblotting.

Mitochondrial and cytosolic proteins were isolated using a mitochondrial enrichment kit (Pierce). Western blots were run using 12-15% SDS-PAGE gels and PVDF membranes and probed with the following primary antibodies: 16B12 anti-HA mouse monoclonal (Covance) for HA-tagged Bax; 631073 Anti-DD monoclonal (Clontech) for DD-Bax; N-20 (Santa Cruz), for endogenous Bax, Ab-2 (Fitzgerald) for prohibitin, C20 (MAPK) (Santa Cruz) for p38 MAP kinase, and rabbit polyclonal for Bcl-2 (Santa Cruz); this is followed by the appropriate secondary antibodies conjugated to horseradish peroxidase (HRP) and visualized with enhanced chemiluminescence kit

(Pierce). Molecular weight markers (SeeBlue Plus 2 (Invitrogen)) were used to approximate the position of protein bands in blots.

Live-Cell Confocal Imaging.

Images were acquired through a PerkinElmer UltraView spinning disc confocal system, with AxioObserver.Z1 stand (Carl Zeiss), in a humidity and temperature-controlled chamber (LiveCell) with cells cultured on MatTek plates (MatTek Corporation). Post-acquisition snapshots were taken from time-lapse movies at time points indicated in the figures. Time-lapse movies were initiated two hours after transfection or expression was induced and images acquired through 12 hours of expression using a Plan-Apochromat 10x objective. For DD-CT20 fusion proteins, cells were incubated with 1nM MitoTracker Red 580 for 30 minutes prior to imaging. Time-lapse movies were recorded for up to 12 hours using a Plan-Apochromat 63x Oil DIC objective.

Visualization of the uptake and effects of the fluorescent dye (DiI)-loaded NPs (prepared as described below) in HCT-116, MCF-7 and MDA-MD-231 cells was observed using a 10x air objective with a numerical aperture of 0.3, using ex/em of 514/587. All cells were loaded with MitoTracker as described above. Visualization of the HCT-116 cell lines was observed using Plan-Apochromat 63x Oil objective. MCF-7 and MDA-MB-231 images were captured using Plan-Apochromat 40x Oil objective. All time-lapse images were generated in 2D by capturing 6 time points per hour for 24 hours of the same field.

Treatments and Detection of Apoptotic Cells and Mitochondrial Membrane Potential by Flow Cytometry.

HCT-116, MCF-7 or MDA-MB-231 cells were collected at a final concentration of 1×10^6 cells/ml and assayed using the SYTOX® AADvanced™ dead cell stain solution (Invitrogen). Cells were analyzed using the BD FACSCanto flow cytometer. SYTOX® AADvanced™ was visualized at 488nm and emissions collected at 695nm. Analysis of data was done using FSC Express software (DeNovo). Membrane asymmetry was assessed using the Violet Ratiometric Membrane Asymmetry Probe/Dead Cell Apoptosis Kit (Invitrogen) according to the manufacturer's protocol.

The cell permeable dye, JC-1 (Molecular Probes), was used to qualitatively assess the mitochondrial membrane potential ($\Delta\Psi\mu$). For detection, JC-1 was excited at 488 nm and fluorescence measured at 530 (JC-1 monomers) and 590 (JC-1 aggregates) nm. JC-1 monomers accumulate in the cytosol while JC-1 aggregates accumulate in the mitochondrial matrix in a manner dependent on the mitochondrial membrane potential. Briefly, MDA-MB-231 cells were seeded in 6 well plates and treated with CT20p or controls as described in Figure Legends. JC-1 was used at $5\mu\text{g/mL}$, and cells were incubated with the dye for 15 minutes in the dark prior to analysis. Cells were analyzed by flow cytometry using the FACSCanto II (BD Biosciences). Data was acquired in the FITC and PE channels for analysis. FCS Express software (DeNovo) was used to analyze data.

To study apoptosis, cells were pre-treated with $100\mu\text{M}$ of the pan-caspase inhibitor Z-VAD-fmk (EMD Biosciences) or transiently transfected with Bcl-2 (as described above), then treated with either CT20p-NPs (see below) or cisplatin (CDDP)

(gift from Dr. Deborah Altomare, UCF) alone or in combination as indicated in figure legends. Following treatment, cells were analyzed as described above for cell death and membrane asymmetry.

Synthesis of Polymeric NPs Encapsulating CT20p.

CT20p was encapsulated into hyperbranched polymeric (HBPE) NPs following a previously reported method [96]. A fluorescent dye (Dil) was co-encapsulated with the peptide. In brief, 1.0 μL of Dil dye (10 $\mu\text{g}/\mu\text{L}$) and 36 μL of CT20p (0.05 $\mu\text{g}/\mu\text{L}$) solution in 250 μL of DMSO were mixed in 250 μL of a DMSO solution containing the HBPE polymer (12 mg) for a ratio of ~ 0.15 μg peptide: 1 mg nanoparticles. The resulting polymer-Dil/CT20p mixture in DMSO was added to deionized water (2.5 mL) to form the HBPE (CT20p/Dil) NPs. The resulting NPs were purified using a PD-10 column and dialyzed (MWCO 6-8K) against PBS (pH=7.4). Dynamic light scattering and zeta potential analysis of the nanoparticle reveals a size diameter of 88 ± 2 nm and zeta potential of -54.5 mV.

Synthesis of Aminated Polymeric NPs Encapsulating CT20p.

The HBPE NPs (above) contain functional carboxylic groups on their surface that results in a negative charge. To introduce a positively charged surface the nanoparticles were aminated using water-soluble carbodiimide chemistry [EDC: 1-ethyl-3-(3-dimethylamino-propyl) carbodiimide hydrochloride and NHS: *N*-hydroxysuccinimide chemistry], following a previously reported method [96]. Briefly, to a solution of HBPE (CT20p/Dil) NPs (1.0 mmol) in PBS (pH = 7.4), a solution of EDC (10 mmol) and NHS (10 mmol) in MES buffer (pH = 6.0) was added. Afterwards, ethylenediamine (10 mmol)

in DMSO was added to obtain aminated Dil/CT20p co-encapsulation polymeric NPs, which were purified and dialyzed as above. Dynamic light scattering and zeta potential analysis of the nanoparticle reveals a nanoparticle size diameter of 91 ± 3 nm and zeta potential of + 10.3 mV. All NPs were stored at 4°C. A final working concentration of 350 pM was determined by testing the toxicity of 7, 1.4, 0.7 and 0.35 nM on HCT116^{+/+} cells.

Calcein Release Experimental Protocol.

Calcein release from artificial membranes was measured on a JASCO 810 spectropolarimeter (Jasco Inc.) with a Peltier water cooled thermostat and a photomultiplier tube mounted at 90 degrees for fluorescence measurements. Large unilamellar vesicles (LUVs) were prepared with the following modifications: Lipids (Avanti Polar Lipids) in chloroform were mixed in the following molar ratios: 52.5% 1-palmitoyl-2-oleyl-sn-glycero-3-phosphatidylcholine (POPC), 21% 1-palmitoyl-2-oleyl-sn-glycero-3-phosphatidylethanolamine (POPE), 13% bovine liver L- α phosphatidylinositol (PI), 10% cholesterol and 3.5% 1-palmitoyl-2-oleyl-sn-glycero-3-phosphatidylglycerol (POPG), in order to mimic the outer mitochondrial membrane. After removing chloroform and desiccating, the dried lipid film was re-suspended in 50 mM HEPES, pH 7, supplemented with 110 mM NaCl and 80 mM calcein and extruded with Avanti's mini extruder (Alabaster, Alabama). External calcein was removed by gel filtration through a 1.5 x 50 cm Econo-Column (Bio-Rad) freshly packed with Sephadex 50 (GE Healthcare). CT20p was added at concentrations equivalent to those used with cells in culture. Calcein fluorescence was excited at 495nm and emission spectra recorded between 510 and 550 nm, (excitation/ emission slits: 10/ 3 nm). Samples were

maintained at 37C and a final measurement taken at 24 hours. Maximum calcein release was obtained by the addition of Triton x100 (0.1% final concentration) to calcein loaded LUVs without nanoparticles that had been incubated at 37C for 24 hours after the addition of 10 μ l DMSO. LUV integrity was monitored by light scattering at an excitation wavelength of 500 nm and detected at 90 degrees to the incident light.

In Vivo Experiment.

Two to five million MBA-MD-231 cells were harvested from culture and injected subcutaneously into the right flanks of 16 female nude mice (nu/nu, Charles River). After 2-3 weeks, tumor volume and growth was assessed by ultrasound (VisualSonics Vevo 2100). Mice with tumors were injected intra-tumorally (IT) or intravenously (IV) with PBS, unloaded NPs, or CT20p-NPs at 4X the concentrations described above. Injections were performed once (IV) or twice (IT) over 4-15 day period. Mice were observed 0-15 days post-treatments and tumor volume assessed by ultrasound. Given the size of the standard deviation and the difference in the means between groups of control and CT20p-NPs treated mice, at n=4 for each group, at 80% power the P values were less than 0.05. This study was carried out in accordance with the recommendations in the Guide for the Care and Use of Laboratory Animals of the National Institutes of Health. The protocol was approved by the Institutional Animal Care and Use Committee at the University of Central Florida. All efforts were made to minimize suffering

Results

CT20p Enables Mitochondrial Membrane Binding and Permeabilization.

The ability to selectively permeabilize membranes and kill cells is a feature of anti-microbial peptides (AMPs), whose fundamental structure involves clusters of hydrophobic and cationic residues (Table 4). Most peptides with these sequences interact well with the negatively charged prokaryotic lipid membranes, but interact poorly with the more zwitterionic eukaryotic plasma membranes [97]. Mitochondria within eukaryotic cells resemble Gram negative bacteria in a number of ways: having a double membrane, circular DNA, and may have arisen through the process of endosymbiosis[98], [99]. Hence, AMPs introduced within eukaryotic cells could disrupt mitochondrial membranes, causing mammalian cell death. As an example, a synthetic, anti-microbial-like peptide, D -(KLAKLAK)₂, disrupts mitochondria and kills cancer cells when tagged with cell-penetrating peptides [100–102]. Based on this information, we sought to develop a new peptide with the features of AMPs that could be used to induce the selective death of cancer cells. To this end, we examined different membrane-binding domains from Bax, a death-inducing member of the Bcl-2 family. We found that the C-terminal α 9 helix of Bax (basis for CT20p) contained clusters of hydrophobic and cationic residues (Table 4). In fact, the arrangement of hydrophobic and cationic residues of CT20p was comparable to a number of AMPs, including those of the Brevinin family as well as Ranalexin. CT20p also shared features with anti-microbial peptides, namely the double-lysines, not found in peptides composed of the α 5- α 6 helices of Bax or BH3 domain peptides (Table 4). In fact, based on their sequences,

these latter peptides are likely to induce apoptosis by interacting with and blocking the activity of anti-apoptotic proteins rather than directly associating with mitochondrial membranes.

To examine the capacity of CT20p to cause cell death by targeting mitochondria, we first examined the involvement of the double lysines in the context of the full-length Bax protein. Mutagenesis of the double lysines in the C-terminus of Bax was performed. Previously we found that constitutive expression of N-terminal-tagged Bax induced spontaneous cell death. To avoid this, we inducibly expressed HA-tagged Bax in stably transfected Flp-In T-REx 293 cells. Bax constructs were integrated into the genome at a single FRT (recombination) site and the levels of Bax expression in these isogenic cell lines did not cause apoptosis. Localization of full-length, wild-type (WT) Bax (Bax-KK) was distributed among cytosolic and mitochondrial lysates (Figure 1A) as we and others have previously shown. We found that N-terminal-deleted Bax (Bax- Δ NT) was localized primarily to mitochondria, while the C-terminal-deleted Bax, (Bax- Δ CT) was retained in the cytosol, indicating the importance of the N- and C-terminal domains in the localization of Bax (Figure 16A). Substitution of the double lysines (K189/K190) with negatively charged residues, aspartic acid (D) or glutamic acid (E), resulted in the cytosolic retention of Bax (Bax-DD, Bax-EE) (Figure 16B). Whereas substitution of the double lysines with positively charged arginine (R) (Bax-RR) led to mitochondrial localization (Figure 16B). Substitution of the double lysines with a polar amino acid, glutamine (Q) (Bax-QQ), led to less mitochondrial Bax, when compared Bax-KK and Bax-RR (Figures. 16A, 16B). Substitution of the double lysines with the hydrophobic

amino acid leucine (L) (Bax-LL) resulted in mitochondrial association, likely through increased hydrophobicity (Figure 16A). Mutation of one lysine, K189, (Bax-EK) also rendered Bax cytosolic, which was not observed by mutation of K190 (Bax-KMGK) (Figures. 16A, 16B). These results deleting or mutating the double lysines at the C-terminus of Bax confirmed that these residues and the C-terminal helix were important for association of the full-length protein with mitochondria.

Next, we determined whether CT20p retained the mitochondrial-binding properties of the full-length protein. To evaluate this, we fused only the CT20p domain to a short destabilization domain (DD) for detection and inducible expression. CT20p fused to DD (DD-CT20) was inducibly expressed in HCT-116 cells. Peptide localization was examined post-expression. As control we compared DD-CT20 (KK and EE, LL and RR mutants) peptides to DD-tagged full-length (FL) Bax. Previously we showed that induced expression of DD-FL Bax did not cause cell death in the absence of apoptotic stimuli [95]. Gene expression was induced for four hours after previous transfection of cells with DD-FL Bax or DD-CT20 peptide cDNA constructs. Constitutive GFP expression from the bi-cistronic plasmid was controlled by an IRES element and used to detect transfected cells. As shown in Figure 16B, most of DD-tagged FL Bax was found in cytosolic extracts, and a fraction of DD-FL-Bax was in mitochondria extracts. The small 15-16 kD band of DD-CT20 peptides or DD-CT20 mutant peptides (EE, LL, and RR (fainter band)) was detected in mitochondrial extracts, indicating that the DD-CT20 peptides were localizing to mitochondria. These results were confirmed by immunofluorescence (Data not shown). Expression of DD-CT20 also caused the

mitochondrial translocation of a small amount of endogenous Bax (Figure 16B). Additional experiments attaching CT20p to EGFP confirmed the findings that fusion of CT20p to a cytosolic protein could confer membrane binding properties. It should be noted that in these experiments, detecting the localization of DD-CT20 or GFP-CT20 proved challenging, even upon a short term of expression, because CT20 expression could cause significant cell death as shown in supplemental figures, indicating that its effects upon mitochondria had lethal consequences.

To examine the effect that CT20p could have upon mitochondrial membranes, we directly evaluated its ability to disrupt lipid membranes and cause the release of sequestered contents. LUVs composed of the phospholipids that make up the mitochondrial outer membrane were made as described in Materials and Methods and were loaded with calcein. The release of calcein was measured by fluorescence spectrometry. Controls were LUVs alone or LUVs treated with Triton X-100, which caused disruption of lipids and release of calcein. The data in Figure 9A demonstrated that CT20p could insert into mitochondrial-like LUVs and cause the release of calcein (Figure 17A), without disrupting the integrity of the LUVs as shown by analysis of the light scattering pattern (Figure 17B). A decrease in light scattering is evident when vesicle integrity is lost as seen in Triton X-100 sample (Figure 17B). The extent of the light scattering was determined by the amount of light detected by the fluorescence detector. Because the detector is mounted at a 90 degree angle from the incident light, any signal detected at the incident wavelength (500 nm) is scattered light. When the double lysines were mutated to leucines (CT20p-LL) or glutamic acids (CT20p-EE), minimal to

no release of calcein was detected and LUVs retained their integrity (Figures. 17A, 17B). In total these findings suggest that CT20p can insert into mitochondrial lipid membranes and permeabilize the membranes, perhaps by forming a pore-like structure.

Delivery of the CT20p Using Polymeric NPs Kills Cancer Cells.

Free peptides in aqueous solutions may not adopt the α -helical conformation needed to penetrate cell membranes. For this reason, modifications, such as chemical stapling [41], or the addition of membrane-penetrating sequences [103] have been tried by others to deliver free peptides to cells. However, none of these methods can inherently target tumors. To develop a robust delivery system for CT20p that could incorporate tumor-targeting ligands as well as conventional drugs, we turned to nanotechnology. As CT20p is soluble in DMSO, it can easily be encapsulated within the hydrophobic pockets of aliphatic, polymeric NPs. A major advantage of such NPs is their ability to be modified with poly(ethylene glycol) (PEG), reducing non-specific interactions with proteins, increasing half-life and improving bio-distribution by increasing blood circulation time [104], [105]. Shown in Figure 11A is the scheme for generating the aliphatic, hyper-branched, polymeric NPs that contain Dil (fluorescent dye) and commercially synthesized CT20p. Two forms of polymeric NPs were made: positively charged, aminated (AM) or negatively charged, carboxylated (COOH) nanoparticles [96]. To verify that the NPs would not release CT20p at neutral pH, calcein loaded liposomes were prepared. While CT20p alone (350 pM) resulted in the release of calcein from liposomes (as shown in Figure 2A), CT20p-NPs (350 pM) failed to do so, indicating that the peptide loaded NPs were intact at pH 7. This confirmed that

cargo is released from NPs only within cells by intracellular esterases or acidic pH [96], indicating that polymeric NPs are a good vehicle in which to incorporate CT20p for delivery to tumor cells.

Next we examined the uptake of Dil-loaded NPs and effect upon the viability of HCT-116 cells. The representative experiment in Figure 18B showed that HCT-116 cells take up NPs, uptake was better for the Bax-deficient cells compared to Bax-containing cells, which could be due to their metabolic state since cells lacking Bax tend to be more glycolytic [95]. While the treatment of HCT-116 cells with unloaded NPs did not cause significant cell death (Figure 18B), treatment of HCT-116 cells with CT20p-NPs (700 pM) resulted in observable morphological changes consistent with cell killing (Figure 18B). As expected, treatment of cells with free peptide at doses equivalent to that available in the NPs, as well as 1000-fold greater, did not cause toxicity (data not shown). To show that NPs alone did not cause death, we used a DNA-binding dye that detects membrane rupture of dead cells (Sytox). In Figure 18C the results show that minimal (in Bax^{+/+} HCT-116 cells) to no (in Bax^{-/-} HCT-116 cells) cell death was detected upon addition of Dil-loaded NPs (5 μg, 10 μg or 15 μg) as compared to positive control (dead cells). From this point on, to minimize off-target effects, all *in vitro* experiments were performed using approximately 350 pM CT20p-NPs.

To visualize the effect of CT20p-NPs upon mitochondria, we stained Bax-containing or Bax-deficient HCT-116 cells with MitoTracker and imaged live cells. In Figure 19A and 19B are “snapshots” at 0, 12 and 24 hour time points revealing changes in cell morphology which include disruption of mitochondria (reduced or faint

MitoTracker staining), cell shrinkage and membrane perturbations, indicative of cell death. Loss of membrane integrity was detected within three hours of treatment with CT20p-NPs (Figure 19C); more so for the Bax deficient cells that we had shown previously were more efficiently taking up NPs. While both AM-NPs and COOH-NPs containing CT20p initiated cell death (Figure 19B-C), the COOH-NPs were more effective. Further, these results with Bax-deficient cells indicated that the death-inducing activity of CT20p was independent of endogenous Bax.

Next, we determined whether CT20p was cytotoxic to the breast cancer cell lines, MCF-7 and MDA-MB-231. In Figure 19A, we observed morphological changes such as diffused MitoTracker staining and cell shrinkage in MCF-7 cells treated with AM- or COOH-NPs containing CT20p, with COOH-NPs being the more effective. Most MCF-7 cells died within 24 hours, while loss of membrane integrity was detected by 3 hours of treatment (Figure 20B). In Figure 19C, the live-cell imaging experiment revealed vacuolization and cell shrinkage of MDA-MB-231 cells treated with CT20p-NPs. Within three hours, increased membrane rupture was detected in MDA-MB-231 cells treated with COOH-NPs loaded with CT20p (Figure 20D). Because the cytotoxic effect of the CT20p was more pronounced for the breast cancer cells (Figure 20) compared to HCT116 cells (especially the Bax-containing HCT116 cells (Figure 19), it remains possible that the CT20p-NP compound could be a potent inducer of death in metabolically active cells. These results show that CT20p, once introduced into cells, can rapidly trigger cell death, detectable by pronounced morphological changes.

Because of these results, Subsequent experiments performed with done using COOH-NPs to encapsulate CT20p.

The Death-Inducing Activity of CT20p is Independent of Caspases and Resistant to Bcl-2, Causing Tumor Regression.

To investigate whether the mechanism by which CT20p induced cell death involved apoptosis through the intrinsic mitochondrial pathway, we treated MDA-MB-231 cells with CT20p-NPs as described in Figure 20, adding a caspase inhibitor or over expressing Bcl-2. Cell death was measured by the uptake of Sytox, an indicator of membrane rupture. As shown in the representative experiment in Figures 21A, CT20p-NPs caused significant loss of membrane integrity, seen as an increase in Sytox staining, which was minimally impaired by caspase inhibition with Z-VAD-FMK. In contrast, treatment of MDA-MB-231 cells with cisplatin (CDDP) induced less cell death detectable by Sytox but was inhibited over 50% by Z-VAD-FMK. These results suggested that the mechanism induced by CT20p could be different than that induced by CDDP, and was largely independent of the effector caspases inhibited by Z-VAD-FMK. We next over expressed Bcl-2 and found that did not impair the death activity of CT20p. Overexpression of Bcl-2 did, however, inhibit the effects of CDDP treatment (Figure 21A). Combination of CDDP followed by treatment with CT20p-NPs proved to be the most effective in inducing cytotoxicity that was not inhibited by Z-VAD-FMK or Bcl-2 (Figure 21A). We confirmed that transfected cells were expressing Bcl-2 by immunoblotting lysates prepared from cells.

While Sytox is good indicator of cell death, it only reveals whether membrane rupture has occurred. To determine whether CT20p could induce apoptotic cell death, we measured membrane asymmetry caused by flipping of phospholipids in the plasma membrane using a violet ratiometric probe. In Figure 21B, dot blots show the comparison of loss of membrane integrity to changes in membrane symmetry in MDA-MB-231 cells treated with CT20p-NPs and/or CDDP. We found that treatment with CT20p-NPs resulted in uptake of the DNA-binding dye (as shown in Figure 21A), indicating membrane disturbance, but did not promote changes in membrane asymmetry typical of apoptosis. Death induced by CT20p-NPs was slightly affected by caspase inhibition (39.5% reduced to 22% Sytox-positive) but did not approach untreated conditions (1.7% Sytox-positive). Over expression of Bcl-2 did not block the death-inducing activity of CT20p-NPs (41% Sytox-positive). In contrast, CDDP induced alterations in the membrane asymmetry (~9%) detectable by the violet ratiometric probe that was inhibited by Z-VAD-FMK (2.6%) or Bcl-2 (4.6%) (Figure 21B). The combination treatment of CDDP followed by CT20p-NPs was effective with increased numbers of cells staining positive for both membrane asymmetry and Sytox uptake (~60% combined Sytox-positive). Caspase inhibition or Bcl-2 over expression minimally affected these results (~58% and ~47% combined Sytox-positive, respectively) (Figure 21B). These findings are suggestive that CT20p could engage a death mechanism distinct from that of CDDP that does not involve the intrinsic mitochondrial pathway, since death induced was independent of Z-VAD-FMK inhibited-caspases and resistant to Bcl-2.

To determine CT20p was directly affecting mitochondrial physiology while triggering a non-apoptotic death mechanism, we examined cells for changes in the mitochondrial membrane potential ($\Delta\psi\mu$). Typically apoptotic activities result in depolarization or low (L) mitochondrial membrane potential. We observed that mitochondria in MDA-MB-231 cells maintained a high (H) to intermediate (I) $\Delta\psi\mu$, that decreased to intermediate (I) levels upon treatment with empty NPs (results from 6 hours of treatment shown; Figure 21C). Note that empty NPs did not cause cell death (Figure 18). In contrast, treatment with CT20p-NPs led to cells containing mitochondria with increased or high $\Delta\psi\mu$ (H) that did result in eventual cell death (Figure 21C). Hyperpolarization of the mitochondrial membrane is not characteristic of apoptosis but rather is associated with conditions that cause necrosis [106]. These results collectively suggest that the activity of CT20p, once delivered and released from NPs, triggers a series of intracellular events that may involve mitochondria but result in the eventual rupture of the plasma membrane and cell lysis more consistent with necrotic-like mechanisms.

To demonstrate that CT20p was cytotoxic *in situ*, a small scale murine tumor experiment was performed. MDA-MB-231 cells were implanted in the flanks of nude mice and intra-tumoral or systemic injections of CT20p-NPs peptide were applied once tumors were detected (~9-17 mm). Intra-tumoral injections with performed twice over a period of week and complete tumor regression was observed (Figure 22A), as visualized in the representative ultrasound images (Figure 22B). Systemic application of pegylated-CT20p-NPs was achieved with a single intravenous injection and tumor

regression was also observed (Figure 22A and 22B). Mice were observed daily for two weeks after systemic treatments with CT20p-NPs and no signs of distress were noted. Upon dissection, tumors in mice that had received injections of CT20p-NPs were undetectable or liquefied, while organs (liver, kidneys, lungs) appeared normal and indistinguishable from control mice. These results are indicative of the potential therapeutic application of CT20p-NPs.

Discussion

Our results revealed that the last 20 amino acid residues of the C-terminus of Bax bear striking similarity to AMPs. Indeed, the presence of cationic and hydrophobic residues, including double lysines, suggests that peptides derived from this C-terminal segment may have the capacity to promote cell death in the absence of an initiating death signal. In addition, the primary sequence of the C-terminal segment of Bax imparts a favorable degree of solubility to CT20p, allowing encapsulation in NPs for delivery to cancer cells. Introduction of CT20p-NPs into colon and breast cancer cells resulted in cell death that is independent of Bax expression and is not suppressed by over-expression of Bcl-2. Unlike the full-length Bax protein, CT20p appears to cause a lethal sequence of events that result in membrane rupture not characteristic of apoptosis. These observations suggest that CT20p has the ability to induce a necrotic-like cell death that is distinct from apoptosis-inducing agents, such as DNA alkylating drugs. Thus, CT20p-NPs could serve as a potent cytotoxic agent for use in combination anticancer regimens together with conventional agents.

Our data suggests that the CT20p may function by forming pores in lipid membranes. This data is bolstered by evidence from a collaborative biophysical study, demonstrating that the structure of CT20p in aqueous solutions was partially α -helical (C-terminus) and partially β -sheet (N-terminus). CT20p could form a pore with a novel structure composed of eight peptide molecules in a strand–turn–helix conformation resulting in an “ α/β ring” (Tatulian et al., submitted). Such pores made by CT20p in zwitterionic and anionic lipid membranes caused the release of calcein from loaded lipid vesicles (Garg et al., submitted). In this same study control peptides did not form pores in lipid membranes that caused calcein release, indicating that the observed pore formation was specific to CT20p. Second-order rate kinetics revealed that initial pore formation by CT20p was slow (involving 2–3 peptides), which was followed by a faster rate of assembly involving up to eight peptide molecules. These studies led to a model of an octameric, trans-membrane pore with an inner diameter of 20–22 Å that could transport calcein, ions or slightly larger molecules (Tatulian et al., submitted). This data coupled with our observation that the CT20p can localize to mitochondria membrane systems in intact cells and cause the release of small molecules from mitochondrial-like lipid vesicles suggests that mitochondria may participate in the necrotic-like cell death we have observed. This implies that CT20p could form pores leading to the release of small ions or molecules sequestered in the mitochondria, consistent with mitochondrial membrane hyperpolarization. These events, in turn, could initiate a lethal cascade of

events causing the morphological changes and membrane rupture that we observed in cells treated with CT20p.

A number of studies have focused on harnessing or regulating the activity of Bcl-2 family members to induce the death of cancer cells. The poration activity of α -helical fragments from Bcl-2 proteins has been documented [107–109]. Such studies showed that peptides composed of the α 5 and α 6 helices of Bax could permeabilize membranes, forming channels that release sequestered contents like calcein [110], [111], providing insights on how the full-length Bax protein may function to permeabilize mitochondria and induce apoptosis. GFP-tagged versions of the α 5 and α 6 helices of Bax induced apoptotic cell death as indicated by increased annexin-V binding, PARP cleavage and caspase 3 activation, and, when fused to a cell-penetrating motif, caused regression of tumors [103]. In the same study, a GFP-tagged, longer version of the α 9 helix of Bax (as compared to CT20p) was tested and did not cause apoptosis [103]. As explanation, the additional residues added to the C-terminal sequence may add rigidity and impair the death-inducing activity we observed with the shorter CT20p. In fact, we previously examined a Bax C-terminal peptide that contained five additional residues (25mer) that was less effective inducing cell death when expressed in cells (data not shown). Other sequences from Bax that have been examined by others include the BH3 domain. In peptide form, the Bax BH3 domain induced apoptosis when used to treat cells [112]. This was mostly due to the BH3 peptide blocking the interaction between Bax and anti-apoptotic proteins like Bcl-XL. The Bax BH3 peptide did not directly activate Bax or trigger the translocation of Bax to the mitochondria [112]. This study

and others have focused efforts on exploring the indirect use of BH3 peptides as inhibitors of anti-apoptotic proteins, such as Bcl-2, rather than as direct activators of cell death via membrane pore formation. The subsequent development and clinical testing of BH3-derived small molecule mimetics [113] is the direct consequence of demonstrating the therapeutic utility of peptides based on functional domains from Bcl-2 proteins.

CT20p shares many of the features of naturally occurring AMPs such as cationic charges (i.e., double C-terminal lysines) and portions of hydrophobic stretches. This may promote selectivity for negatively charged membranes, like those of prokaryotes and also cancer cells. The membranes of cancer cells, because of increased exposure of phosphatidylserine (PS) [114], the presence of sialic acid residues linked to glycoproteins like mucins [115], and the altered expression of proteoglycans with highly negatively charged side chains [116], [117], tend to accumulate negative charges. Once attracted to membranes, AMPs can kill by necrotic (lysing cell membranes) or apoptotic (disrupting mitochondria) mechanisms. AMPs can also form pores; however, the structural features of these remain to be fully elucidated. A good model from which to compare the action of CT20p is the synthetic peptide, (KLAKLAK)₂ (KLA peptide), made to replicate the amphipathic features of AMPs [118]. KLA peptide is poorly permeable to mammalian cells and requires fusion with a cell membrane penetrating agent to enter cells. Most studies report that, once introduced into a cell, the KLA peptide (like CT20p) localizes to mitochondria [100]. Unlike CT20p, however, the KLA peptide causes depolarization of the mitochondrial membrane and apoptosis under most conditions

tested [101], [102], [119], [120]. Interestingly, a dose effect was observed when the KLA peptide was fused to prostate cancer antigen in that low doses caused apoptosis, while high doses led to necrosis [121]. We did not observe such effects with CT20p, which caused non-apoptotic cell death with cell lysis at all doses tested, with the major portion of experiments performed in the picomolar range.

In summary, our results suggest that CT20p acts through a non-apoptotic pathway to induce cancer cell death and thereby has potential application with apoptosis-inducing agents in combination therapies to activate multiple death pathways. This is a potent approach to treat cancer in that the targeting of membranes, the rapid mode of action and the necrotic-like death pathway make CT20p an unlikely inducer of cancer drug resistance. We demonstrated herein that CT20p can be encapsulated in polymeric NPs, which increases its bioavailability and enables delivery to tumor cells. We observed tumor regression under both intra-tumoral and systemic applications, suggesting that CT20p-NPs were accessing the tumor sites through tissue and through the blood. One explanation for this is that the leakiness of the tumor vasculature, the so-called enhanced permeability and retention effect (EPR) [122], helped the CT20p-loaded NPs accumulate within tumors. These results justify the next phase of testing using tumor-targeting nanoparticles for optimal delivery of CT20p in combination treatments to effectively eradicate cancerous cells.

Figures and Tables

Table 4. Comparison of CT20p with Anti-Microbial Peptides and Apoptosis-Inducing Peptides

Comparison of CT20p with Anti-Microbial Peptides and Apoptosis-Inducing Peptides					
PEPTIDE	SOURCE	SEQUENCE	% HYD	NET CHARGE	Structure
CT20p	Human	VITFVAGVLTASLTWKKMG	60	2	alpha
lactoferricin	Bos taurus	FKCRRWQWRMKKLGAPSITCVRRAF	48	1	beta
Indolicidin	Bos taurus	ILPWKWPWWPWRR	53	3	beta
Mellitin	Honey Bee	GIGAVLKVLTTGLPALISWIKRKRQQ	46	5	alpha
Brevinin 1	Frog	FLPVLAGIAAKVVPALFCKITKKC	66	4	unknown
Ranalexin	Frog	FLGGLIK/VPAMICAVTKKC	65	3	alpha
Cecropin A	Insect	KWKLFKKIEKVGQNIRDG/KAGPAVAVVGQATQIAK	45	6	alpha
Dermaseptin B2	Frog	ALWKTMLKKGLTMALHAGKAALGAAADTISQGTQ	54	3	alpha
Magainin 2	Frog	GIGKFLHSAKKGKAFVGEIMNS	43	3	alpha
CT20p REV	n/a	GMKKWITLSATLVGAVFTIV	60	2	n/a
KLA peptide	synthetic	KLAKLAKKLAKLAK	57	6	alpha
Bax a5-a6	Human	DGNFNWGRVVALFYFASKLVLKVPELIRT	52	2	alpha
BIM BH3	Human	MRPEIWI AQELRRIGDEFNA	40	0	unknown
BID BH3	Human	EDIIRNIARHLAQVGDSDR	40	0	unknown
BAK BH3	Human	GQVGRQLA/GDDINR	40	0	unknown

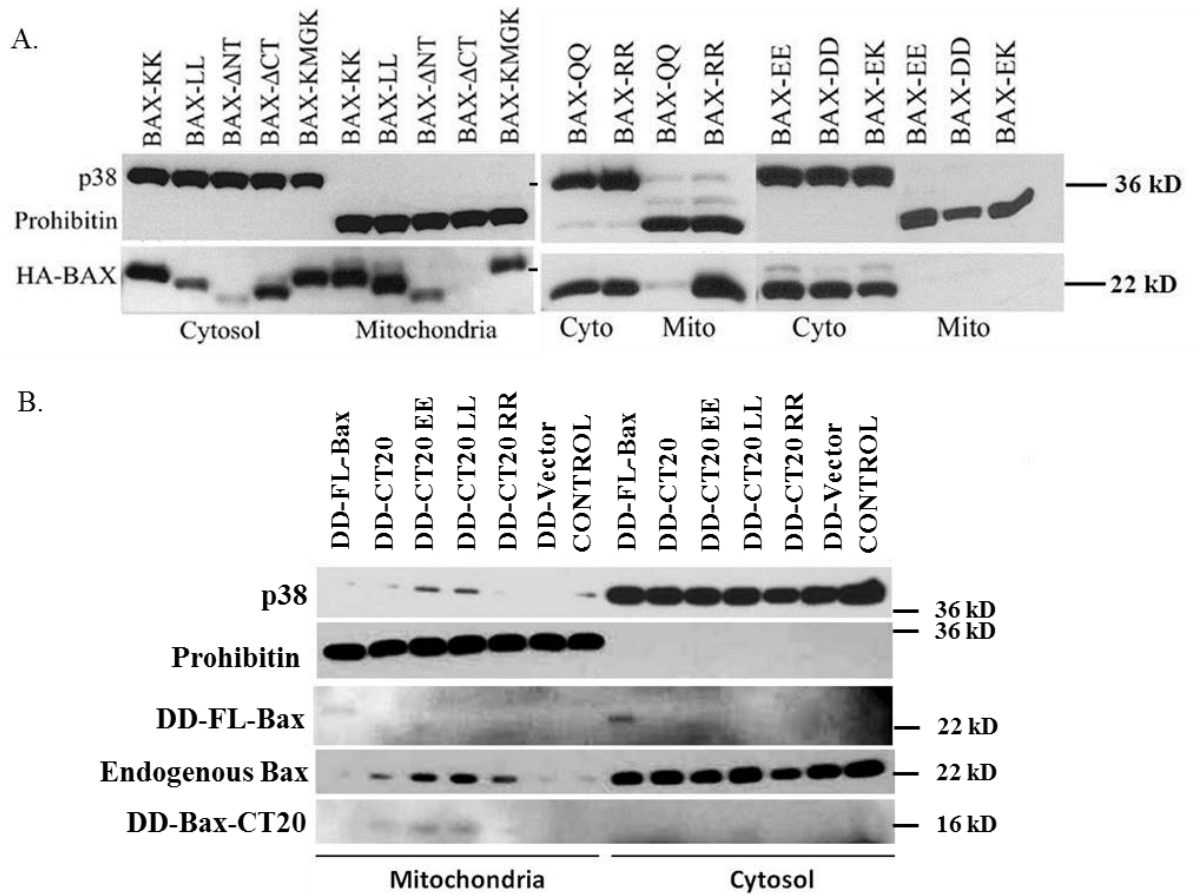


Figure 16 Lysines in CT20p, which is Based on the C-terminus of Bax, Contribute to Intracellular Localization.

(A-B) Mitochondrial translocation of HA-tagged wild type Bax (Bax-KK) and K189/K190 mutants, expressed in 293 cells using the Flp-In T-Rex system, was examined by immunoblot. p38 MAPK and Prohibitin were blotted for cytosolic and mitochondrial content, respectively. Data are representative of five independent assays. Images from full-length blots were cropped for concise presentation. (C) The mitochondrial translocation of DD-tagged Bax full-length (FL-Bax) and DD-tagged CT20 peptides, wild-type and EE, LL and RR mutants, was examined in Bax^{+/+} HCT-116 cells by immunoblot. Endogenous Bax was probed with anti-Bax antibody. p38 MAPK and prohibitin indicated cytosolic and mitochondrial content, respectively. DD-fusions were detected with an anti-DD antibody. Controls are cells transfected with empty vector or untransfected. Data are representative of two independent assays. Images from full-length blots were cropped for concise presentation.

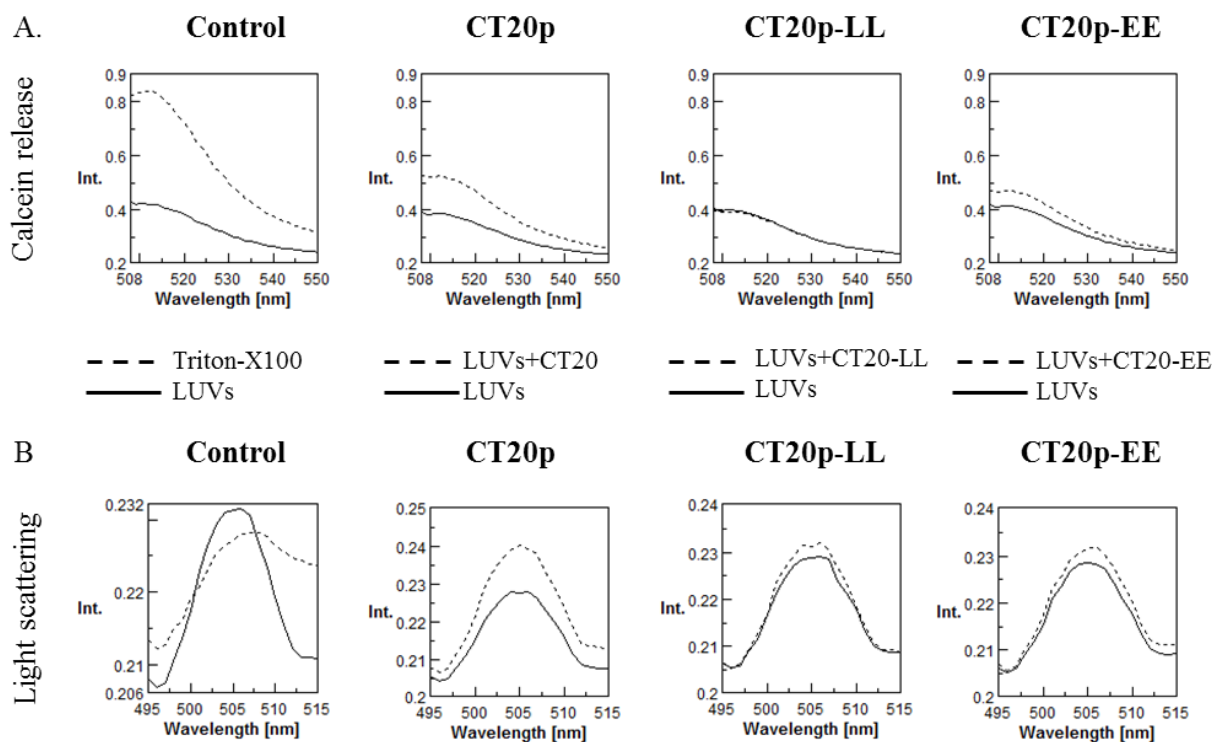


Figure 17. CT20p causes the Release of Sequestered Contents from Mitochondrial-like Lipid Vesicles without Loss of Membrane Integrity.

(A) CT20p was commercially synthesized and calcein-loaded mitochondrial-like LUVs prepared. Calcein release from CT20p-treated LUVs was measured as described in Experimental Procedures. Red lines indicate maximal release of calcein with Triton X-100. Blue lines indicate addition of LUVs and green lines (except for control) indicate treatment with CT20p or mutants. Dotted line is buffer alone. CT20 is the wild-type peptide and CT20-LL and CT20-EE are mutations of the double lysines (K189/K190 in the full-length Bax protein). (B) Light scatter analysis of LUVs from (A).

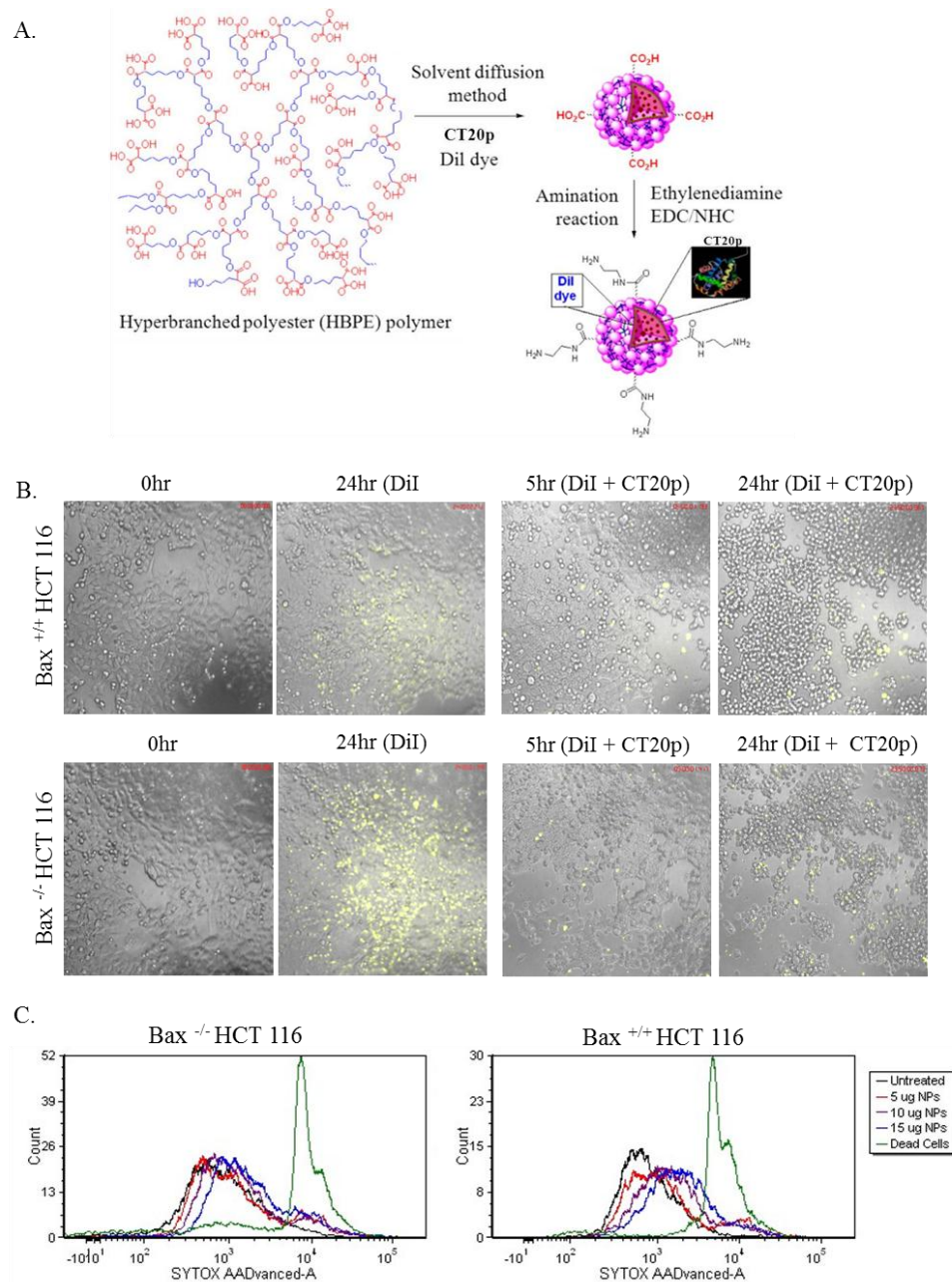


Figure 18. CT20pe can be Encapsulated in NPs for Delivery to Cells.

(A) Schematic representation of the three dimensional structure of aliphatic hyperbranched NPs. (B) HCT-116 cells were treated with NPs loaded with Dil or Dil + CT20p (0.07 nM) for 24 hours. Time-lapse movies were acquired as described in Experimental Procedures using a 10x air objective. For each sample, three different fields of view were acquired. (C) Bax^{+/+} and Bax^{-/-} HCT-116 cells were treated with NPs loaded with Dil at amounts of 5, 10 and 15 μ g for 24 hours and cell death was measured using Sytox AAD as described in Experimental Procedures. Results or images are representative “snapshots” of three independent experiments.

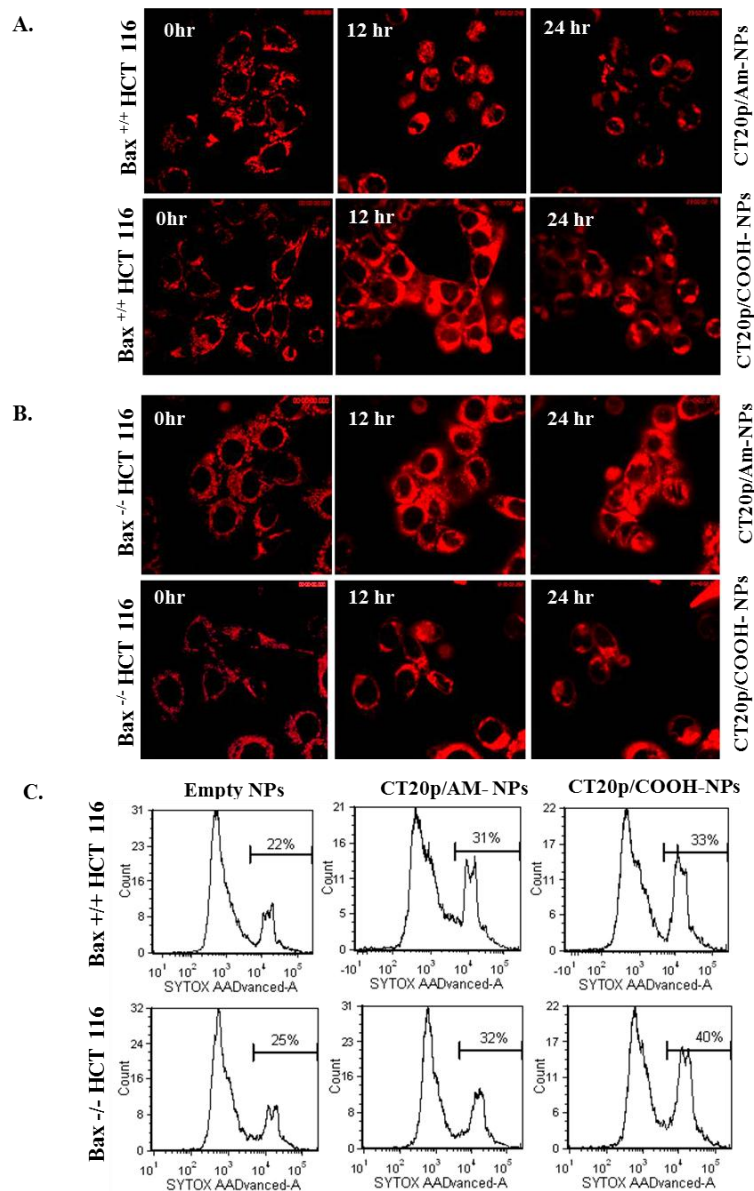


Figure 19. CT20p-NPs Kill Bax-containing or Bax-deficient HCT116 cells.

(A-B) Bax^{+/+} (A) and Bax^{-/-} (B) HCT-116 cells were treated with AM- or COOH-NPs loaded with CT20p (350 pM) for 24 hours. To visualize mitochondria, cells were treated with MitoTracker Red 580 and time-lapse movies were acquired as described in Experimental Procedures using a 63x Oil objective. For each sample, three different fields of view were acquired. Images are representative “snapshots” of three independent experiments. (C) HCT-116 cells were treated with CT20p-NPs (350 pM) and, after three hours, cell death was measured using Sytox AAD as described in Experimental Procedures.

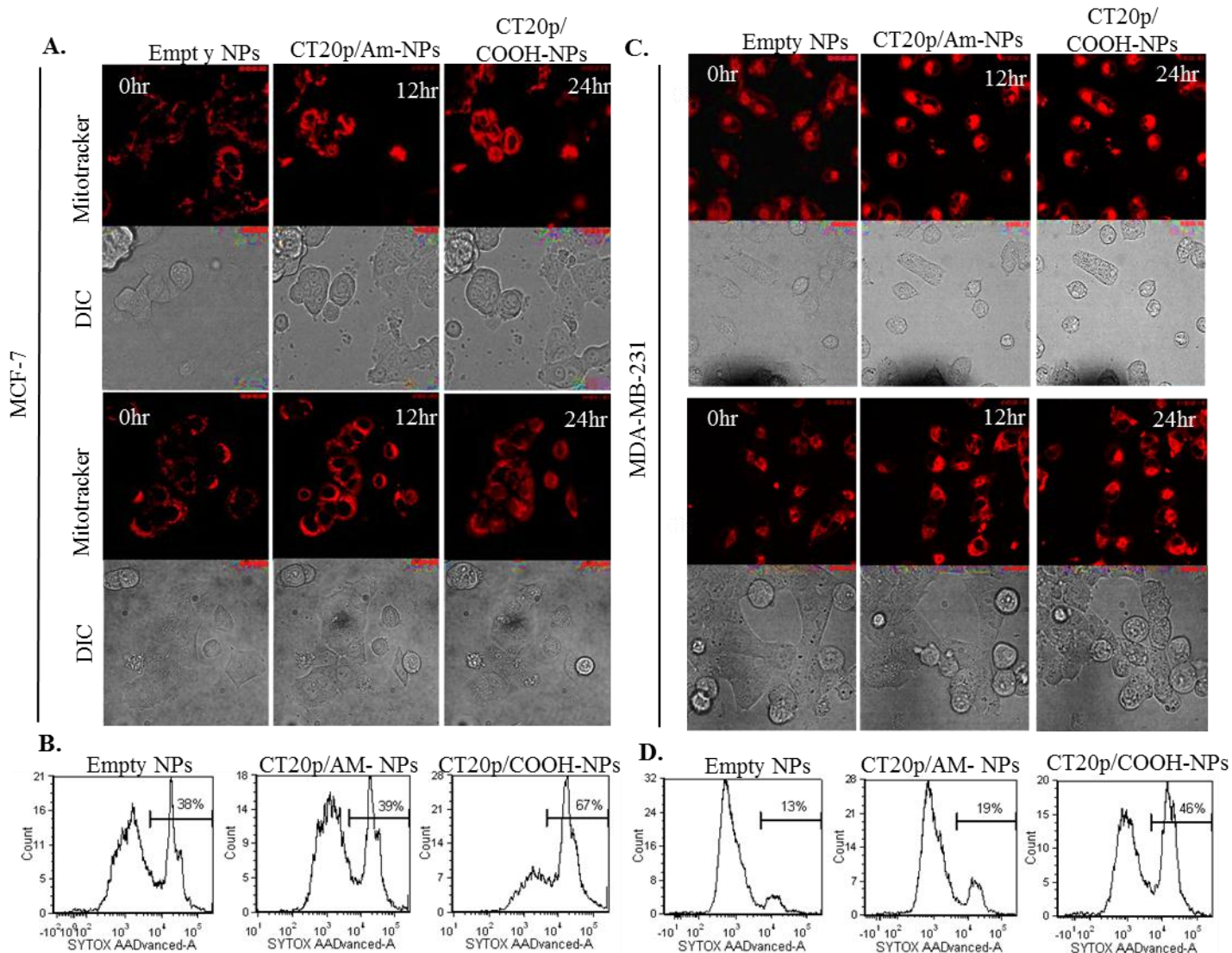


Figure 20. CT20p-NPs Kill Breast Cancer Cells.

(A, C) MCF-7 (A) or MDA-MB-231 (C) cells were treated with AM- or COOH-NPs loaded with CT20p (350 pM) for 24 hours. To visualize mitochondria, cells were treated with MitoTracker Red 580 and time-lapse movies were acquired as described in Experimental Procedures using a 40x Oil objective. Images are representative “snapshots” of three independent experiments. (B, D) MCF-7 (B) or MDA-MB-231 (D) cells were treated CT20p-NPs (350 pM) and, after three hours, cell death was measured using Sytox AAD as described in Experimental Procedures.

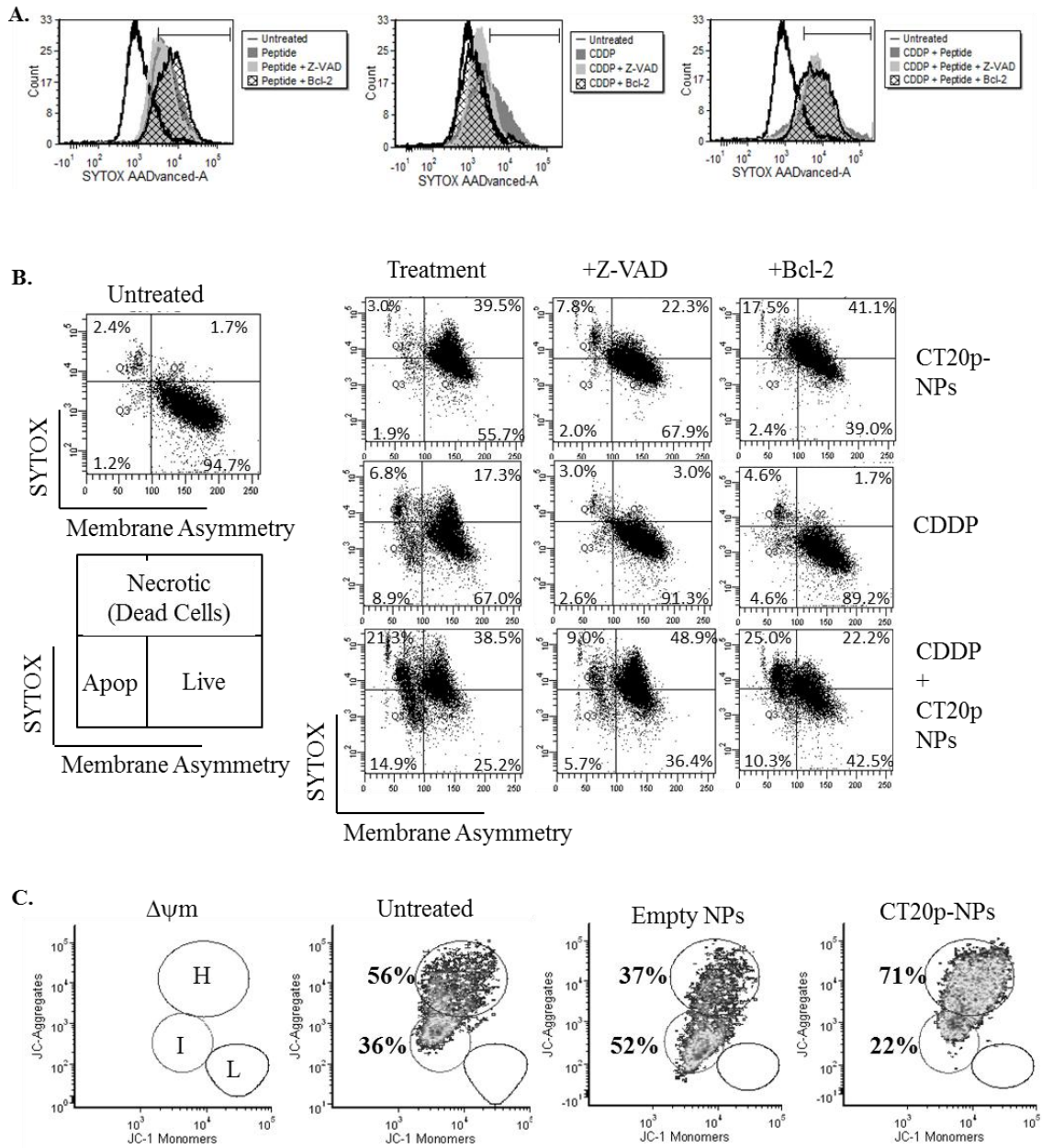
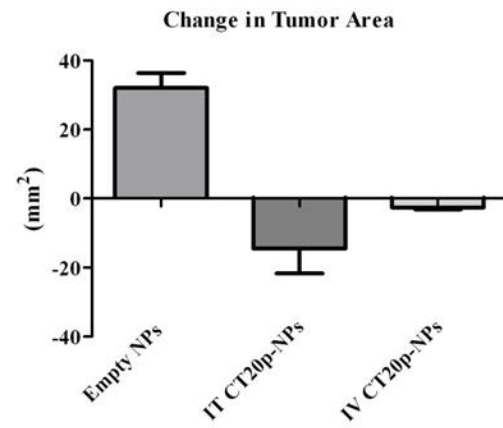


Figure 21. Mechanism of Death Mediated by CT20p is Effector Caspase Independent and Resistant to Bcl-2.

(A) MDA-MB-231 cells were treated with COOH-NPs encapsulated with CT20p (350 pM) and treated with ZVAD-Fmk and/or CDDP as described in Experimental Procedures. Cells were also transiently transfected with Bcl-2. Cell death was assayed with Sytox AAD. (B) MDA-MB-231 cells were treated as described in (A) and membrane asymmetry measured with a violet radiometric probe. Dot blots show a combination of results from Sytox (cell death) and changes in membrane symmetry. Data shown is representative of at least three independent experiments.

A.



B.

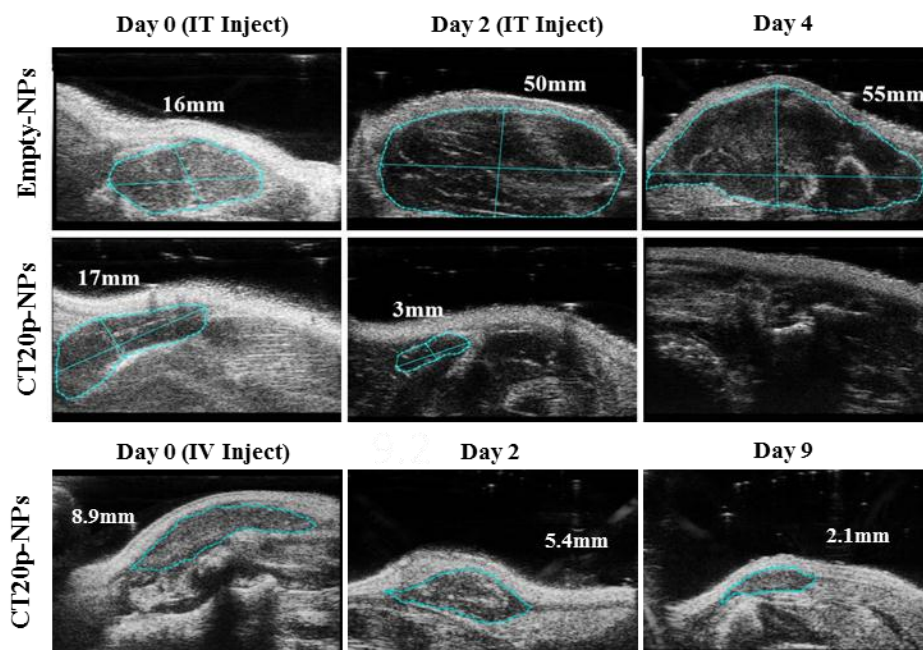


Figure 22. CT20p Induces Tumor Cell Death in vivo.

(A) MDA-MB-231 cells were implanted in nude mice and changes in tumor volume assessed by ultrasound as described in Methods. (D) Representative ultrasound image of tumor regression induced by treatment with the CT20 peptide. Results shown are representative of n=5.

CHAPTER 4: STABILIZATION OF THE TERTIARY STRUCTURE OF BAX IS DEPENDENT ON THE C-TERMINAL HELIX

Introduction

Molecular dynamics (MD) simulations of solved structures can give insight into the mechanism by which proteins fold, unfold and interact with the surrounding environment. This is a particularly powerful tool in understanding the dynamic nature of the Bcl-2 (B-cell lymphoma 2) family of proteins. Despite the functional division of the family into pro- and anti-apoptotic proteins, the tertiary structure and arrangement of amphipathic helices around a core hydrophobic helix is maintained throughout [53]. Additionally, these proteins retain a hydrophobic groove that is required for dimerization events that regulate the balance between survival and cell death [3]. Mutations within this groove have a deleterious effect on dimerization and subsequent activity of the affected proteins [59].

Bax, a member of the pro-apoptotic sub-family of Bcl-2 proteins, retains the characteristic helical packing and hydrophobic groove that are the hallmarks of this family. The NMR solved structure [10] shows 9 alpha helices, of which the $\alpha 5$ helix, imbedded within the protein, is the most hydrophobic [123], [124]. Bax also has an extensive hydrophobic groove spanning one face of the protein, and is comprised of helices 2, 3, 4, and 5. When Bax is in its cytosolic, monomeric form, the amphipathic $\alpha 9$ helix resides within the groove, and upon conformational change, the helix dissociates from the groove allowing for oligomerization [124]. This conformational change is purported to allow for translocation of Bax to the mitochondrial membrane due to the

exposure of the C-terminal helix and relaxation of the bulk of the protein releasing the $\alpha 5$ – $\alpha 6$ helices [17], [50].

Molecular dynamics simulations of Bax, and most other Bcl-2 proteins, are most commonly performed in an effort to better design inhibitors or activators [41], [52], [53]. Recently, however, a study of the stability of the protein under elevated temperatures revealed that the $\alpha 5$ helix maintained its secondary structure at 500K despite the apparent melting of the surrounding helices [123]. This suggests that the application of appropriate force fields in a generated, controlled environment can yield information on the stability or weaknesses of micro-domains within the protein. This information can be used to direct the generation of point mutations and deletion mutants of Bax to elucidate the mechanism by which it transitions from cytosolic to membrane bound form.

Previous *in silico* studies in our lab suggest that it is energetically favorable for the $\alpha 9$ helix to bind in a reverse orientation in the hydrophobic groove. In this orientation, the positively charged Lysine residues at positions 189/190 interact with the negatively charged glutamic acid and asparagine residues at positions 69 and 73 respectively. Analysis of the existing structure in comparison with selected mutations to residues 69 and 73 at the boundary of the hydrophobic groove will allow for a comparison of the global fluctuations in the tertiary structure of the protein, as well as localized distortions within the binding pocket. Similarly analysis of the C-terminal deletion mutant will indicate whether the occupation of the groove by the $\alpha 9$ helix contributes to stability of the protein.

Currently, there is one solved structure of isolated Bax (PDB ID 1F16) [10], with the only other complete structure (PDB ID 2K7W) complexed with a BH3 peptide [125]. The solution structure 1F16 is based on a purified protein expressed in *E.coli* and then isolated from the bacterial lysate with a cleavable N-terminal Chitin Binding Domain (CBD) [10]. This poses a challenge for accurate MD description of the behavior of the protein as proper folding of the N-terminus is essential for the maintenance of the inactive form of Bax [49]. Described within is a method by which an untagged, properly folded Bax and mutant variants can be expressed and purified in order to characterize the transition from monomer to oligomer.

Materials and Methods

Generation of Bax Mutants in Silico.

Based on the existing PDB file generated from the solved NMR structure of Bax [10], groove mutants were generated within the Visual Molecular Dynamics (VMD version 1.9) program [126]. Briefly of the 20 models generated from the NMR structure, model 6 was isolated from the source PDB file 1F16. This model was then used as the base model for subsequent deletions and point mutations. The single and double mutations generated were selected to simulate a charge reversal on residues 69 and 73. Additionally a CT20 deletion mutant was generated to remove the C-terminal 20 residues from full-length protein. The mutations function within the analysis component of VMD allowed for the generation of single point mutations, once the residue was mutated *in silico* the X, Y, and Z coordinates of the source PDB file were used to generate a new point spread function to describe the orientation of the atoms in the

mutated residue and any other changes in orientation in surrounding atoms. From this, VMD was directed to generate new PDB files containing the mutated residues.

Molecular Dynamics Simulations.

All MD simulations were carried out using GROMACS (GRoningen MACHine for Chemical Simulation) version 4.5.5 [127], [128], and computations were carried out on the Stokes Advanced Research Computing Center (The University of Central Florida). This was conducted in two steps. First the PDB files generated in VMD were ported into GROMACS using the *pdb2gmx* command. The protein was then placed in a box so that the distance between the protein and the edge of the box was 1.5 nm to satisfy the periodic boundary conditions. Since periodic boundary conditions are applied to the system, long-range interactions in the box were calculated using the smooth particle mesh Ewald algorithm [129]. Then using the *genbox* program, the box was filled and the protein solvated with water using either the TIP3P or SPC/E water model [130], [131]. Any latent charge on the protein was neutralized by the addition of either sodium or chloride ions. The applied force field for the generated topology used for these simulations was AMBER99SB-ILDN [132] because of the ability of the force field to describe torsional motion in side chains. To ensure that the AMBER99SB-ILDN force field contained sufficient parameters to describe the effects of the programmed constraints on the protein, the same simulations were run applying different force fields to the system. The force fields used were AMBER99SB [133], an less descriptive version of the AMBER99SB-ILDN force field, CHARMM27 [134], and OPLS-AA/L[135] all atom force field. MD runs to equilibrate the system were conducted using the

grompp preprocessor to prepare the topology files to determine the energy minimization (EM), temperature (300K, or 300-500K), and pressure equilibrium (2 bar). Once equilibrated, the position restraints were released and the production MD was run using a leap-frog algorithm to couple the position restraints with constant temperature and pressure [136] and data was collected. Data from the simulations was then analyzed for variations.

Analysis of Simulations.

The data generated from the wild type and mutant forms of Bax were analyzed after each MD run. The EM, temperature and pressure equilibration, density, root mean square deviation (RMSD), and radius of gyration were derived and plotted using GraphPad 5. The effects of the MD simulation on the molecule were able to be visualized in VMD.

Expression and Purification of the Full Length Bax Protein

Full-length Bax cDNA with a HMM sequence: (ATG TGG TGG CGC CTG TGG TGG CTG CTG CTG CTG CTG CTG CTG CTG TGG CCC ATG GTG TGG GCC) was cloned into pcDNA6/His B vector for expression in mammalian system. Sequencing was done to ensure that the ATG was on the HMM sequence and that the FL BAX was properly oriented in the vector. 293T cells were grown in T75 flasks in 20mL DMEM supplemented with 10% FBS and treated with 1% penicillin/streptomycin. Cells were grown to 75% confluence before transfection.

Cells were transfected according to Mirus LT1 protocol in complete DMEM. The cells were also treated with blastocidin to select for cells expressing the vector. Stably

expressing cells were expanded into T75 flasks to maximize protein yield. The cells were transitioned to a serum free media to facilitate the purification process. Media from the flasks was collected every 48 hours and concentrated through 3kD concentrator down to 2mL volumes. The media was then buffer exchanged with 20 mM Bis-Tris buffer supplemented with 50mM L-Glutamic acid and 50 mM L-Arginine at pH 7 to prepare for ion exchange chromatography (IEX). The protein was passed over a UnoQ anion exchange column (BioRad). The protein was eluted with a Bis-Tris buffer containing 1M KCl and was collected for size exclusion chromatography (SEC).

The eluted protein was then run through a de-salting column prior to SEC. Bax was then run through a Superdex 200 (GE) size exclusion column using the Bis-Tris buffer from the IEX for elution (flow rate 0.10 mL/min). The peak fractions were collected for analysis.

SDS-PAGE and Western Blotting.

Western blots on the Bax fractions were run at each step of the purification process using 12-15% SDS-PAGE gels, with the protein transferred to PVDF membranes and probed with N-20 (Santa Cruz), for endogenous Bax, this was followed by the appropriate secondary antibodies conjugated to horseradish peroxidase (HRP) and visualized with enhanced chemiluminescence kit (Pierce). Molecular weight markers (SeeBlue Plus 2 (Invitrogen)) were used to approximate the position of protein bands in blots. Gels were also stained with coomassie blue to check for protein purity.

Results

The ability for Bax to undergo conformational change during apoptosis is necessary for the protein to translocate to the mitochondria. A thorough analysis of the wild type protein analyzed against the individual amino acid contribution of specified point mutations and C-terminal deletion mutant will provide insight into the regions of instability within the protein that may contribute to its transition state. The findings of the molecular dynamics simulations yield important information as to the ability for mutant variations of the protein to function in a predicted manner, and therefore serve as a guide for the design of the expression system to purify Bax.

Energy Minimization and Validation of Force Fields.

The initial Bax structure, obtained from set of coordinates model 6 of the 20 representative NMR structures was solvated, neutralized, then relaxed through energy minimization using the GROMACS MD engine, mdrun. This is necessary prior to running a production MD to ensure that the applied force field adequately describes the system. The minimization process allows for the determination of the potential energy (E_{pot}), which is measured in kJ/mol. For the energy minimization to be considered successful the graph of the potential energy should converge and the value on which it converges should be negative. An analysis of the potential energies of 1F16 (WT Bax), the groove mutants (E69R, N73R, and E69R,N73R), and the C-terminal deletion mutant (DCT) (Figure 23) show that the applied force field, AMBER99SB-ILDN, is sufficient to describe the system as all structures converged and were negative with values ranging between -2.0×10^6 - 11.85×10^6 kJ/mol. The initial stability of the structure is linked to the potential energy in that the lower the E_{pot} the more stable the structure is prior to the

dynamics run. Based on an analysis of the E_{pot} for each structure, the least stable is the DCT and the most is the N73R mutant.

As stated previously, the applied force field for these simulations was the AMBER99SB-ILDN force field. This was chosen in part because of the refinement of the AMBER99SB protein force field. The force field better describes χ_1 torsional potentials determined by rotation about the Φ angle [132]. This allows for a better assessment of the contribution from the torsional energies over the AMBER99SB force field, and more completely describes the protein energetics. Because of this, the AMBER99SB-ILDN provides a better description of the contribution of point mutations to the stability and structure of the system.

The Validity of this force field on the system was tested by evaluating and comparing the E_{pot} of the WT Bax and DCT models minimized with different force fields applied to the system. The tested force fields were CHARMM 27, AMBER99SB, and OPLS-AA/L, and the E_{pot} for WT Bax and DCT under each force field was compared for variation (Figure 24). Based on the energy minimization, the CHARMM27 force field is a not suitable for this system as determined by the difference in E_{pot} compared to the other force fields. This is expected because CHARMM27 is optimized for describing nucleotides and small peptides [134]. The E_{pot} for the structure as described by the AMBER99SB force field is comparable to that of the AMBER99SB-ILDN also as expected since the only significant difference is the inclusion of the contribution of the χ_1 torsional potential by the ILDN variation. There was a measurable, but acceptable difference in the E_{pot} when the OPLS-AA/L force field was applied to the structure. The

energy minimization was calculated to be the lowest with this force field, despite the fact that is very similar to the AMBER force field. The difference lies in the AA portion of the OPLS parameters includes all of the atoms explicitly [135]. There also may be a contribution of the water model to the energy of the system as the SPC/E water model was used instead of the TIP3P water model. The potential for the TIP3P model is represented as such:

$$E_{ab} = \sum_i^{\text{on } a} \sum_j^{\text{on } b} \frac{k_C q_i q_j}{r_{ij}} + \frac{A}{r_{00}^{12}} - \frac{B}{r_{00}^6}$$

Where q_i and q_j partial charges, r_{ij} is the distance between charged sites (the oxygen atoms in the water molecules), and A and B are the Lennard-Jones parameters [130].

In the SPC/E water model, the potential is adjusted to correct for the dipole moment on a polarized water molecule:

$$E_{pol} = \frac{1}{2} \sum_i \frac{(\mu - \mu^0)^2}{\alpha_i}$$

This allows for a more accurate representation of the contribution of water to the system, and its effects on the structure [130].

MD Simulations and Analysis of Protein Stability.

MD simulations conducted within GROMACS show movement of the structures over time and under constant temperature and pressure. The constrained atomic positions were released and the protein was allowed to move freely for 10ns. The initial runs on the WTBox, the groove mutants and the DCT were run at 300K and 2 bar pressure. Figure 25 shows the radius of gyration of the each structure. The gyration, or

general movement about the center of the protein, is an indicator of the stability of the structure over time. All mutations were relatively stable as indicated by the relatively static movement, with the exception of DCT which began to fluctuate greatly as the simulation progressed. A calculation of the root mean square deviation (RMSD) of each structure shows (Figure 26) that, relative to the original positions, there is very little movement, again with the exception of DCT. The increase in the RMSD corresponds with the increase in the radius of gyration in the simulation indicating that the deleted C-terminus was conveying some stability to the overall structure.

In order to further probe the contribution of the C-terminus to the overall stability, the protein was subjected to a series of temperature increases. This melt study was conducted using the OPLS-AA/L force field and validated in the other force fields described above. The temperature intervals were 300K, 400K, and 500K, and both WT_{Bax} and DCT were subjected to these conditions. Figure 27 shows the modeled structures at each temperature with the applied trajectories from each simulation. The structures were visualized in VMD. The WT_{Bax} was able to retain its secondary structure as the protein was melted. This is particularly evident in the maintained helicity of the hydrophobic core ($\alpha 5$ helix). This corresponds to the findings in a previous study that reported that the core stability of Bax lies in the helix [123]. To determine if the absence of the C-terminus would affect the stability of the protein the same conditions were applied to the DCT structure. The absence of the C-terminal helix has a dramatic effect on the stability of the protein as the protein lost a majority of its secondary structure with each increase in temperature. A look at the change in the

RMSD (Figure 28) verified that WT Bax is a far more stable structure than its DCT derivative.

Protein Expression.

One of the challenges to studying Bax is that, because its activity is regulated through the proper folding of both the N- and C- termini, expressing the protein with a terminal tag may affect the activity. To combat this, a novel expression scheme was developed. Rather than expressing the protein in bacteria, the protein was expressed in 293T cells with a cleavable synthetic secretion sequence attached to the N-terminus. This sequence was derived from Hidden Markov Modeling of known native secretory sequences [137]. The addition of this sequence allows Bax to be directed to the endoplasmic reticulum and then shuttled out of the cell. Figure 28 shows that Bax is contained in the media as shown by coomassie stain and western blot (Figure 28A).

The concentrated protein from the media was then run through a size exclusion column. Based on the dimensions of the column and the pores of the resin, a protein of Bax 's size (22kD) is expected to elute off of the column at approximately 17mLs. An analysis of the absorbance at 280 shows a very intense peak that apex is at ~17.8mLs (Figure 28B). The presence of Bax in this fraction was verified again by western blot (Figure 28C). The recovered protein from the purification can now be assessed for function and also, depending on purity, for structure.

Discussion

Within the Bcl-2 family there is a conserved series of structural motifs and functional homology [3]. Since Bax is dynamic in that it has a cytosolic and membrane

bound form, any insight into what regulates the transition can be leveraged into the design of inhibitors or activators to manipulate the protein function. The molecular dynamics approach used in this study examines the contributions of functional domains and specific residues on the stability of the overall structure. These simulations indicate that helical packing about the hydrophobic core is dependent on the occupation of the hydrophobic groove. In the absence of the C-terminus the protein relaxes compared to the wild type protein. This relaxation would allow for membrane docking as the relaxed structure would expose hydrophobic region to lipid membranes.

Validation of the *in silico* modeling with expressed, purified Bax and Bax mutants can ultimately elucidate the mechanism of action by which the protein makes its transition to the membrane and adopts its oligomeric form. While this work is incomplete, the simulations component alone gives a good deal of information regarding the stability of various mutants, and also illustrates the need for additional structural studies, particularly a resolved structure of Bax that is not obtained from a tagged expression of the protein. Since most molecular dynamics simulations of Bcl-2 family members seek to determine binding partners for the design of inhibiting or activating compounds and peptides, the solved structure of the protein must be accurate. Additionally, the generation of pure, properly folded Bax can be used in a variety of biophysical and molecular biology approaches to determine structural and functional characteristics that have not been previously described.

Figures and Tables

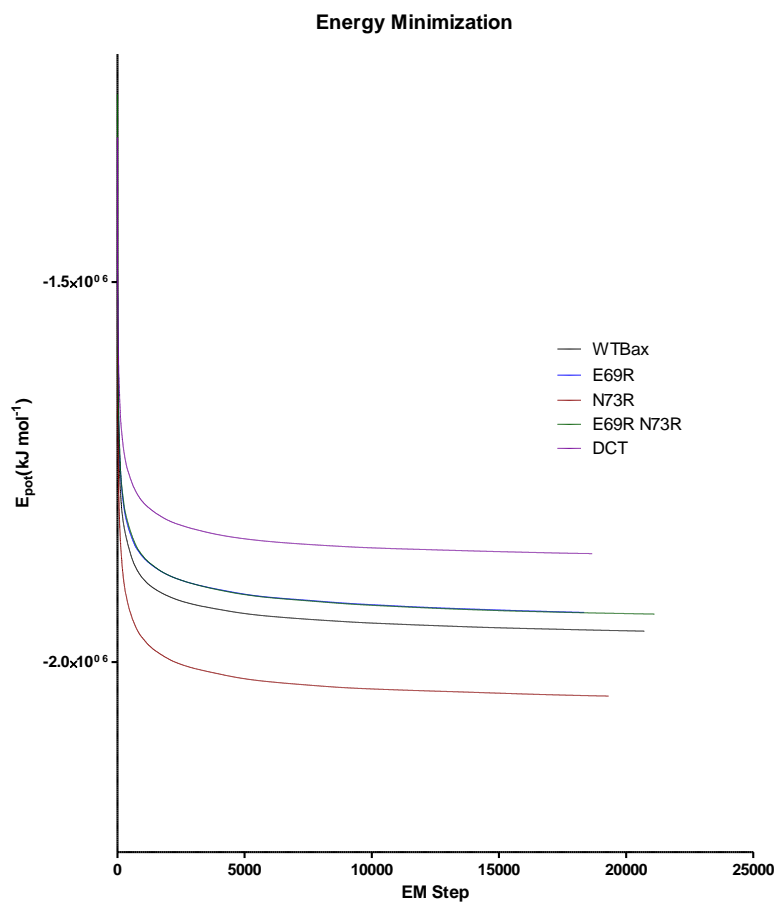


Figure 23. A Comparison of the Energy Minimization of Bax Variants.

The energy minimization of WTBox and four mutant variants were compared. The E_{pot} is calculated in kJ/mol and is used as a measure of the stability of a system. Convergent curves indicate that the applied force fields are correct. The more negative the E_{pot} the more potential energy the system has at the onset of the simulation.

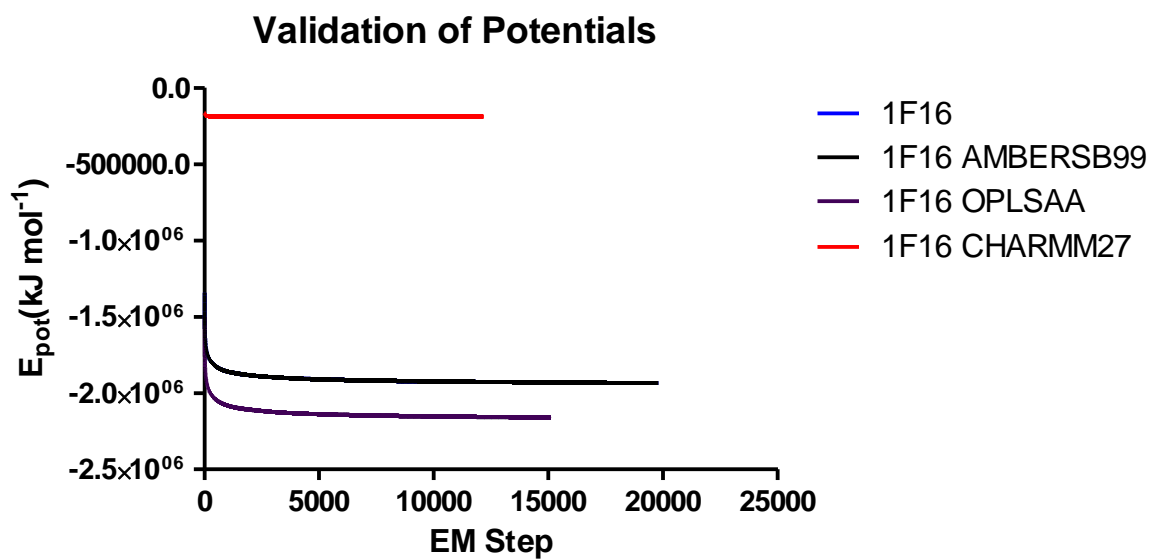


Figure 24. Validation of the AMBER99SB-ILDN Force Field.

Validation of the AMBERSB99-ILDN force field was conducted by running the WTBox model system through an energy minimization. The validation force fields chosen were a less descriptive AMBERSB99, a more descriptive OPLS-AA/L, and a non-descriptive CHARMM 27 force field.

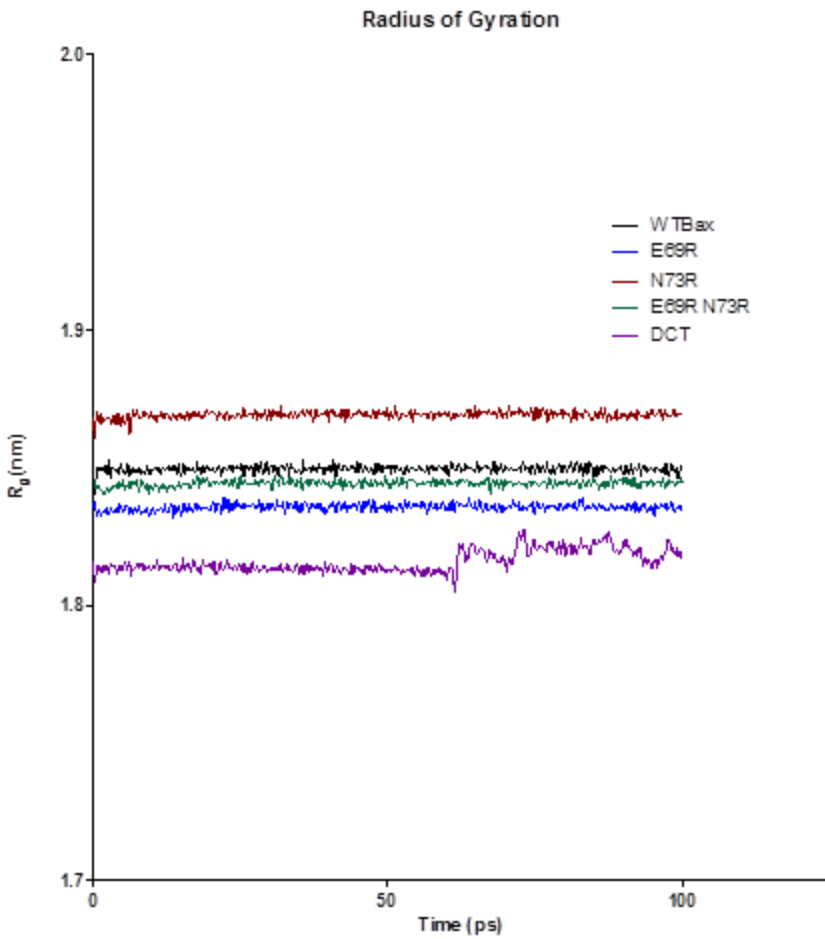


Figure 25. Radius of Gyration Indicates Stability of the Structure in the System.

Radius of gyration about the center was measured for each structure. The linearity of the plot for each structure is indicative of the stability of the protein in the system. Variations in the linearity, as seen in the DCT are due to instability in the backbone structure of the protein.

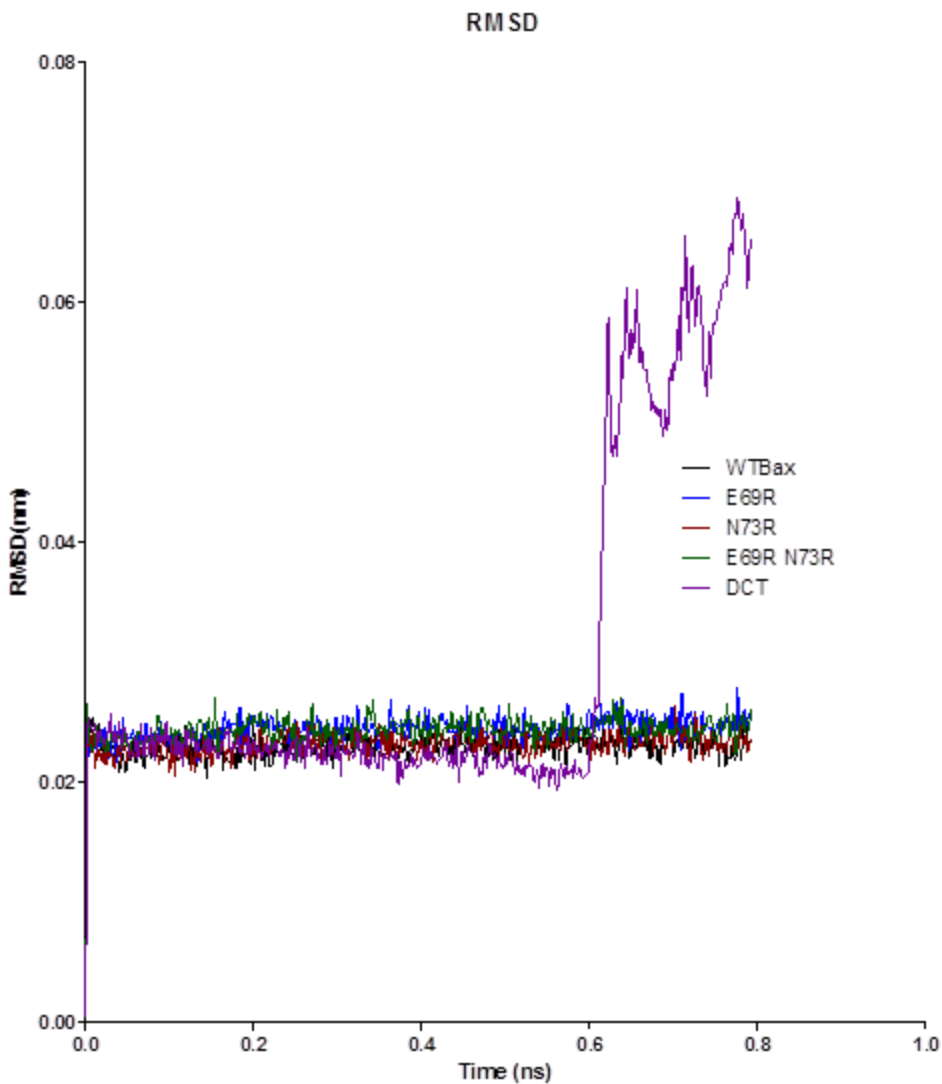


Figure 26. Root Mean Square Deviation of the Structure as Compared to the Initial PDB File.

The RMSD of each structure was calculated for the atomic positions after simulation as compared to the initial atomic position from the PDB file. The linearity correlates to the stability of the structure. Variations in the linearity indicate significant movement of the atomic positions during the simulation

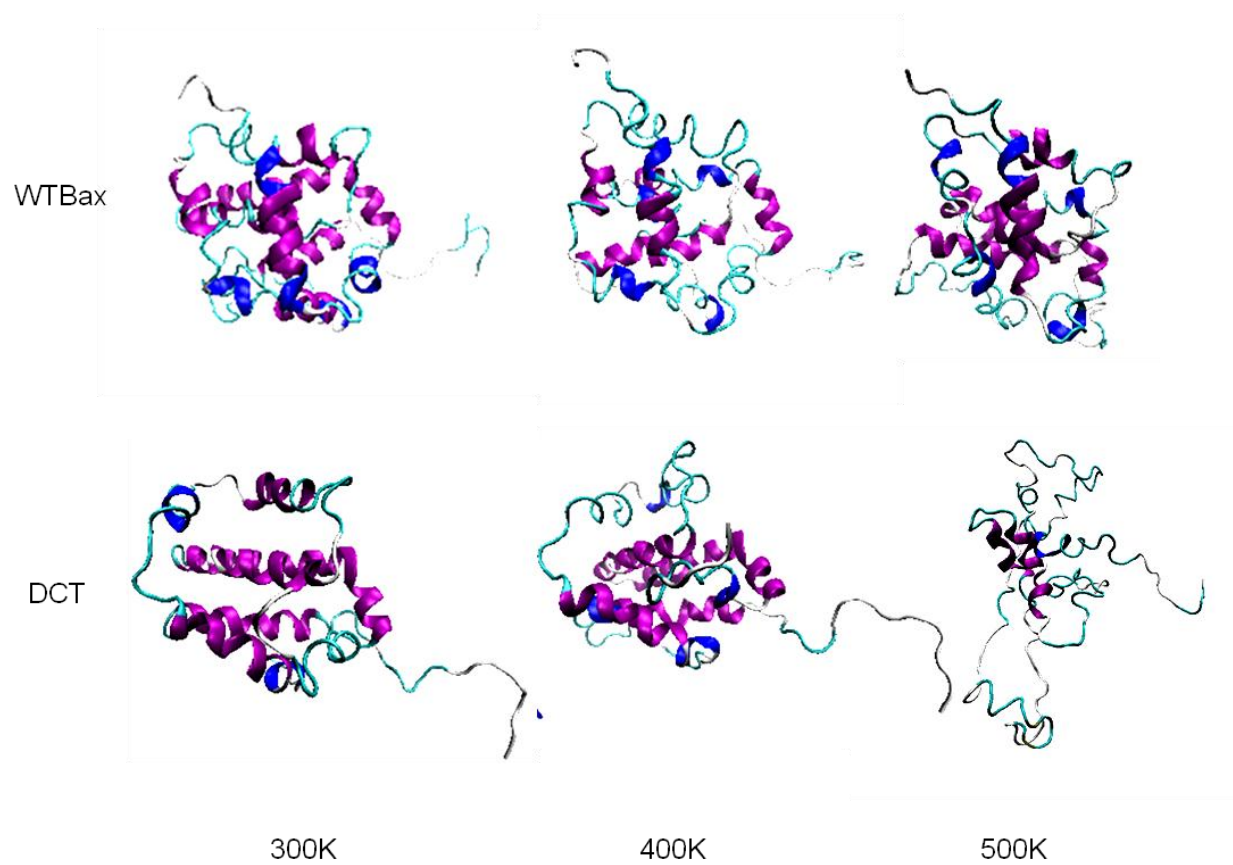


Figure 27. Structural Changes as a Result of Increase in Temperature

Visualization of the protein after simulation at each time step shows significant difference in the secondary structure. Alpha helices are denoted in purple, light blue indicates an elongated or random structure, and white sections are disordered.

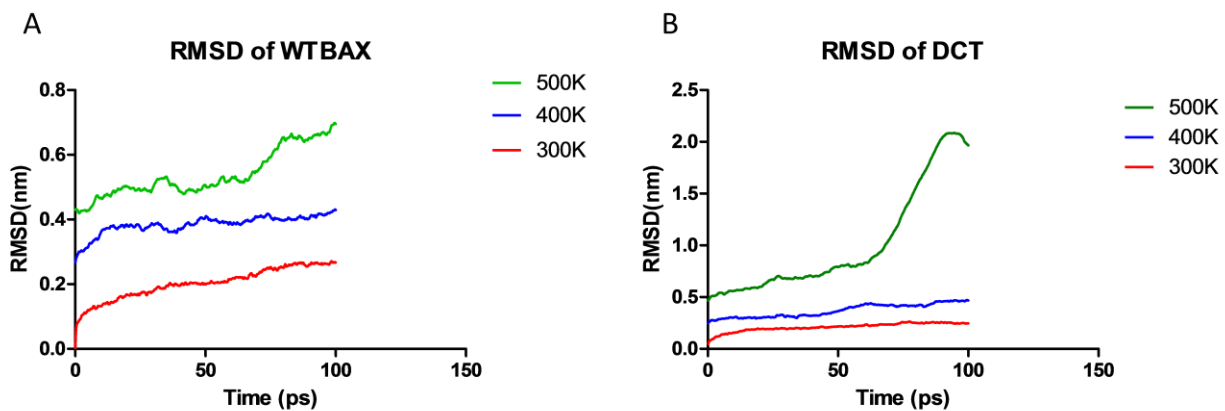


Figure 28. RMSD of WTBox and DCT at Each Temperature Step.

RMSD calculations for both WTBox and DCT were measured for each temperature step. The RMSD is measured in nm from the original position. Increase in RMSD correlates to protein instability. The contribution of the C-terminus is seen in a comparison of the RMSD from WTBox and DCT.

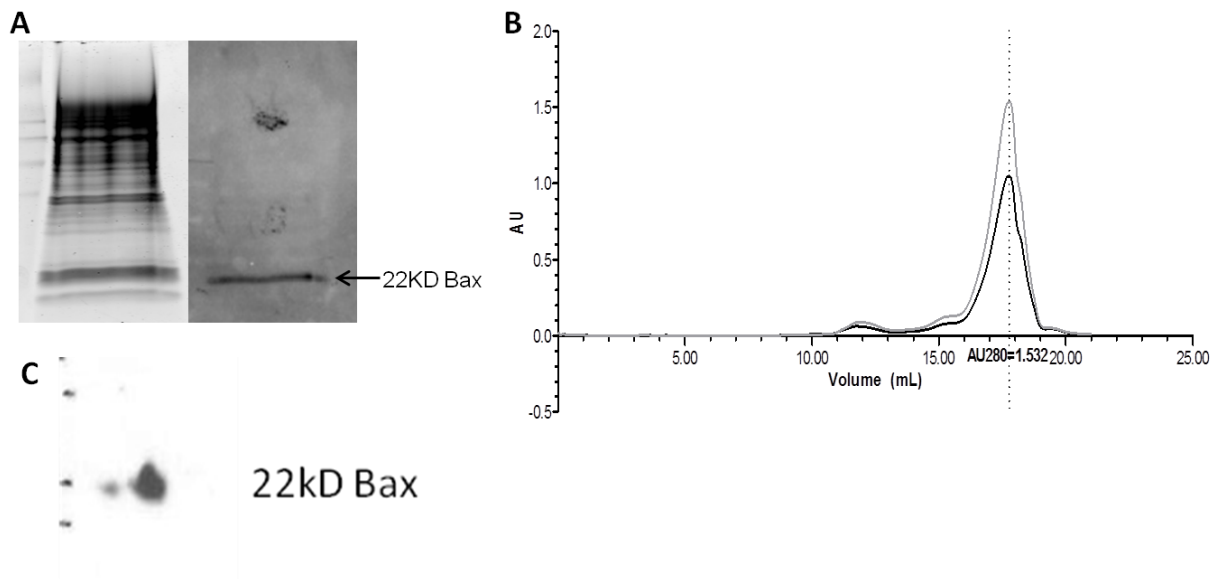


Figure 29. Verification of the Presence of Bax from the Mammalian Expression System.

(A) Coomassie stain of Bax in DMEM media after expression and secretion in 293T cells. Bax was detected by western blot in this sample. (B) Concentrated protein was run through a size exclusion column and the peak fraction was collected. (C) Western blot analysis of peak fraction proteins shows a strong 22kD band corresponding to Bax.

CHAPTER 5: CONCLUSION

The results presented in the preceding chapters describe a previously unrecognized role for the pro-apoptotic protein known as Bax in the regulation of bioenergetics. This observation prompted further exploration into the structure and function of Bax. These studies have revealed that the C-terminal helix retains the ability to translocate to the mitochondria and can promote a non-apoptotic cell death. These results are consistent with data from structural studies of full-length, untagged Bax which show that the C-terminal trans-membrane domain plays a key role in the overall stability of Bax. When taken together, these results have laid the groundwork for additional studies on Bax structure and function and have shed light on a viable path towards developing new therapeutic agents to modulate Bax activity.

During embryogenesis, Bax plays a crucial role in normal tissue development; the absence of Bax/Bak either results in death *in utero*, or severe developmental defects, usually involving an abnormal accumulation of cells [138]. Classically described as a killer protein, overexpression of Bax in cell culture leads to mitochondrial membrane disruption and propagation of the apoptotic signal. Like many of the Bcl-2 family members, Bax is a target for drug design because of its role in apoptosis. Efforts to design drugs to activate Bax, particularly in cancer cells, have been met with limited success. Attempts to understand the mechanism of Bax translocation and poration of the mitochondria have had limited success.

The dynamic functionality of the protein is apparent from the determination that Bax has a supporting role in mitochondrial energy production. While a majority of the

protein does reside in the cytosol in the absence of an apoptotic signal, there is a detectable amount of Bax at the mitochondrial membrane. The mechanism by which Bax contributes to the maintenance of bioenergetics in the cell remains to be elucidated. However, it was determined that this non-apoptotic function was not dependent on the C-terminus, and the effect could be diminished by over-expression of Bcl-2. This discovery indicates that modulation of Bax activity, or its interactors in this yet to be described mechanism can skew the cell's bioenergetics to either a glycolytic or oxidative phosphorylation state. With Bax being reported to bind to voltage regulating proteins at the mitochondrial membrane interface, exploring these interactions is the most reasonable direction to pursue in an attempt to elucidate a mechanism for this previously undescribed, non-apoptotic function.

To utilize Bax therapeutically, particularly in cancer, the classical approach has been to activate it using small molecules or peptides to bind to the BH3 region and force the conformational change into the active form. Furthermore, peptides derived from Bax are typically used to tease out the function of the whole protein, but not as therapy. Examination of the C-terminus of Bax, the putative membrane binding domain of the protein, reveals that it bears many of the features of antimicrobial peptides. Herein is the discovery that the CT20p, derived from the C-terminus conveys cytotoxicity to cells through a non-apoptotic mechanism. The membrane binding region, when isolated and delivered into the cell, triggers a series of events that are quantifiable, but do not correspond with classical apoptotic events such as the activation of caspases. This unique characteristic offers a therapy that is potent with limited off target effects

because the therapeutic target is negatively charged membranes such as the mitochondrial membrane. The CT20p also increases the sensitivity of cells towards existing chemotherapies, indicating that the peptide is a sensitizer that can be used in combination therapy. While the true mechanism of the peptide is not described here, further examination of how the peptide conveys cytotoxicity will help to direct the design of more potent membrane disrupting peptides, which can prove to be more effective than commonly used chemotherapies in the treatment of certain cancers.

These two discoveries on the function of Bax lead back to a poor understanding of the structure and the ability of the protein to self-regulate. The bio-energetic function is not dependent on the C-terminus outside of the specific targeting to the mitochondria. Likewise, the cytotoxicity of the CT20p is not dependent on the other putative membrane binding regions of the protein. The contribution of computational modeling, in an effort to understand the molecular dynamics of Bax, yields vital information in terms of regions of instability. Also, it indicates the generation of a deletion mutant may not result in a protein that functions as anticipated. These discoveries underscore the need to re-examine the way that Bax behaves, and precisely how the conformational change is regulated. Without a clear understanding of the means by which Bax is regulated, the potential utility of these discoveries loses value.

The therapeutic mechanisms behind the manipulation of Bax regulation are often overlooked possibly because the protein is characterized in the literature solely as a driver of apoptosis. As a result, the typical techniques, such as generating deletion mutants or isolating regions to study Bax components are not as informative as they

could be because success of the manipulation is measured in terms of activation of the intrinsic apoptotic cascade. A thorough examination of how the Bax structure changes in response to environmental cues could yield insight into its oligomerization and membrane binding activities. The preliminary success of the CT20p is because it was isolated not to study how it functions as part of Bax, but rather to see if it could retain its membrane binding ability absent of the rest of the protein. The potent cytotoxic effect of the peptide alone opens up a series of questions involving the evolution of Bax and the evolutionary, endosymbiotic relationship of the mitochondria in the cell. Computational modeling of the behavior of the protein in the presence and absence of the C-terminus yields insight into how Bax may have adapted to modulate its interactions with the mitochondria.

Collectively, this work brings to the field a novel, homeostatic function of Bax through the activation of a small fraction of the monomeric, cytosolic Bax under non-apoptotic conditions. Because of this, inhibition of Bax may be used to sensitize a cell to nutrient deprivation or chemotherapies by forcing the cell into a certain metabolic state. The last 20 residues of the C-terminus of Bax are not required for this function, but do contain a number of features characteristic of antimicrobial and membrane disrupting peptides. As such, the CT20p derived from these residues is able to convey cytotoxicity in the absence of death signals, and this cytotoxicity appears to be independent of the apoptotic machinery. Additionally these terminal residues may also serve as a regulatory domain for the protein as a whole.

APPENDIX A: COPYRIGHT PERMISSION

7/9/12

Rightslink® by Copyright Clearance Center



RightsLink®

Home

Account Info

Help



ACS Publications

High quality. High impact.

Title: Rational Development of a Cytotoxic Peptide To Trigger Cell Death

Author: Rebecca J. Boohaker, Ge Zhang, Michael W. Lee, Kathleen N. Nemeč, Santimukul Santra, J. Manuel Perez, and Annette R. Khaled

Publication: Molecular Pharmaceutics

Publisher: American Chemical Society

Date: Jul 1, 2012

Copyright © 2012, American Chemical Society

Logged in as:
Rebecca Boohaker

LOGOUT

PERMISSION/LICENSE IS GRANTED FOR YOUR ORDER AT NO CHARGE

This type of permission/license, instead of the standard Terms & Conditions, is sent to you because no fee is being charged for your order. Please note the following:

- Permission is granted for your request in both print and electronic formats, and translations.
- If figures and/or tables were requested, they may be adapted or used in part.
- Please print this page for your records and send a copy of it to your publisher/graduate school.
- Appropriate credit for the requested material should be given as follows: "Reprinted (adapted) with permission from (COMPLETE REFERENCE CITATION). Copyright (YEAR) American Chemical Society." Insert appropriate information in place of the capitalized words.
- One-time permission is granted only for the use specified in your request. No additional uses are granted (such as derivative works or other editions). For any other uses, please submit a new request.

BACK

CLOSE WINDOW

Copyright © 2012 [Copyright Clearance Center, Inc.](#) All Rights Reserved. [Privacy statement.](#) Comments? We would like to hear from you. E-mail us at customercare@copyright.com

<https://s100.copyright.com/AppDispatchServlet>

APPENDIX B: IACUC APPROVAL LETTERS



Office of Research & Commercialization

9/30/2011

Dr. Annette Khaled
Biomolecular Science Center
BRA
12722 Research Parkway
Orlando, FL 32826

Subject: Institutional Animal Care and Use Committee (IACUC) Protocol Submission

Dear Dr. Annette Khaled:

This letter is to inform you that your following animal protocol was re-approved by the IACUC. The IACUC Animal Use Renewal Form is attached for your records.

Animal Project #: 10-45
Title: Identification of regulatory domains that mediate the membrane-binding of BAX.

First Approval Date: 10/6/2010

Please be advised that IACUC approvals are limited to one year maximum. Should there be any technical or administrative changes to the approved protocol, they must be submitted in writing to the IACUC for approval. Changes should not be initiated until written IACUC approval is received. Adverse events should be reported to the IACUC as they occur. Furthermore, should there be a need to extend this protocol, a renewal must be submitted for approval at least three months prior to the anniversary date of the most recent approval. If the protocol is over three years old, it must be rewritten and submitted for IACUC review.

Should you have any questions, please do not hesitate to call me at (407) 882-1164.

Please accept our best wishes for the success of your endeavors.

Best Regards,

A handwritten signature in cursive script, appearing to read 'Cristina Caamaño'.

Cristina Caamaño
Assistant Director

Copies: Facility Manager (when applicable.)



THE UNIVERSITY OF CENTRAL FLORIDA
INSTITUTIONAL ANIMAL CARE and USE COMMITTEE (IACUC)
Re-Approval to Use Animals

Dear Dr. Annette Khaled,

Your application for IACUC Re-Approval has been reviewed and approved by the UCF IACUC Committee Reviewers.

Approval Date: 9/29/2011

Title: Identification of regulatory domains that mediate the membrane-binding of BAX.

Department: Biomolecular Science Center

Animal Project #: 10-45

Expiration: 10/5/2012

You may purchase and use animals according to the provisions outlined in the above referenced animal project. This project will expire as indicated above. You will be notified 2-3 months prior to your expiration date regarding your need to file another renewal.

Christopher Parkinson, Ph.D.
IACUC Chair

Approved Renewed



Office of Research & Commercialization

9/30/2011

Dr. Annette Khaled
Biomolecular Science Center
BRA
12722 Research Parkway
Orlando, FL 32826

Subject: Institutional Animal Care and Use Committee (IACUC) Protocol Submission

Dear Dr. Annette Khaled:

This letter is to inform you that your following animal protocol was approved by the IACUC. The IACUC Use Approval Form is attached for your records.

Animal Project #: 11-56
Title: Pilot study to Examine Anti-tumor Activity of Bax Peptide

First Approval Date: 9/29/2011

Please be advised that IACUC approvals are limited to one year maximum. Should there be any technical or administrative changes to the approved protocol, they must be submitted in writing to the IACUC for approval. Changes should not be initiated until written IACUC approval is received. Adverse events should be reported to the IACUC as they occur. Furthermore, should there be a need to extend this protocol, a renewal must be submitted for approval at least three months prior to the anniversary date of the most recent approval. If the protocol is over three years old, it must be rewritten and submitted for IACUC review.

Should you have any questions, please do not hesitate to call me at (407) 882-1164.

Please accept our best wishes for the success of your endeavors.

Best Regards,

Cristina Caamaño
Assistant Director, Research Program Services
Office of Research and Commercialization

Copies: Appropriate Facility Manager (when applicable).

12201 Research Parkway • Suite 501 • Orlando, FL 32826-3246 • 407-823-3778 • Fax 407-823-3299

An Equal Opportunity and Affirmative Action Institution



THE UNIVERSITY OF CENTRAL FLORIDA
INSTITUTIONAL ANIMAL CARE and USE COMMITTEE (IACUC)
Approval to Use Animals

Dear Dr. Annette Khaled,

Your application for IACUC Approval has been reviewed and approved by the UCF IACUC Committee Reviewers.

Approval Date: 9/29/2011

Title: Pilot study to Examine Anti-tumor Activity of Bax Peptide

Department: Biomolecular Science Center

Animal Project #: 11-56

Expiration: 9/28/2012

You may purchase and use animals according to the provisions outlined in the above referenced animal project.

Christopher Parkinson, Ph.D.
IACUC Chair



Office of Research & Commercialization

November 4, 2011

Dr. Annette Khaled
6900 Lake Nona Blvd
Burnett School of Biomedical Sciences
Orlando, FL 32827

Subject: Institutional Animal Care Use Committee (IACUC) Addendum Submission.

Dear Dr. Khaled,

This letter is to inform you that the following addendum submitted was approved by the IACUC.

Animal Project: 11-56
Title: Pilot study to Examine Anti-tumor Activity of Bax Peptide (Addendum #1)
Approval Date: 11/3/2011

Please see the attached copy of the approved addendum and please keep a copy for your records. Should you have any questions, please do not hesitate to call me at (407) 822-1164.

Sincerely,

A handwritten signature in cursive script that reads 'Cristina Caamaño'.

Cristina Caamaño
Assistant Director, Research Program Services
Office of Research & Commercialization



UCF IACUC Addendum/Modification Form

Office Use Only:
Date Received: 11/1/11
Approval Date: 11/3/11

This addendum form does NOT extend the IACUC approval period or replace the Continuing Review form for renewal of the study.

INSTRUCTIONS: Use this form to request IACUC review of a minor change in an approved IACUC protocol and submit the request via e-mail to IACUC@mail.ucf.edu or mailed to the IACUC Office: ATTN: Cristina Caamaño, IACUC Coordinator, 12201 Research Parkway, Suite 502, Orlando, FL 32826-3246 or campus mail 32816-0150. Phone: 407-882-1164, Fax: 407-823-3299.

All Addendums must be approved by the IACUC prior to implementation.

Protocol Number: 11-56

Addendum #1

Principal Investigator: Annette Khaled

Title of Protocol: Pilot study to Examine Anti-tumor Activity of Bax Peptide

Type of Project: Category A Category B Category C Category D Category E

Changes to be Made: (provide sufficient detail to allow evaluation by the IACUC)
If new personnel will be added, training information for each procedure involved needs to be provided on this form.

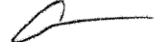
In order to better monitor the introduction of nanoparticles containing the Bax peptide and fluorescent dye will be injected into tumors growing in mice. Mice will be anesthetized and imaged as follows:

Mice injected with tumor cells are housed in mouse room 152 (Lake Nona) or equivalent to facilitate movement for imaging. Mice will be anesthetized using ~2% isoflurane with 1% oxygen in an induction chamber. The anesthetized state will be maintained using a nose cone. Eyes will be protected from drying with ointment. If imaging is longer than ~10 minutes, mice may be placed on a thermostatically controlled heating surface to maintain body temperature. Since we are expecting the tumors to be near the surface as a result of a subcutaneous injection of the cells, fluorescent nanoparticles will be injected directly into the tumor. If at a later time, we could perform an alternate means of tumor injection (e.g., intraperitoneal injection), we then may need to do tail vein or i.p. injection of the fluorescent nanoparticles. The expected site of injection will be swabbed with betadine (or equivalent) to clean the area. Sterile needles will be used for injection.

Fluorescent imaging will be performed with the Carestream multispectral FX imaging station in the Vivarium. Alternatively, if ultrasound imaging is needed to locate the tumor or to do needle guided injections, we will use the VisualSonics Vevo 2100 in the Vivarium, and warmed aqueous ultrasonic gel will be applied to the mouse. Following imaging, the mouse will be observed for recovery. Once it is alert and walking around in the cage, it can be taken back to the housing room. Alternately, the mouse can be euthanized by CO2 for termination of the experiment and collection of tissue/tumor.

Reasons for Addendum/Modification:
The recent availability of nanoparticles with a near infrared dye will allow us to monitor the introduction of nanoparticles into tumors without the need of invasive procedures.

If more space is needed, please attach an additional page to this form.

Signature of Principal Investigator  Date 11/1/11

REFERENCES

- [1] V. P. Skulachev, "Mitochondria in the programmed death phenomena; a principle of biology: 'it is better to die than to be wrong'," *IUBMB Life*, vol. 49, no. 5, pp. 365–373, May 2000.
- [2] C. A. Pettigrew and T. G. Cotter, "Deregulation of cell death (apoptosis): implications for tumor development," *Discov Med*, vol. 8, no. 41, pp. 61–63, Aug. 2009.
- [3] A. M. Petros, E. T. Olejniczak, and S. W. Fesik, "Structural biology of the Bcl-2 family of proteins," *Biochim. Biophys. Acta*, vol. 1644, no. 2–3, pp. 83–94, Mar. 2004.
- [4] P. N. Kelly and A. Strasser, "The role of Bcl-2 and its pro-survival relatives in tumorigenesis and cancer therapy," *Cell Death & Differentiation*, vol. 18, no. 9, pp. 1414–1424, 2011.
- [5] J. Lindsay, M. D. Esposti, and A. P. Gilmore, "Bcl-2 proteins and mitochondria--specificity in membrane targeting for death," *Biochim. Biophys. Acta*, vol. 1813, no. 4, pp. 532–539, Apr. 2011.
- [6] J. W. Lee, W. H. Kim, J. H. Lim, E. H. Song, J. Song, K. Y. Choi, and M. H. Jung, "Mitochondrial dysfunction: glucokinase downregulation lowers interaction of glucokinase with mitochondria, resulting in apoptosis of pancreatic beta-cells," *Cell. Signal.*, vol. 21, no. 1, pp. 69–78, Jan. 2009.

- [7] C. Pepper, T. Hoy, and D. P. Bentley, "Bcl-2/Bax ratios in chronic lymphocytic leukaemia and their correlation with in vitro apoptosis and clinical resistance," *Br. J. Cancer*, vol. 76, no. 7, pp. 935–938, 1997.
- [8] L. F. D[ia]z, M. Chiong, A. F. G. Quest, S. Lavandero, and A. Stutzin, "Mechanisms of cell death: molecular insights and therapeutic perspectives," *Cell Death & Differentiation*, vol. 12, no. 11, pp. 1449–1456, 2005.
- [9] C.-M. Shih, J.-S. Wu, W.-C. Ko, L.-F. Wang, Y.-H. Wei, H.-F. Liang, Y.-C. Chen, and C.-T. Chen, "Mitochondria-mediated caspase-independent apoptosis induced by cadmium in normal human lung cells," *J. Cell. Biochem.*, vol. 89, no. 2, pp. 335–347, May 2003.
- [10] M. Suzuki, R. J. Youle, and N. Tjandra, "Structure of Bax: coregulation of dimer formation and intracellular localization," *Cell*, vol. 103, no. 4, pp. 645–654, Nov. 2000.
- [11] C. A. Jette, A. M. Flanagan, J. Ryan, U. J. Pyati, S. Carbonneau, R. A. Stewart, D. M. Langenau, A. T. Look, and A. Letai, "BIM and other BCL-2 family proteins exhibit cross-species conservation of function between zebrafish and mammals," *Cell Death & Differentiation*, vol. 15, no. 6, pp. 1063–1072, 2008.
- [12] M. O. Péquignot, A. C. Provost, S. Sallé, P. Taupin, K. M. Sainton, D. Marchant, J. C. Martinou, J. C. Ameisen, J.-P. Jais, and M. Abitbol, "Major role of BAX in apoptosis during retinal development and in establishment of a functional postnatal retina," *Dev. Dyn.*, vol. 228, no. 2, pp. 231–238, Oct. 2003.

- [13] X.-F. Song, H. Ren, A. Andreasen, J. S. Thomsen, and X.-Y. Zhai, "Expression of Bcl-2 and Bax in mouse renal tubules during kidney development," *PLoS ONE*, vol. 7, no. 2, p. e32771, 2012.
- [14] K. Vekrellis, M. J. McCarthy, A. Watson, J. Whitfield, L. L. Rubin, and J. Ham, "Bax promotes neuronal cell death and is downregulated during the development of the nervous system," *Development*, vol. 124, no. 6, pp. 1239–1249, Mar. 1997.
- [15] R. J. Lutz, "Role of the BH3 (Bcl-2 homology 3) domain in the regulation of apoptosis and Bcl-2-related proteins," *Biochem. Soc. Trans.*, vol. 28, no. 2, pp. 51–56, Feb. 2000.
- [16] B. Antonsson, S. Montessuit, B. Sanchez, and J. C. Martinou, "Bax is present as a high molecular weight oligomer/complex in the mitochondrial membrane of apoptotic cells," *J. Biol. Chem.*, vol. 276, no. 15, pp. 11615–11623, Apr. 2001.
- [17] G. Heimlich, A. D. McKinnon, K. Bernardo, D. Brdiczka, J. C. Reed, R. Kain, M. Krönke, and J. M. Jürgensmeier, "Bax-induced cytochrome c release from mitochondria depends on alpha-helices-5 and -6," *Biochem. J.*, vol. 378, no. Pt 1, pp. 247–255, Feb. 2004.
- [18] J. M. Jürgensmeier, Z. Xie, Q. Deveraux, L. Ellerby, D. Bredesen, and J. C. Reed, "Bax directly induces release of cytochrome c from isolated mitochondria," *Proc. Natl. Acad. Sci. U.S.A.*, vol. 95, no. 9, pp. 4997–5002, Apr. 1998.
- [19] I. Milisav and D. Suput, "Procaspase-9 is attached to the mitochondrial outer membrane in the early stages of apoptosis," *Cell. Mol. Biol. Lett.*, vol. 12, no. 4, pp. 509–522, 2007.

- [20] H. Düßmann, M. Rehm, D. Kögel, and J. H. M. Prehn, "Outer Mitochondrial Membrane Permeabilization During Apoptosis Triggers Caspase-Independent Mitochondrial and Caspase-Dependent Plasma Membrane Potential Depolarization: A Single-Cell Analysis," *J Cell Sci*, vol. 116, no. 3, pp. 525–536, Feb. 2003.
- [21] A. V. F. Teles, R. P. Ureshino, D. J. Dorta, G. S. Lopes, Y.-T. Hsu, and S. S. Smaili, "Bcl-x(L) inhibits Bax-induced alterations in mitochondrial respiration and calcium release," *Neurosci. Lett.*, vol. 442, no. 2, pp. 96–99, Sep. 2008.
- [22] D. L. Bratton, V. A. Fadok, D. A. Richter, J. M. Kailey, L. A. Guthrie, and P. M. Henson, "Appearance of phosphatidylserine on apoptotic cells requires calcium-mediated nonspecific flip-flop and is enhanced by loss of the aminophospholipid translocase," *J. Biol. Chem.*, vol. 272, no. 42, pp. 26159–26165, Oct. 1997.
- [23] N. N. Danial, C. F. Gramm, L. Scorrano, C.-Y. Zhang, S. Krauss, A. M. Ranger, S. R. Datta, M. E. Greenberg, L. J. Licklider, B. B. Lowell, S. P. Gygi, and S. J. Korsmeyer, "BAD and glucokinase reside in a mitochondrial complex that integrates glycolysis and apoptosis," *Nature*, vol. 424, no. 6951, pp. 952–956, Aug. 2003.
- [24] N. N. Danial, "BAD: undertaker by night, candyman by day," *Oncogene*, vol. 27 Suppl 1, pp. S53–70, Dec. 2008.
- [25] K. N. Alavian, H. Li, L. Collis, L. Bonanni, L. Zeng, S. Sacchetti, E. Lazrove, P. Nabili, B. Flaherty, M. Graham, Y. Chen, S. M. Messerli, M. A. Mariggio, C. Rahner, E. McNay, G. C. Shore, P. J. S. Smith, J. M. Hardwick, and E. A. Jonas, "Bcl-xL regulates metabolic efficiency of neurons through interaction with the mitochondrial

- F1FO ATP synthase,” *Nature Cell Biology*, vol. 13, no. 10, pp. 1224–1233, Sep. 2011.
- [26] G. Yeretssian, R. G. Correa, K. Doiron, P. Fitzgerald, C. P. Dillon, D. R. Green, J. C. Reed, and M. Saleh, “Non-apoptotic role of BID in inflammation and innate immunity,” *Nature*, vol. 474, no. 7349, pp. 96–99, Jun. 2011.
- [27] Y.-L. P. Ow, D. R. Green, Z. Hao, and T. W. Mak, “Cytochrome c: functions beyond respiration,” *Nat. Rev. Mol. Cell Biol.*, vol. 9, no. 7, pp. 532–542, Jul. 2008.
- [28] O. WARBURG, “On the origin of cancer cells,” *Science*, vol. 123, no. 3191, pp. 309–314, Feb. 1956.
- [29] R. K. KIELLEY, “Oxidative phosphorylation by mitochondria of transplantable mouse hepatoma and mouse liver,” *Cancer Res.*, vol. 12, no. 2, pp. 124–128, Feb. 1952.
- [30] B. O’Rourke, S. Cortassa, and M. A. Aon, “Mitochondrial Ion Channels: Gatekeepers of Life and Death,” *Physiology*, vol. 20, no. 5, pp. 303–315, Oct. 2005.
- [31] I. E. Scheffler, “Mitochondria,” in *Mitochondria*, John Wiley & Sons, Inc., 2007, pp. c1–c12.
- [32] N. Khalifat, J.-B. Fournier, M. I. Angelova, and N. Puff, “Lipid packing variations induced by pH in cardiolipin-containing bilayers: the driving force for the cristae-like shape instability,” *Biochim. Biophys. Acta*, vol. 1808, no. 11, pp. 2724–2733, Nov. 2011.

- [33] B. Heit, T. Yeung, and S. Grinstein, "Changes in mitochondrial surface charge mediate recruitment of signaling molecules during apoptosis," *Am. J. Physiol., Cell Physiol.*, vol. 300, no. 1, pp. C33–41, Jan. 2011.
- [34] V. Shoshan-Barmatz and D. Ben-Hail, "VDAC, a multi-functional mitochondrial protein as a pharmacological target," *Mitochondrion*, vol. 12, no. 1, pp. 24–34, Jan. 2012.
- [35] C. R. Pestana, C. H. T. P. Silva, S. A. Uyemura, A. C. Santos, and C. Curti, "Impact of adenosine nucleotide translocase (ANT) proline isomerization on Ca²⁺-induced cysteine relative mobility/mitochondrial permeability transition pore," *J. Bioenerg. Biomembr.*, vol. 42, no. 4, pp. 329–335, Aug. 2010.
- [36] A. Biroccio, A. Candiloro, M. Mottolese, O. Sapora, A. Albini, G. Zupi, and D. Del Bufalo, "Bcl-2 Overexpression and Hypoxia Synergistically Act to Modulate Vascular Endothelial Growth Factor Expression and in Vivo Angiogenesis in a Breast Carcinoma Line," *FASEB J*, vol. 14, no. 5, pp. 652–660, Apr. 2000.
- [37] F. Ciardiello and G. Tortora, "Inhibition of Bcl-2 as Cancer Therapy," *Ann Oncol*, vol. 13, no. 4, pp. 501–502, Apr. 2002.
- [38] K. D. Mason, S. L. Khaw, K. C. Rayeroux, E. Chew, E. F. Lee, W. D. Fairlie, A. P. Grigg, J. F. Seymour, J. Szer, D. C. S. Huang, and A. W. Roberts, "The BH3 mimetic compound, ABT-737, synergizes with a range of cytotoxic chemotherapy agents in chronic lymphocytic leukemia," *Leukemia*, vol. 23, no. 11, pp. 2034–2041, Nov. 2009.

- [39] T. Oltersdorf, S. W. Elmore, A. R. Shoemaker, R. C. Armstrong, D. J. Augeri, B. A. Belli, M. Bruncko, T. L. Deckwerth, J. Dinges, P. J. Hajduk, M. K. Joseph, S. Kitada, S. J. Korsmeyer, A. R. Kunzer, A. Letai, C. Li, M. J. Mitten, D. G. Nettesheim, S. Ng, P. M. Nimmer, J. M. O'Connor, A. Oleksijew, A. M. Petros, J. C. Reed, W. Shen, S. K. Tahir, C. B. Thompson, K. J. Tomaselli, B. Wang, M. D. Wendt, H. Zhang, S. W. Fesik, and S. H. Rosenberg, "An inhibitor of Bcl-2 family proteins induces regression of solid tumours," *Nature*, vol. 435, no. 7042, pp. 677–681, Jun. 2005.
- [40] W. H. Wilson, O. A. O'Connor, M. S. Czuczman, A. S. LaCasce, J. F. Gerecitano, J. P. Leonard, A. Tulpule, K. Dunleavy, H. Xiong, Y.-L. Chiu, Y. Cui, T. Busman, S. W. Elmore, S. H. Rosenberg, A. P. Krivoshik, S. H. Enschede, and R. A. Humerickhouse, "Navitoclax, a targeted high-affinity inhibitor of BCL-2, in lymphoid malignancies: a phase 1 dose-escalation study of safety, pharmacokinetics, pharmacodynamics, and antitumour activity," *Lancet Oncol.*, vol. 11, no. 12, pp. 1149–1159, Dec. 2010.
- [41] L. D. Walensky, A. L. Kung, I. Escher, T. J. Malia, S. Barbuto, R. D. Wright, G. Wagner, G. L. Verdine, and S. J. Korsmeyer, "Activation of apoptosis in vivo by a hydrocarbon-stapled BH3 helix," *Science*, vol. 305, no. 5689, pp. 1466–1470, Sep. 2004.
- [42] S. Conus, T. Kaufmann, I. Fellay, I. Otter, T. Ross[acute], and C. Borner, "Bcl-2 is a monomeric protein: prevention of homodimerization by structural constraints," *The EMBO Journal*, vol. 19, no. 7, pp. 1534–1544, Apr. 2000.

- [43] L. M. Yin, M. A. Edwards, J. Li, C. M. Yip, and C. M. Deber, "Roles of hydrophobicity and charge distribution of cationic antimicrobial peptides in peptide-membrane interactions," *J. Biol. Chem.*, vol. 287, no. 10, pp. 7738–7745, Mar. 2012.
- [44] L.-L. Cai, P. Liu, X. Li, X. Huang, Y.-Q. Ye, F.-Y. Chen, H. Yuan, F.-Q. Hu, and Y.-Z. Du, "RGD peptide-mediated chitosan-based polymeric micelles targeting delivery for integrin-overexpressing tumor cells," *Int J Nanomedicine*, vol. 6, pp. 3499–3508, 2011.
- [45] F. Pinheiro da Silva and M. C. C. Machado, "Antimicrobial peptides: Clinical relevance and therapeutic implications," *Peptides*, Jun. 2012.
- [46] E. Koren and V. P. Torchilin, "Cell-penetrating peptides: breaking through to the other side," *Trends in Molecular Medicine*, Jun. 2012.
- [47] S. Qian, W. Wang, L. Yang, and H. W. Huang, "Structure of transmembrane pore induced by Bax-derived peptide: evidence for lipidic pores," *Proc. Natl. Acad. Sci. U.S.A.*, vol. 105, no. 45, pp. 17379–17383, Nov. 2008.
- [48] D. L. Vaux, S. Cory, and J. M. Adams, "Bcl-2 gene promotes haemopoietic cell survival and cooperates with c-myc to immortalize pre-B cells," *Nature*, vol. 335, no. 6189, pp. 440–442, Sep. 1988.
- [49] J.-P. Upton, A. J. Valentijn, L. Zhang, and A. P. Gilmore, "The N-terminal conformation of Bax regulates cell commitment to apoptosis," *Cell Death Differ*, vol. 14, no. 5, pp. 932–942, May 2007.
- [50] N. Parikh, C. Koshy, V. Dhayabaran, L. R. Perumalsamy, R. Sowdhamini, and A. Sarin, "The N-terminus and alpha-5, alpha-6 helices of the pro-apoptotic protein

- Bax, modulate functional interactions with the anti-apoptotic protein Bcl-xL,” *BMC Cell Biol.*, vol. 8, p. 16, 2007.
- [51] A. J. Valentijn, J.-P. Upton, N. Bates, and A. P. Gilmore, “Bax targeting to mitochondria occurs via both tail anchor-dependent and -independent mechanisms,” *Cell Death Differ.*, vol. 15, no. 8, pp. 1243–1254, Aug. 2008.
- [52] E. Gavathiotis, D. E. Reyna, J. A. Bellairs, E. S. Leshchiner, and L. D. Walensky, “Direct and selective small-molecule activation of proapoptotic BAX,” *Nature Chemical Biology*, vol. 8, no. 7, pp. 639–645, 2012.
- [53] D. Lama and R. Sankararamakrishnan, “Anti-apoptotic Bcl-XL protein in complex with BH3 peptides of pro-apoptotic Bak, Bad, and Bim proteins: Comparative molecular dynamics simulations,” *Proteins: Structure, Function, and Bioinformatics*, vol. 73, no. 2, pp. 492–514, 2008.
- [54] A. L. Grenier, K. Abu-ihweij, G. Zhang, S. M. Ruppert, R. Boohaker, E. R. Slepko, K. Pridemore, J.-J. Ren, L. Fliegel, and A. R. Khaled, “Apoptosis-induced alkalization by the Na⁺/H⁺ exchanger isoform 1 is mediated through phosphorylation of amino acids Ser726 and Ser729,” *Am. J. Physiol., Cell Physiol.*, vol. 295, no. 4, pp. C883–896, Oct. 2008.
- [55] D. T. Chao and S. J. Korsmeyer, “BCL-2 family: regulators of cell death,” *Annu. Rev. Immunol.*, vol. 16, pp. 395–419, 1998.
- [56] N. Motoyama, F. Wang, K. A. Roth, H. Sawa, K. Nakayama, K. Nakayama, I. Negishi, S. Senju, Q. Zhang, and S. Fujii, “Massive cell death of immature

hematopoietic cells and neurons in Bcl-x-deficient mice,” *Science*, vol. 267, no. 5203, pp. 1506–1510, Mar. 1995.

- [57] D. J. Veis, C. M. Sorenson, J. R. Shutter, and S. J. Korsmeyer, “Bcl-2-deficient mice demonstrate fulminant lymphoid apoptosis, polycystic kidneys, and hypopigmented hair,” *Cell*, vol. 75, no. 2, pp. 229–240, Oct. 1993.
- [58] T. Chittenden, C. Flemington, A. B. Houghton, R. G. Ebb, G. J. Gallo, B. Elangovan, G. Chinnadurai, and R. J. Lutz, “A conserved domain in Bak, distinct from BH1 and BH2, mediates cell death and protein binding functions,” *EMBO J.*, vol. 14, no. 22, pp. 5589–5596, Nov. 1995.
- [59] X. M. Yin, Z. N. Oltvai, and S. J. Korsmeyer, “BH1 and BH2 domains of Bcl-2 are required for inhibition of apoptosis and heterodimerization with Bax,” *Nature*, vol. 369, no. 6478, pp. 321–323, May 1994.
- [60] L. A. O’Reilly, D. C. Huang, and A. Strasser, “The cell death inhibitor Bcl-2 and its homologues influence control of cell cycle entry,” *EMBO J.*, vol. 15, no. 24, pp. 6979–6990, Dec. 1996.
- [61] G. Vairo, K. M. Innes, and J. M. Adams, “Bcl-2 has a cell cycle inhibitory function separable from its enhancement of cell survival,” *Oncogene*, vol. 13, no. 7, pp. 1511–1519, Oct. 1996.
- [62] R. A. Kirkland and J. L. Franklin, “Bax affects production of reactive oxygen by the mitochondria of non-apoptotic neurons,” *Exp. Neurol.*, vol. 204, no. 1, pp. 458–461, Mar. 2007.

- [63] R. G. Jones, T. Bui, C. White, M. Madesh, C. M. Krawczyk, T. Lindsten, B. J. Hawkins, S. Kubek, K. A. Frauwirth, Y. L. Wang, S. J. Conway, H. L. Roderick, M. D. Bootman, H. Shen, J. K. Foskett, and C. B. Thompson, "The proapoptotic factors Bax and Bak regulate T Cell proliferation through control of endoplasmic reticulum Ca(2+) homeostasis," *Immunity*, vol. 27, no. 2, pp. 268–280, Aug. 2007.
- [64] P.-F. Cartron, L. Oliver, S. Martin, C. Moreau, M.-T. LeCabellec, P. Jezequel, K. Meflah, and F. M. Vallette, "The Expression of a New Variant of the Pro-Apoptotic Molecule Bax, Bax ψ , Is Correlated with an Increased Survival of Glioblastoma Multiforme Patients," *Hum. Mol. Genet.*, vol. 11, no. 6, pp. 675–687, Mar. 2002.
- [65] L. Zhang, J. Yu, B. H. Park, K. W. Kinzler, and B. Vogelstein, "Role of BAX in the apoptotic response to anticancer agents," *Science*, vol. 290, no. 5493, pp. 989–992, Nov. 2000.
- [66] C. M. Knudson, K. S. Tung, W. G. Tourtellotte, G. A. Brown, and S. J. Korsmeyer, "Bax-deficient mice with lymphoid hyperplasia and male germ cell death," *Science*, vol. 270, no. 5233, pp. 96–99, Oct. 1995.
- [67] A. R. Khaled, K. Kim, R. Hofmeister, K. Muegge, and S. K. Durum, "Withdrawal of IL-7 induces Bax translocation from cytosol to mitochondria through a rise in intracellular pH," *Proc. Natl. Acad. Sci. U.S.A.*, vol. 96, no. 25, pp. 14476–14481, Dec. 1999.
- [68] W. Pendergrass, N. Wolf, and M. Poot, "Efficacy of MitoTracker Green and CMXrosamine to measure changes in mitochondrial membrane potentials in living cells and tissues," *Cytometry A*, vol. 61, no. 2, pp. 162–169, Oct. 2004.

- [69] C. Ferlini and G. Scambia, "Assay for apoptosis using the mitochondrial probes, Rhodamine123 and 10-N-nonyl acridine orange," *Nat Protoc*, vol. 2, no. 12, pp. 3111–3114, 2007.
- [70] P. Xia, H.-X. An, C.-X. Dang, R. Radpour, C. Kohler, E. Fokas, R. Engenhart-Cabillic, W. Holzgreve, and X. Y. Zhong, "Decreased mitochondrial DNA content in blood samples of patients with stage I breast cancer," *BMC Cancer*, vol. 9, p. 454, 2009.
- [71] M. Garcia Fernandez, L. Troiano, L. Moretti, M. Nasi, M. Pinti, S. Salvioli, J. Dobrucki, and A. Cossarizza, "Early changes in intramitochondrial cardiolipin distribution during apoptosis," *Cell Growth Differ.*, vol. 13, no. 9, pp. 449–455, Sep. 2002.
- [72] J. Yang, X. Liu, K. Bhalla, C. N. Kim, A. M. Ibrado, J. Cai, T. I. Peng, D. P. Jones, and X. Wang, "Prevention of apoptosis by Bcl-2: release of cytochrome c from mitochondria blocked," *Science*, vol. 275, no. 5303, pp. 1129–1132, Feb. 1997.
- [73] Z. N. Oltvai, C. L. Milliman, and S. J. Korsmeyer, "Bcl-2 heterodimerizes in vivo with a conserved homolog, Bax, that accelerates programmed cell death," *Cell*, vol. 74, no. 4, pp. 609–619, Aug. 1993.
- [74] H. Zha, C. Aimé-Sempé, T. Sato, and J. C. Reed, "Proapoptotic protein Bax heterodimerizes with Bcl-2 and homodimerizes with Bax via a novel domain (BH3) distinct from BH1 and BH2," *J. Biol. Chem.*, vol. 271, no. 13, pp. 7440–7444, Mar. 1996.

- [75] F. W. Peyerl, S. Dai, G. A. Murphy, F. Crawford, J. White, P. Murrack, and J. W. Kappler, "Elucidation of some Bax conformational changes through crystallization of an antibody-peptide complex," *Cell Death Differ.*, vol. 14, no. 3, pp. 447–452, Mar. 2007.
- [76] K. N. Nemeč and A. R. Khaled, "Therapeutic modulation of apoptosis: targeting the BCL-2 family at the interface of the mitochondrial membrane," *Yonsei Med. J.*, vol. 49, no. 5, pp. 689–697, Oct. 2008.
- [77] A. Torrecillas, M. M. Martínez-Senac, A. Ausili, S. Corbalán-García, and J. C. Gómez-Fernández, "Interaction of the C-terminal domain of Bcl-2 family proteins with model membranes," *Biochim. Biophys. Acta*, vol. 1768, no. 11, pp. 2931–2939, Nov. 2007.
- [78] Y. Tsujimoto and S. Shimizu, "Role of the mitochondrial membrane permeability transition in cell death," *Apoptosis*, vol. 12, no. 5, pp. 835–840, May 2007.
- [79] J. G. Pastorino, N. Shulga, and J. B. Hoek, "Mitochondrial binding of hexokinase II inhibits Bax-induced cytochrome c release and apoptosis," *J. Biol. Chem.*, vol. 277, no. 9, pp. 7610–7618, Mar. 2002.
- [80] M. Karbowski, Y.-J. Lee, B. Gaume, S.-Y. Jeong, S. Frank, A. Nechushtan, A. Santel, M. Fuller, C. L. Smith, and R. J. Youle, "Spatial and temporal association of Bax with mitochondrial fission sites, Drp1, and Mfn2 during apoptosis," *J. Cell Biol.*, vol. 159, no. 6, pp. 931–938, Dec. 2002.
- [81] C. Brooks, Q. Wei, L. Feng, G. Dong, Y. Tao, L. Mei, Z.-J. Xie, and Z. Dong, "Bak regulates mitochondrial morphology and pathology during apoptosis by

- interacting with mitofusins,” *Proc. Natl. Acad. Sci. U.S.A.*, vol. 104, no. 28, pp. 11649–11654, Jul. 2007.
- [82] Y. Takahashi, M. Karbowski, H. Yamaguchi, A. Kazi, J. Wu, S. M. Sebti, R. J. Youle, and H.-G. Wang, “Loss of Bif-1 suppresses Bax/Bak conformational change and mitochondrial apoptosis,” *Mol. Cell. Biol.*, vol. 25, no. 21, pp. 9369–9382, Nov. 2005.
- [83] R. Kumarswamy and S. Chandna, “Putative partners in Bax mediated cytochrome-c release: ANT, CypD, VDAC or none of them?,” *Mitochondrion*, vol. 9, no. 1, pp. 1–8, Feb. 2009.
- [84] P. Wang, A. Lo, J. B. Young, J. H. Song, R. Lai, N. M. Kneteman, C. Hao, and L. Li, “Targeted quantitative mass spectrometric identification of differentially expressed proteins between Bax-expressing and deficient colorectal carcinoma cells,” *J. Proteome Res.*, vol. 8, no. 7, pp. 3403–3414, Jul. 2009.
- [85] Y. Ionov, H. Yamamoto, S. Krajewski, J. C. Reed, and M. Perucho, “Mutational inactivation of the proapoptotic gene BAX confers selective advantage during tumor clonal evolution,” *Proc. Natl. Acad. Sci. U.S.A.*, vol. 97, no. 20, pp. 10872–10877, Sep. 2000.
- [86] M. Wu, A. Neilson, A. L. Swift, R. Moran, J. Tamagnine, D. Parslow, S. Armistead, K. Lemire, J. Orrell, J. Teich, S. Chomicz, and D. A. Ferrick, “Multiparameter metabolic analysis reveals a close link between attenuated mitochondrial bioenergetic function and enhanced glycolysis dependency in human tumor cells,” *Am. J. Physiol., Cell Physiol.*, vol. 292, no. 1, pp. C125–136, Jan. 2007.

- [87] R. Elkholi, K. V. Floros, and J. E. Chipuk, "The Role of BH3-Only Proteins in Tumor Cell Development, Signaling, and Treatment," *Genes Cancer*, vol. 2, no. 5, pp. 523–537, May 2011.
- [88] G. Kroemer, L. Galluzzi, and C. Brenner, "Mitochondrial membrane permeabilization in cell death," *Physiol. Rev.*, vol. 87, no. 1, pp. 99–163, Jan. 2007.
- [89] I. Sturm, A. G. Bosanquet, S. Hermann, D. Güner, B. Dörken, and P. T. Daniel, "Mutation of p53 and consecutive selective drug resistance in B-CLL occurs as a consequence of prior DNA-damaging chemotherapy," *Cell Death Differ.*, vol. 10, no. 4, pp. 477–484, Apr. 2003.
- [90] M. Kuhar, S. Sen, and N. Singh, "Role of mitochondria in quercetin-enhanced chemotherapeutic response in human non-small cell lung carcinoma H-520 cells," *Anticancer Res.*, vol. 26, no. 2A, pp. 1297–1303, Apr. 2006.
- [91] A. B. Castoreno and U. S. Eggert, "Small molecule probes of cellular pathways and networks," *ACS Chem. Biol.*, vol. 6, no. 1, pp. 86–94, Jan. 2011.
- [92] S. Pillarisetti, "Are peptides the future? Small molecule versus peptides," *Curr Pharm Biotechnol*, vol. 7, no. 4, pp. 225–227, Aug. 2006.
- [93] A. W. Roberts, J. F. Seymour, J. R. Brown, W. G. Wierda, T. J. Kipps, S. L. Khaw, D. A. Carney, S. Z. He, D. C. S. Huang, H. Xiong, Y. Cui, T. A. Busman, E. M. McKeegan, A. P. Krivoschik, S. H. Enschede, and R. Humerickhouse, "Substantial susceptibility of chronic lymphocytic leukemia to BCL2 inhibition: results of a phase I study of navitoclax in patients with relapsed or refractory disease," *J. Clin. Oncol.*, vol. 30, no. 5, pp. 488–496, Feb. 2012.

- [94] R. J. Boohaker, M. W. Lee, P. Vishnubhotla, J. M. Perez, and A. R. Khaled, "The Use of Therapeutics Peptides to Target and to Kill Cancer Cells.," *Curr Med Chem*, 2012.
- [95] R. J. Boohaker, G. Zhang, A. L. Carlson, K. N. Nemecek, and A. R. Khaled, "BAX supports the mitochondrial network, promoting bioenergetics in nonapoptotic cells," *Am. J. Physiol., Cell Physiol.*, vol. 300, no. 6, pp. C1466–1478, Jun. 2011.
- [96] S. Santra, C. Kaittanis, and J. M. Perez, "Aliphatic hyperbranched polyester: a new building block in the construction of multifunctional nanoparticles and nanocomposites," *Langmuir*, vol. 26, no. 8, pp. 5364–5373, Apr. 2010.
- [97] D. W. Hoskin and A. Ramamoorthy, "Studies on anticancer activities of antimicrobial peptides," *Biochim. Biophys. Acta*, vol. 1778, no. 2, pp. 357–375, Feb. 2008.
- [98] M. W. Gray, "The endosymbiont hypothesis revisited," *Int. Rev. Cytol.*, vol. 141, pp. 233–357, 1992.
- [99] C. W. Morden, C. F. Delwiche, M. Kuhsel, and J. D. Palmer, "Gene phylogenies and the endosymbiotic origin of plastids," *BioSystems*, vol. 28, no. 1–3, pp. 75–90, 1992.
- [100] H. M. Ellerby, W. Arap, L. M. Ellerby, R. Kain, R. Andrusiak, G. D. Rio, S. Krajewski, C. R. Lombardo, R. Rao, E. Ruoslahti, D. E. Bredesen, and R. Pasqualini, "Anti-cancer activity of targeted pro-apoptotic peptides," *Nat. Med.*, vol. 5, no. 9, pp. 1032–1038, Sep. 1999.

- [101] B. Law, L. Quinti, Y. Choi, R. Weissleder, and C.-H. Tung, "A mitochondrial targeted fusion peptide exhibits remarkable cytotoxicity," *Mol. Cancer Ther.*, vol. 5, no. 8, pp. 1944–1949, Aug. 2006.
- [102] L. Agemy, D. Friedmann-Morvinski, V. R. Kotamraju, L. Roth, K. N. Sugahara, O. M. Girard, R. F. Mattrey, I. M. Verma, and E. Ruoslahti, "Targeted nanoparticle enhanced proapoptotic peptide as potential therapy for glioblastoma," *Proc. Natl. Acad. Sci. U.S.A.*, vol. 108, no. 42, pp. 17450–17455, Oct. 2011.
- [103] J. G. Valero, L. Sancey, J. Kucharczak, Y. Guillemin, D. Gimenez, J. Prudent, G. Gillet, J. Salgado, J.-L. Coll, and A. Aouacheria, "Bax-derived membrane-active peptides act as potent and direct inducers of apoptosis in cancer cells," *J. Cell. Sci.*, vol. 124, no. Pt 4, pp. 556–564, Feb. 2011.
- [104] Y. Li, Y. Pei, X. Zhang, Z. Gu, Z. Zhou, W. Yuan, J. Zhou, J. Zhu, and X. Gao, "PEGylated PLGA nanoparticles as protein carriers: synthesis, preparation and biodistribution in rats," *J Control Release*, vol. 71, no. 2, pp. 203–211, Apr. 2001.
- [105] F. Alexis, E. Pridgen, L. K. Molnar, and O. C. Farokhzad, "Factors affecting the clearance and biodistribution of polymeric nanoparticles," *Mol. Pharm.*, vol. 5, no. 4, pp. 505–515, Aug. 2008.
- [106] T. Vanden Berghe, N. Vanlangenakker, E. Parthoens, W. Deckers, M. Devos, N. Festjens, C. J. Guerin, U. T. Brunk, W. Declercq, and P. Vandenabeele, "Necroptosis, necrosis and secondary necrosis converge on similar cellular disintegration features," *Cell Death Differ.*, vol. 17, no. 6, pp. 922–930, Jun. 2010.

- [107] G. Basañez, J. C. Sharpe, J. Galanis, T. B. Brandt, J. M. Hardwick, and J. Zimmerberg, "Bax-type apoptotic proteins porate pure lipid bilayers through a mechanism sensitive to intrinsic monolayer curvature," *J. Biol. Chem.*, vol. 277, no. 51, pp. 49360–49365, Dec. 2002.
- [108] A. J. García-Sáez, I. Mingarro, E. Pérez-Payá, and J. Salgado, "Membrane-insertion fragments of Bcl-xL, Bax, and Bid," *Biochemistry*, vol. 43, no. 34, pp. 10930–10943, Aug. 2004.
- [109] P. H. Schlesinger and M. Saito, "The Bax pore in liposomes, Biophysics," *Cell Death Differ.*, vol. 13, no. 8, pp. 1403–1408, Aug. 2006.
- [110] A. J. García-Sáez, M. Coraiola, M. D. Serra, I. Mingarro, P. Müller, and J. Salgado, "Peptides corresponding to helices 5 and 6 of Bax can independently form large lipid pores," *FEBS J.*, vol. 273, no. 5, pp. 971–981, Mar. 2006.
- [111] A. J. García-Sáez, M. Coraiola, M. Dalla Serra, I. Mingarro, G. Menestrina, and J. Salgado, "Peptides derived from apoptotic Bax and Bid reproduce the poration activity of the parent full-length proteins," *Biophys. J.*, vol. 88, no. 6, pp. 3976–3990, Jun. 2005.
- [112] C. Moreau, P.-F. Cartron, A. Hunt, K. Meflah, D. R. Green, G. Evan, F. M. Vallette, and P. Juin, "Minimal BH3 peptides promote cell death by antagonizing anti-apoptotic proteins," *J. Biol. Chem.*, vol. 278, no. 21, pp. 19426–19435, May 2003.

- [113] L. Zhang, L. Ming, and J. Yu, "BH3 mimetics to improve cancer therapy; mechanisms and examples," *Drug Resist. Updat.*, vol. 10, no. 6, pp. 207–217, Dec. 2007.
- [114] S. Riedl, B. Rinner, M. Asslaber, H. Schaidler, S. Walzer, A. Novak, K. Lohner, and D. Zweytick, "In search of a novel target - phosphatidylserine exposed by non-apoptotic tumor cells and metastases of malignancies with poor treatment efficacy," *Biochim. Biophys. Acta*, vol. 1808, no. 11, pp. 2638–2645, Nov. 2011.
- [115] S. Bafna, S. Kaur, and S. K. Batra, "Membrane-bound mucins: the mechanistic basis for alterations in the growth and survival of cancer cells," *Oncogene*, vol. 29, no. 20, pp. 2893–2904, May 2010.
- [116] B. Fadnes, O. Rekdal, and L. Uhlin-Hansen, "The anticancer activity of lytic peptides is inhibited by heparan sulfate on the surface of the tumor cells," *BMC Cancer*, vol. 9, p. 183, 2009.
- [117] S. Aviel-Ronen, S. K. Lau, M. Pintilie, D. Lau, N. Liu, M. S. Tsao, and S. Jothy, "Glypican-3 is overexpressed in lung squamous cell carcinoma, but not in adenocarcinoma," *Mod. Pathol.*, vol. 21, no. 7, pp. 817–825, Jul. 2008.
- [118] M. M. Javadpour, M. M. Juban, W. C. Lo, S. M. Bishop, J. B. Alberty, S. M. Cowell, C. L. Becker, and M. L. McLaughlin, "De novo antimicrobial peptides with low mammalian cell toxicity," *J. Med. Chem.*, vol. 39, no. 16, pp. 3107–3113, Aug. 1996.

- [119] J. C. Mai, Z. Mi, S. H. Kim, B. Ng, and P. D. Robbins, "A proapoptotic peptide for the treatment of solid tumors," *Cancer Res.*, vol. 61, no. 21, pp. 7709–7712, Nov. 2001.
- [120] N. Kolevzon, U. Kuflik, M. Shmuel, S. Benhamron, I. Ringel, and E. Yavin, "Multiple triphenylphosphonium cations as a platform for the delivery of a proapoptotic peptide," *Pharm. Res.*, vol. 28, no. 11, pp. 2780–2789, Nov. 2011.
- [121] K. Rege, S. J. Patel, Z. Megeed, and M. L. Yarmush, "Amphipathic peptide-based fusion peptides and immunoconjugates for the targeted ablation of prostate cancer cells," *Cancer Res.*, vol. 67, no. 13, pp. 6368–6375, Jul. 2007.
- [122] Y. Matsumura and H. Maeda, "A new concept for macromolecular therapeutics in cancer chemotherapy: mechanism of tumoritropic accumulation of proteins and the antitumor agent smancs," *Cancer Res.*, vol. 46, no. 12 Pt 1, pp. 6387–6392, Dec. 1986.
- [123] J. L. Rosas-Trigueros, J. Correa-Basurto, C. G. Benítez-Cardoza, and A. Zamorano-Carrillo, "Insights into the structural stability of Bax from molecular dynamics simulations at high temperatures," *Protein Sci.*, vol. 20, no. 12, pp. 2035–2046, Dec. 2011.
- [124] "Conformational change of Bax: a question of life or death," , *Published online: 08 August 2001*; | doi:10.1038/sj.cdd.4400910, vol. 8, no. 9, Aug. 2001.
- [125] E. Gavathiotis, M. Suzuki, M. L. Davis, K. Pitter, G. H. Bird, S. G. Katz, H.-C. Tu, H. Kim, E. H.-Y. Cheng, N. Tjandra, and L. D. Walensky, "BAX activation is initiated at a novel interaction site," *Nature*, vol. 455, no. 7216, pp. 1076–1081, Oct. 2008.

- [126] W. Humphrey, A. Dalke, and K. Schulten, "VMD: visual molecular dynamics," *J Mol Graph*, vol. 14, no. 1, pp. 33–38, 27–28, Feb. 1996.
- [127] H. J. C. Berendsen, D. van der Spoel, and R. van Drunen, "GROMACS: A message-passing parallel molecular dynamics implementation," *Computer Physics Communications*, vol. 91, no. 1–3, pp. 43–56, Sep. 1995.
- [128] B. Hess, C. Kutzner, D. van der Spoel, and E. Lindahl, "GROMACS 4: Algorithms for Highly Efficient, Load-Balanced, and Scalable Molecular Simulation," *J. Chem. Theory Comput.*, vol. 4, no. 3, pp. 435–447, 2008.
- [129] U. Essmann, L. Perera, M. Berkowitz, T. Darden, H. Lee, and L. Pedersen, "A smooth particle mesh Ewald method," *The Journal of Chemical Physics*, vol. 103, no. 19, pp. 8577–8593, 1995.
- [130] P. Mark and L. Nilsson, "Structure and Dynamics of the TIP3P, SPC, and SPC/E Water Models at 298 K," *The Journal of Physical Chemistry A*, vol. 105, no. 43, pp. 9954–9960, 2001.
- [131] P. T. Kiss and A. Baranyai, "Sources of the deficiencies in the popular SPC/E and TIP3P models of water.," *The Journal of chemical physics*, vol. 134, no. 5, p. 054106, 2011.
- [132] K. Lindorff-Larsen, S. Piana, K. Palmo, P. Maragakis, J. L. Klepeis, R. O. Dror, and D. E. Shaw, "Improved side-chain torsion potentials for the Amber ff99SB protein force field," *Proteins*, vol. 78, no. 8, pp. 1950–1958, Jun. 2010.
- [133] S. A. Showalter and R. Brüschweiler, "Validation of Molecular Dynamics Simulations of Biomolecules Using NMR Spin Relaxation as Benchmarks:

- Application to the AMBER99SB Force Field,” *J. Chem. Theory Comput.*, vol. 3, no. 3, pp. 961–975, 2007.
- [134] E. Mayaan, A. Moser, A. D. MacKerell, and D. M. York, “CHARMM force field parameters for simulation of reactive intermediates in native and thio-substituted ribozymes,” *Journal of Computational Chemistry*, vol. 28, no. 2, pp. 495–507, 2007.
- [135] W. L. Jorgensen, D. S. Maxwell, and J. Tirado-Rives, “Development and Testing of the OPLS All-Atom Force Field on Conformational Energetics and Properties of Organic Liquids,” *J. Am. Chem. Soc.*, vol. 118, no. 45, pp. 11225–11236, 1996.
- [136] H. J. C. Berendsen, J. P. M. Postma, W. F. van Gunsteren, A. DiNola, and J. R. Haak, “Molecular dynamics with coupling to an external bath,” *The Journal of Chemical Physics*, vol. 81, no. 8, p. 3684, 1984.
- [137] S. Barash, W. Wang, and Y. Shi, “Human secretory signal peptide description by hidden Markov model and generation of a strong artificial signal peptide for secreted protein expression,” *Biochem. Biophys. Res. Commun.*, vol. 294, no. 4, pp. 835–842, Jun. 2002.
- [138] T. Lindsten, A. J. Ross, A. King, W. X. Zong, J. C. Rathmell, H. A. Shiels, E. Ulrich, K. G. Waymire, P. Mahar, K. Frauwirth, Y. Chen, M. Wei, V. M. Eng, D. M. Adelman, M. C. Simon, A. Ma, J. A. Golden, G. Evan, S. J. Korsmeyer, G. R. MacGregor, and C. B. Thompson, “The combined functions of proapoptotic Bcl-2 family members bak and bax are essential for normal development of multiple tissues,” *Mol. Cell*, vol. 6, no. 6, pp. 1389–1399, Dec. 2000.